Interlibrary Loan Services,

Copyright Notice: By accessing this attached article, you are agreeing to abide by the Copyright Laws of the United States
(Title 17, United States Code).

Sincerely,

Sherry Chastain

Sherry Chastain, Outreach-Ill. Dept.
Arkansas State Library
900 W. Capitol, Suite 100
Little Rock, Ar. 72201
(501) 682-1792 / ILL. office
(501) 682-2053/ library
sherry@library.arkansas.gov

NOAA Technical Report ERL 418-AOML 32

The Structure of Typhoon Irma (1974) as Revealed by 700-mb Aircraft Data

David P. Jorgensen

April 1982

U.S. DEPARTMENT OF COMMERCE
National Oceanic and Atmospheric Administration
Environmental Research Laboratories

NOAA Technical Report ERL 418-AOML 32

The Structure of Typhoon Irma (1974) as Revealed by 700-mb Aircraft Data

David P. Jorgensen

Atlantic Oceanographic and Meteorological Laboratories
Miami, Florida

April 1982

U.S. Department of Commerce
Malcolm Baldrige, Secretary

National Oceanic and Atmospheric Administration
John V. Byrne, Administrator

Environmental Research Laboratories
Boulder, Colorado
George H. Ludwig, Director

CONTENTS

The Structure of Typhoon Irma (1974) As Revealed by 700-mb Aircraft Data

David P. Jorgensen

ABSTRACT. Instrumented-aircraft data for five days representing, roughly, the entire life cycle of the typhoon are analyzed. The data analyses are presented as horizontal cross sections and profiles of eight meteorological parameters: relative tangential wind, actual and relative radial wind, adjusted temperature, relative humidity, mixing ratio, adjusted D-value, and adjusted equivalent potential temperature. From computations of the degree of balance between the tangential wind field and the pressure gradient field of the typhoon it is found that on all days, regardless of storm state or motion, the pressure field was almost exactly in gradient balance with the relative tangential wind field in the eyewall region, at 700 mb. The feature of the wind field that primarily distinguished the most intense phase of the storm (November 26) from the other days was the sharp decrease in the windspeed profile with radial distance away from the storm center. The windspeed profile on the other days was very flat, with little dropoff in windspeed with radial distance.

1. INTRODUCTION

The gathering of meteorological data from tropical cyclones by instrumented aircraft has been a regular procedure since the early 1950's. Thorough examination of storms of different character has been conducted, principally by LaSeur and Hawkins (1963), Colon (1964), Hawkins and Rubsam (1968), Hawkins and Imbembo (1976), and Shea and Gray (1973), who composited 13 years of radial profile observations of Atlantic hurricanes. Recently, Willoughby et al. (1981) have noted the occurrence of secondary wind maxima, and their propagation and apparent effect on storm evolution in rather symmetric Atlantic hurricanes. The majority of these analyses, however, were carried out on Atlantic hurricanes. Recent investigations by a U.S. Air Force C-130 aircraft equipped with the new Airborne Weather Recording System (AWRS) in the Western Pacific provided an opportunity to examine the structure of a typhoon. This is the first case of a well-instrumented aircraft gathering data in a Western Pacific typhoon. The goals of this research were (1) to judge the quality of the Western Pacific data in respect to data gathered by research aircraft in Atlantic hurricanes, and (2) to compare structures of a mature Western Pacific typhoon and Atlantic hurricanes.

Typhoon Irma developed in the Western Pacific south of Guam on November 21, 1974, as a depression in the monsoon trough (fig. 1) and was the last typhoon of the 1974 season. The storm drifted northwestward from November 21 to 25; then its track became westerly (Annual Typhoon Report, 1974). The periods of aircraft investigations are indicated in fig. 1. The data gathered

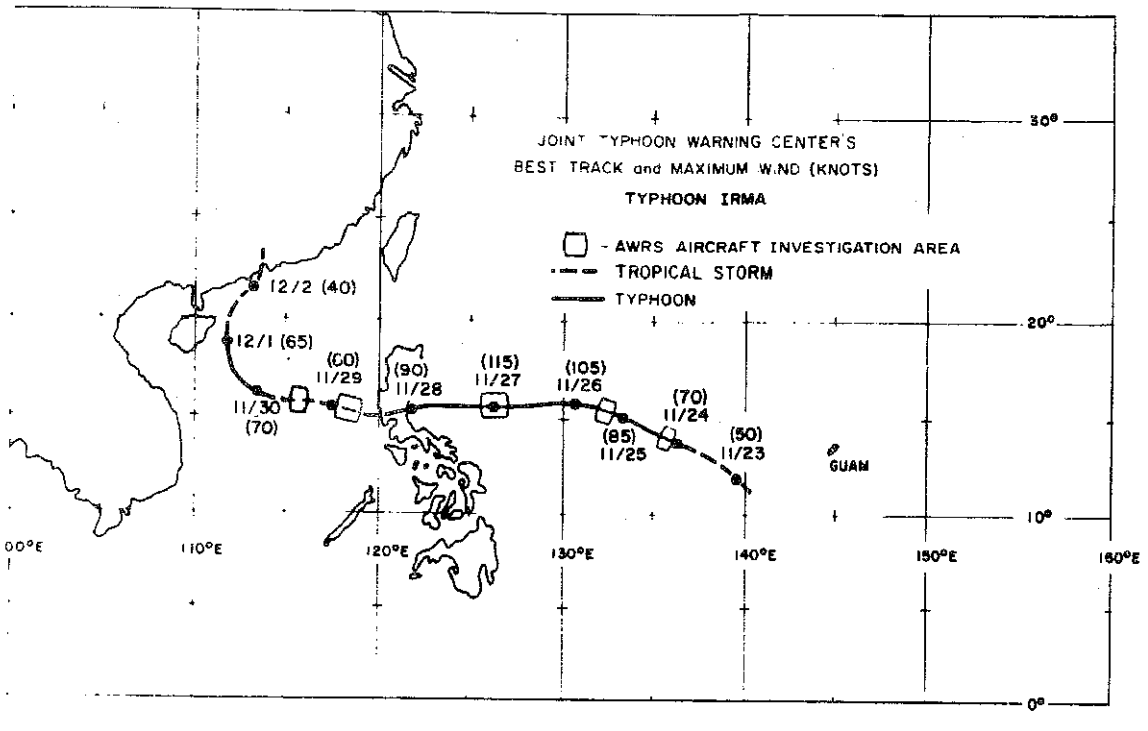

Figure 1.--Joint Typhoon Warning Center's best track of Typhoon Irma (from the Annual Typhoon Report, 1974).

by the aircraft represent several phases of the storm as it underwent development. Starting as a weak-to-moderate typhoon (November 24 and 25, with maximum flight level winds* 38 and 52 m s^{-1}, respectively), Irma developed into a strong, late-season typhoon (November 26, with maximum flight level winds at 72 m s^{-1}) and returned to tropical storm strength after passage over Manila (maximum flight level winds were 26 m s^{-1} on November 28 and 29) before curving northward.

The synoptic conditions on November 24 (not shown) indicate the relative weakness of the 700-mb flow, which was characteristic of the period November 24 through 29, the strong anticyclone south of China, and the weak trough to the north of the storm. Ley and Elsberry (1976) studied the track of this storm and tried to predict it with a nested-grid model, with some success. Although the storm was forecast in real time to recurve to the north because of its interaction with the trough, the building of the ridge to the north and west apparently influenced the storm to take a westward course. The abnormally large size of Irma (as compared with Atlantic hurricanes) is also indicated by the extent of its circulation. Defense Meteorological Satellite Program (DMSP) photographs (fig. 2) for November 25-28 show the cloud cover extending over 10° of longitude and latitude before landfall at Manila.

* The maximum winds tabulated on the track in fig. 1 are from the Annual Typhoon Report (1974) and are not necessarily the same as those recorded by the aircraft. Typhoon forecasters use several data sources, including aircraft, to arrive at best-track and intensity estimates. The track and intensities indicated in fig. 1 represent a compromise (or a smooth) over the many data sources to maintain a consistent picture.

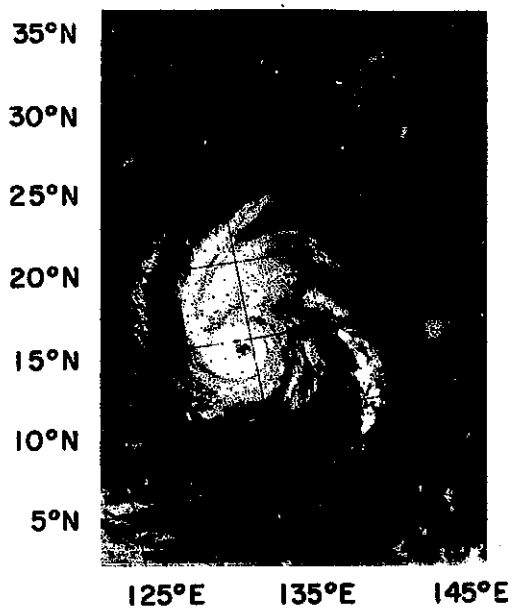

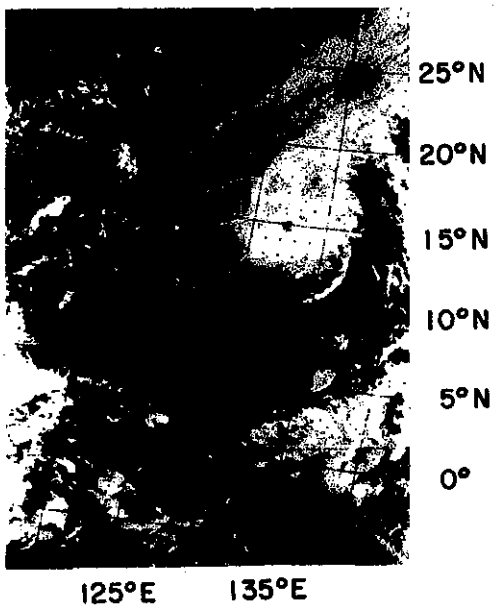

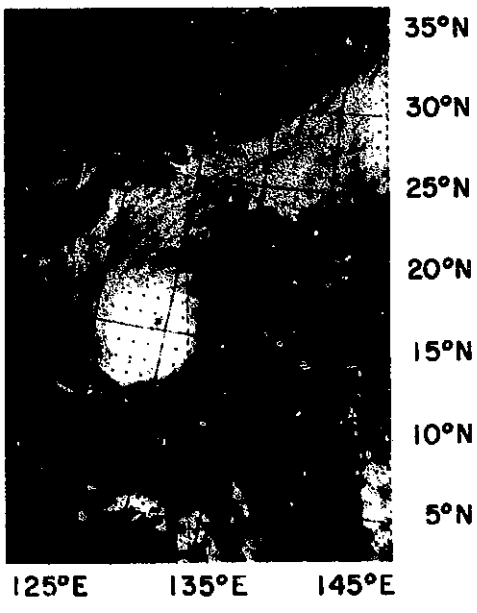

Figure 2.--Series of Defense Meteorological Satellite Program (DMSP) visible photographs of Irma from November 24 through November 28, 1974.

The aircraft were sent out from Anderson Air Force Base, Guam, and Kadena Air Force Base, Okinawa. The AWRS system was undergoing operational testing and evaluation in tropical cyclone reconnaissance. A complete description of the AWRS test and evaluation can be found in Melhart and Fister (1975). The AWRS was so developed that a high degree of confidence can be placed in the inertial navigation system and the determination of flight level winds. The primary parameters measured by the system and recorded on magnetic tape at the rate of one observation per second are radar altitude, pressure altitude, drift angle, magnetic heading, ground speed, true air speed, wind direction, windspeed, latitude, longitude, air temperature, dew point, and static pressure. All other parameters, such as equivalent potential temperature (θ_E), mixing ratio, and D-value (difference between the absolute and pressure altitude), are computed from these basic parameters. No radar data were available from this aircraft. Data were recorded on magnetic tape at the rate of one observation per second. In this study, however, only one observation per 10 seconds is used, primarily to speed the processing. The data were not smoothed or despiked, except when gradient wind was computed.

2. DATA COMPOSITING METHOD

Data gathered from these investigative flights were composited with respect to the storm center. The storm's motion has been removed from the relative wind plots. This method assumes that the storm is in a steady state over the data collection interval and that the storm's motion is accurately known. The usual method is to compute the storm track from radar positions. This was not possible for the Irma data set, since no on-board radar was being photographed. Instead, the storm track was computed by "fixing" the apparent center from the aircraft data (centering D-value profile, looking for wind minima) on each pass through Irma's eye. Only data within the radius of maximum wind were used to define the storm center. A linear storm track was then fitted to these eye observations. There were, in general, two or three eye penetrations, except on November 24 when only one pass was made through the eye. In that case, the Joint Typhoon Warning Center's best track was used in conjunction with the one observation.

The thermodynamic data (temperature and dewpoint) were adjusted to the 700-mb level by the mean tropical lapse rate to compensate for small departures (±10 mb) of the aircraft from this level. This adjustment would result in no more than a few tenths of a degree correction no matter what realistic lapse rates were used (standard atmospheric, mean tropical, or mean hurricane); for simplicity and the maintenance of continuity with other studies, the mean tropical lapse rate was used. The D-value (departure from standard atmosphere) was adjusted with the hypsometric equation (see Appendix).

Temperature data were also corrected for an apparent 1.5°C too-cold bias that was deduced by a hydrostatic consistency check when the aircraft ascended/descended upon takeoff/landing. This bias was also noted by Lewis and Jorgensen (1978) in a study of Atlantic Hurricane Gertrude based upon data from the same aircraft taken on October 1, 1974.

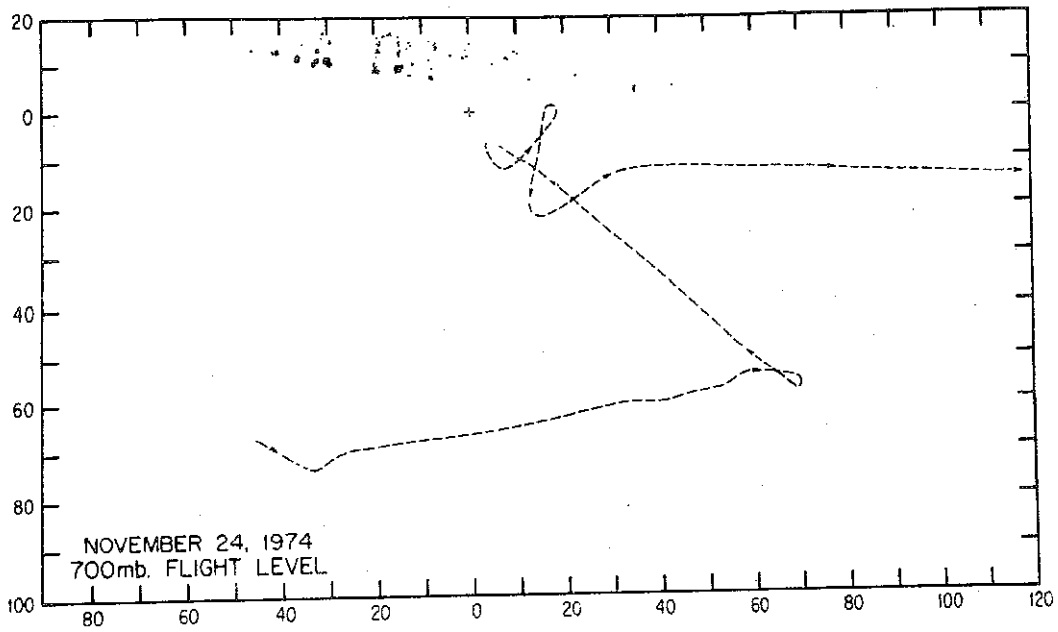

Figure 3.--November 24 flight track.

3. STORM STRUCTURE ON NOVEMBER 24

At 0000Z on November 24, Irma was approximately 100 km due west of Guam, moving west-northwest at about 5 m s^{-1}. The AWRS aircraft flew a 9.7-hour mission from Guam; however, a tape malfunction on board destroyed most of the data gathered. Figure 3 presents the part of the flight track for which data are available.

The profiles for the first penetration are presented in fig. 4. The radius of maximum winds (defined here as the distance from the center of the eye at which the windspeed first stops increasing) was 130 km, and the maximum wind was 39 m s^{-1}. By definition, the eye is considered to be the relatively calm area enclosed by the ring of clouds (eyewall) that mark a transition zone of sharpest inward increase of equivalent potential temperature and cyclonic wind shear. The eyewall boundary customarily is determined visually or by radar. The Shea and Gray composites indicate that the radius of maximum wind is displaced 5-10 km radially outward from the radius of the inner radar eye boundary, with a weak dependence on storm strength; that is, the stronger storms have less displacement. Displacement is also related to eyewall slope, as indicated by Jorgensen (1982). In this study no information is available on the location of the eyewall clouds, and the eye is considered bounded by the maximum wind. The extreme size of Irma's eye is the most unusual aspect of these data compared with other observations of both Atlantic hurricanes and Western Pacific typhoons. The Shea and Gray composites indicate that roughly 3% of the radius of maximum wind observations are >90 km. Bell (1975) has compiled data based on 10 years of airborne reconnaissance observations of reported eye diameter of Western Pacific typhoons (usually visible or radar

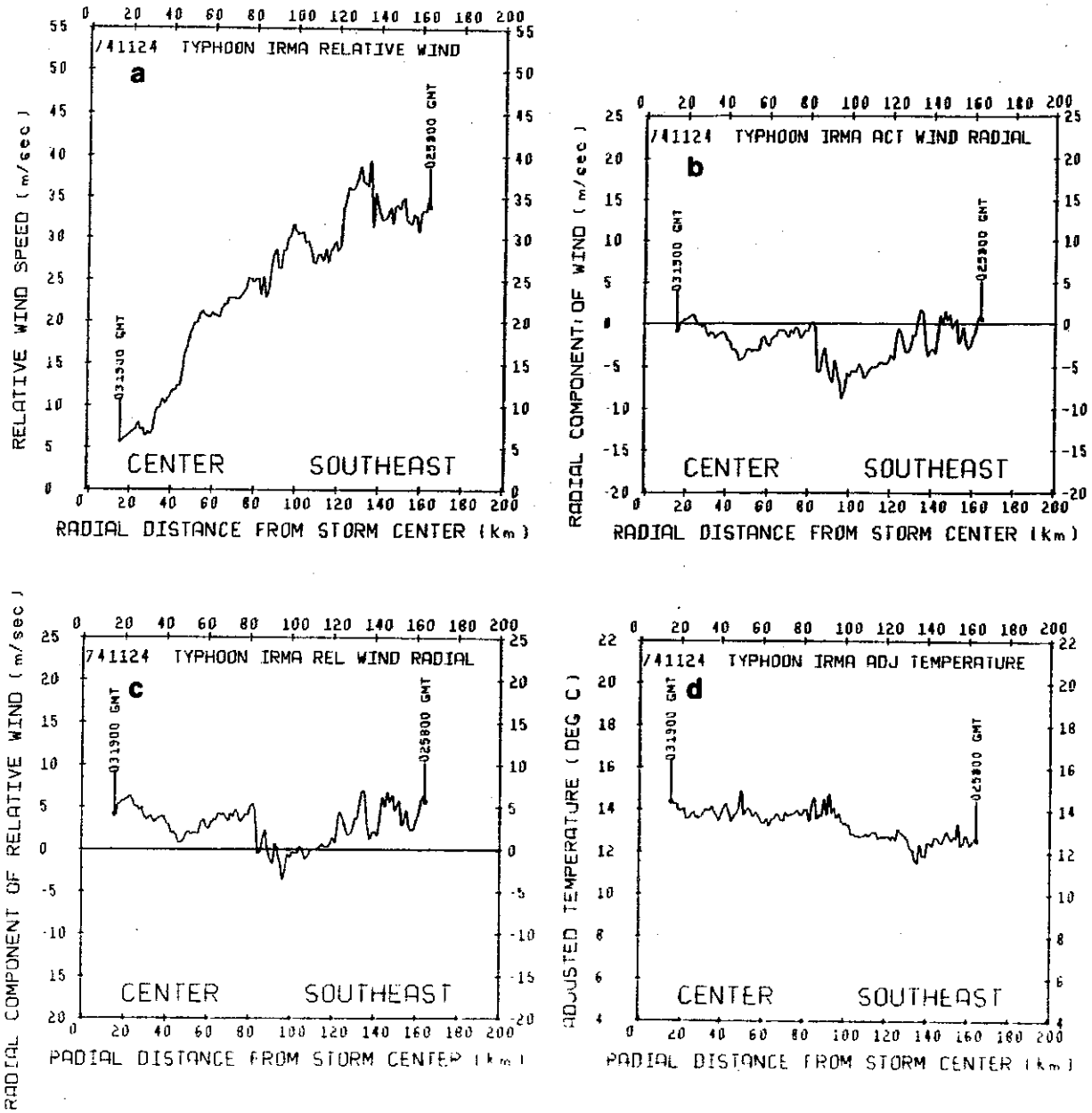

Figure 4.--November 24 southeast-center inbound leg profiles: (a) relative tangential wind; (b) actual radial wind; (c) relative radial wind; (d) adjusted temperature.

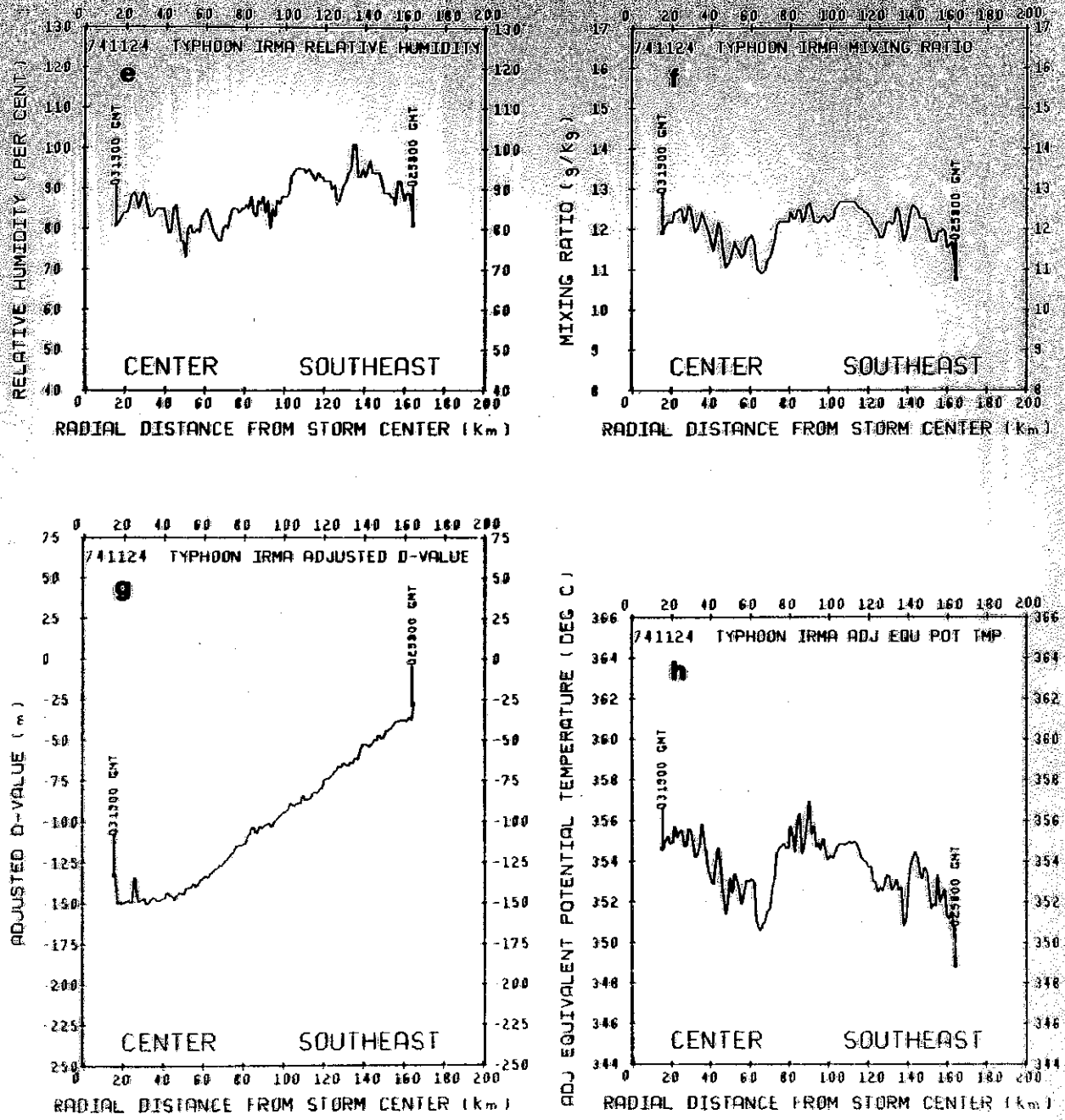

Figure 4.--Continued: (e) relative humidity; (f) mixing ratio; (g) adjusted D-value; (h) adjusted equivalent potential temperature.

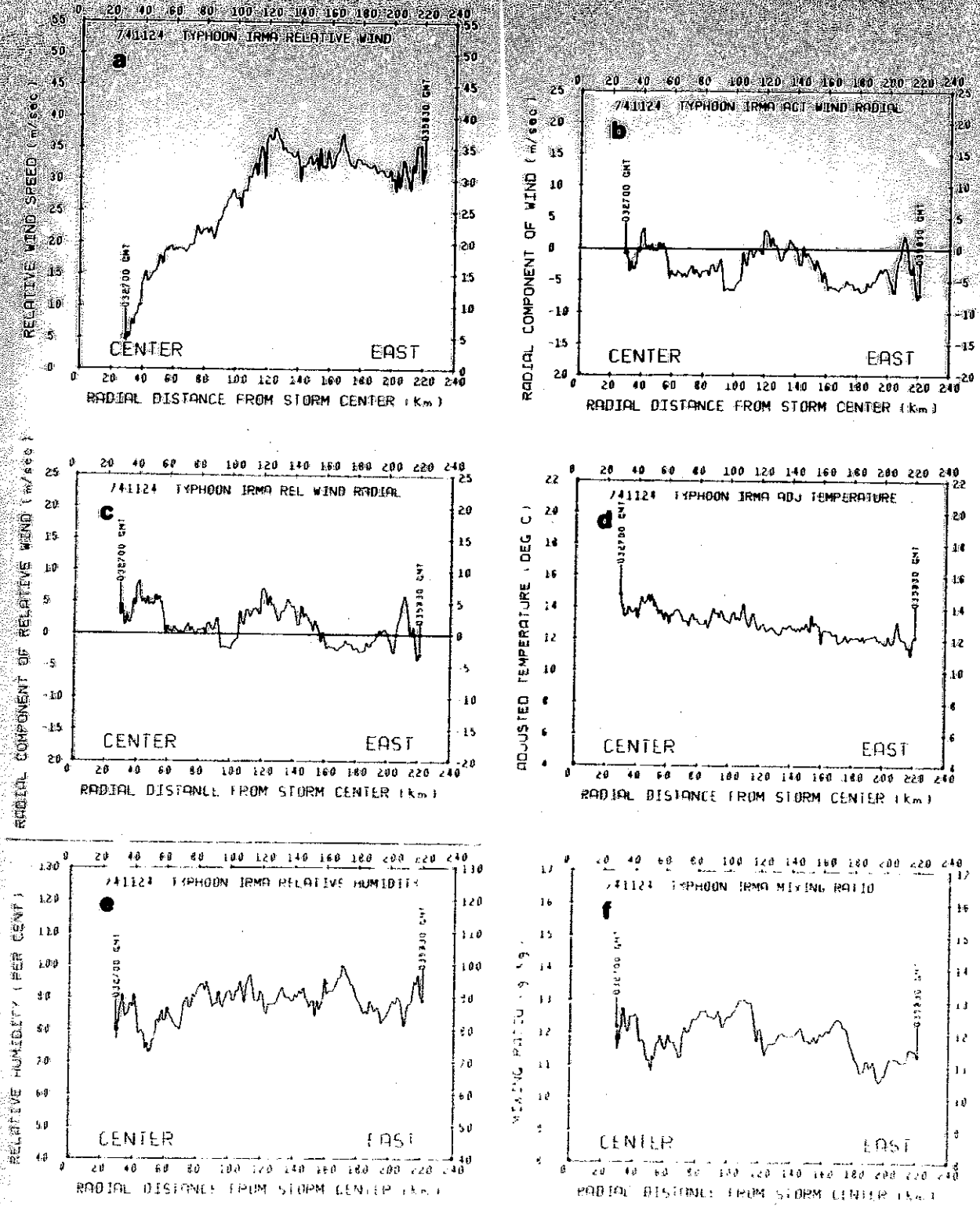

Figure 5.--November 24 east-center outbound leg profiles: (a) relative tangential wind; (b) actual radial wind; (c) relative radial wind; (d) adjusted temperature; (e) relative humidity; (f) mixing ratio.

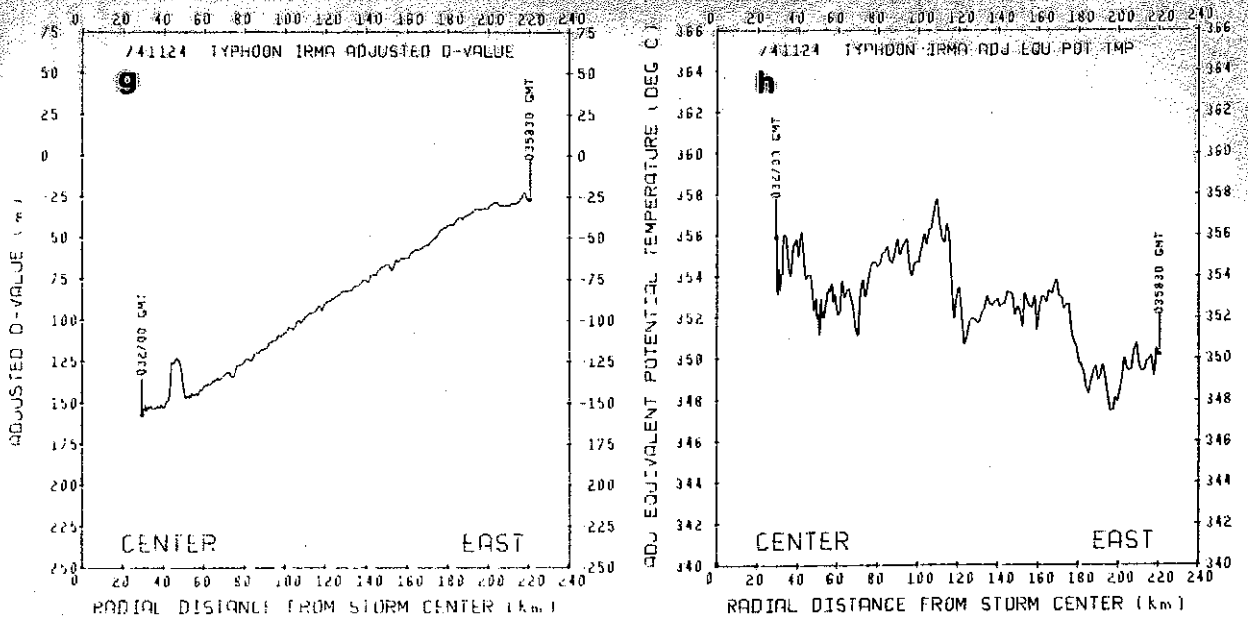

Figure 5.--Continued: (g) adjusted D-value; (h) adjusted equivalent potential temperature.

reports of eye size) and found that only 2% have eye radii >80 km. As will be seen, the large eye size was a characteristic of Irma, in spite of substantial changes in the maximum wind speed.

Most of the flight leg on November 24 was within the broad eye. The relative radial component of the wind shows a small outflow component (positive) over most of the flight leg, except for a narrow region near the radius of maximum winds. Comparison of the actual radial profile with the relative radial component profile illustrates the effect of removing the storm motion from the data. Even though the actual and relative wind profiles were nearly the same, the effect of removal of storm motion is to change the sign of the radial components, since the storm motion is along the direction of the flight leg presented in fig. 5. Outflow from the eye into the eyewall clouds, even at 700 mb, is a common occurrence, as Jorgensen (1982) points out for Atlantic hurricanes.

The relative humidity profile reveals the generally subsaturated conditions within the broad eye. The eye temperatures were approximately 1° to 2° warmer in the eye center than near the eyewall, and the moisture content, mixing ratio, and absolute humidity profiles were relatively constant through the eye except for a decrease between 40 and 70 km radial distance. The adjusted equivalent potential temperature profile showed an increase of Θ_E in the presumed eyewall region between about 120 and 140 km radial distance. The relative Θ_E minimum at 60 km radial distance was in response to the moisture minimum.

Figure 5 shows the profiles for the outbound leg from the center to the east. Again, the relative wind profile shows no clearly defined radius of maximum wind, but a rather broad zone from about 120 km outward that approaches 40 m s^{-1}. The eye size is not readily apparent, but can be

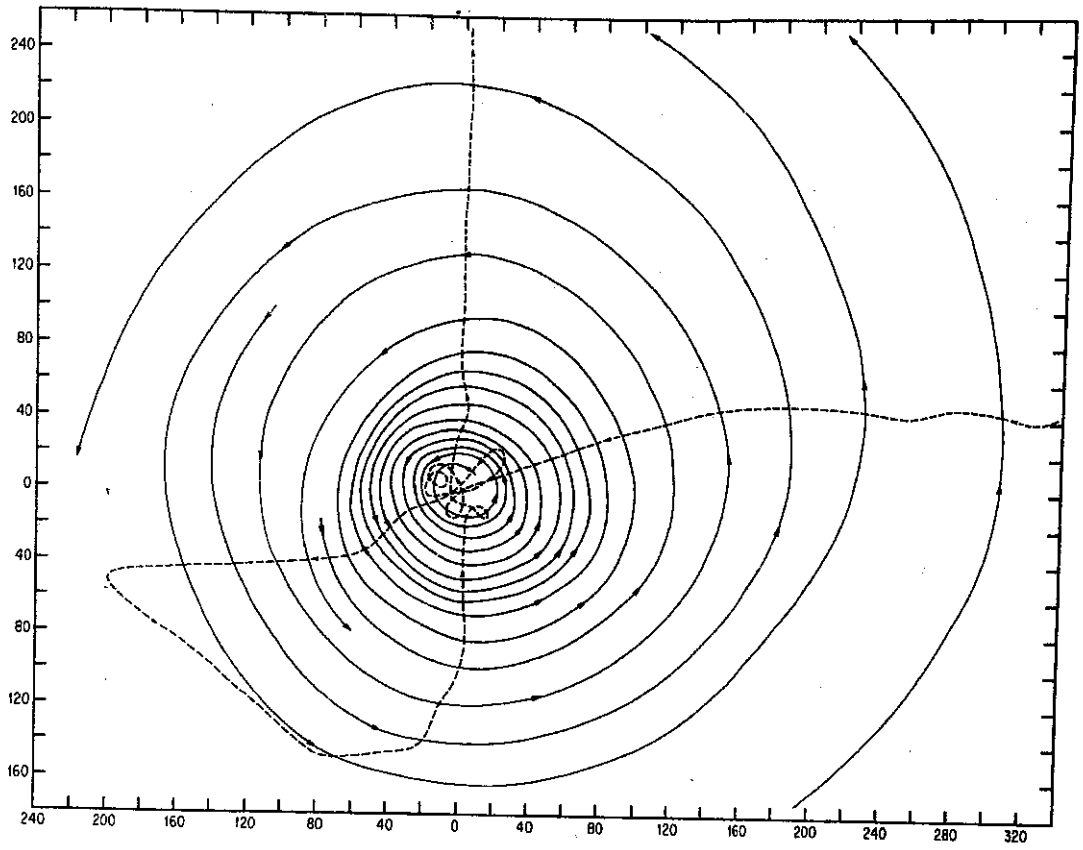

Figure 6.--The 700-mb relative wind streamlines on November 25 in storm-relative coordinates. Aircraft's flight track is indicated by dashed line.

inferred to be about 240 km in diameter. Small (<8 m s^{-1}) relative outflow occurred out to about 160 km. The thermodynamic quantities were similar to the first leg. As before, the highest temperatures were about 2°C, in the eye center with the moisture profiles showing relative minimums in central region (inward from 120 km radial distance). The location of the eyewall region can be inferred from the Θ_E profile, since the eye boundary of the storm would be expected to have a relative maximum of Θ_E and the most rapid increase of Θ_E would be presumed to have occurred in the convectively active regions surrounding the eye (Hawkins and Imbembo, 1976). The Θ_E profile reveals such an increase at radial distances from 110 to 120 km.

4. STORM STRUCTURE ON NOVEMBER 25

Irma's structure on November 25 is revealed by the horizontal analyses of streamlines, isotachs, and isotherms, as well as by the profiles for the two traverses of the eye. The storm was more intense on this day than the day before, and the aircraft's flight pattern consisted of much longer radial legs.

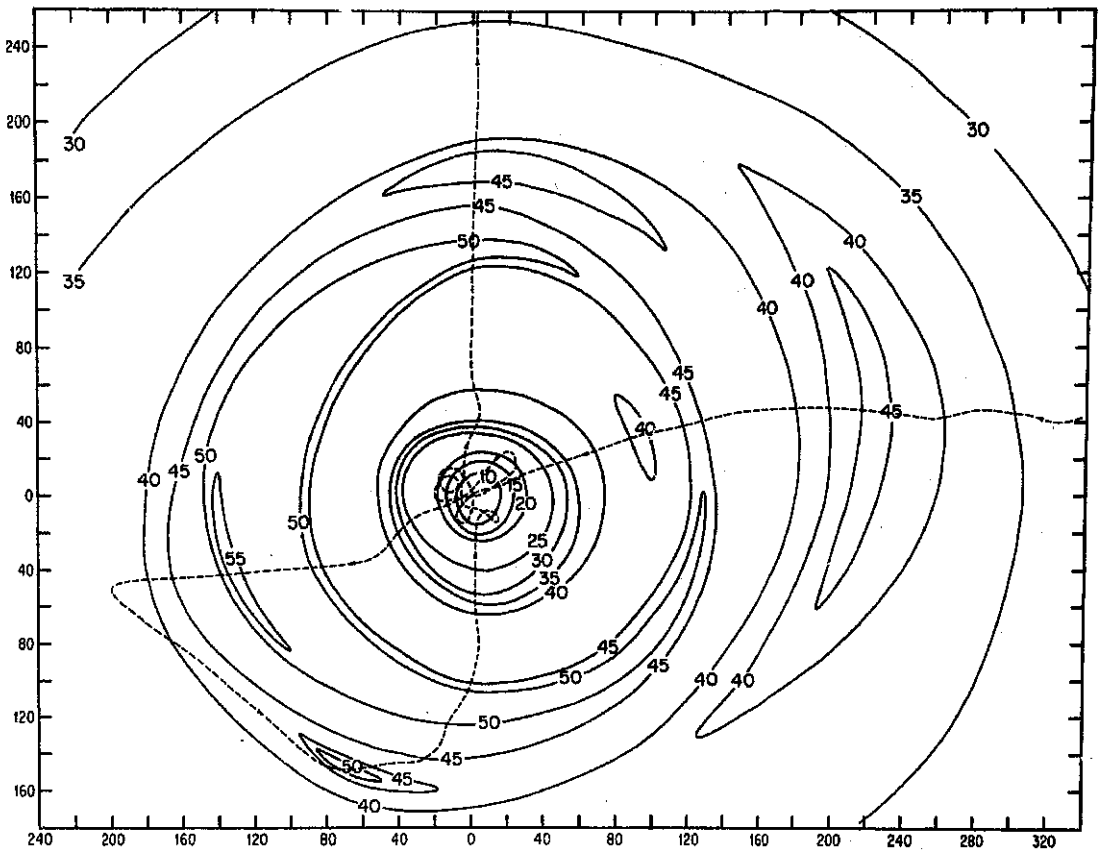

Figure 7.--Horizontal isotach analysis at 700 mb on November 25, in storm-relative coordinates.

4.1 Horizontal Analysis

The streamline analysis of November 25 (fig. 6) reveals a nearly symmetric flow pattern with only a hint of cyclonic outflow, which is revealed more clearly in the profiles. This would seem to indicate that the inflow layer was confined to levels below 700 mb. The Shea and Gray composites show that the inflow layer was primarily constrained to levels below 900 mb, or just within the surface frictional boundary layer. Hawkins and Imbembo (1976) also show this result for the small, intense Hurricane Inez (1966).

The isotach analysis (fig. 7) illustrates the absence of any well-defined radius of maximum wind. Rather, there was a broad zone of nearly symmetric 40- to 50-m-s^{-1} wind. The highest wind speeds were in an area slightly left of the moving storm front (storm motion on this day was 2.2 m s^{-1} toward 301°). The location of any asymmetric wind maximum in Atlantic hurricanes is generally the right front quadrant (Shea and Gray, 1973).

Analysis of the adjusted temperature field is presented in fig. 8. Here, the area of highest temperatures is of particular interest. The most anomalously warm areas were not in the center of the eye (nor distributed evenly across it), but in a ring 5 to 10 km wide, just inside the radius of

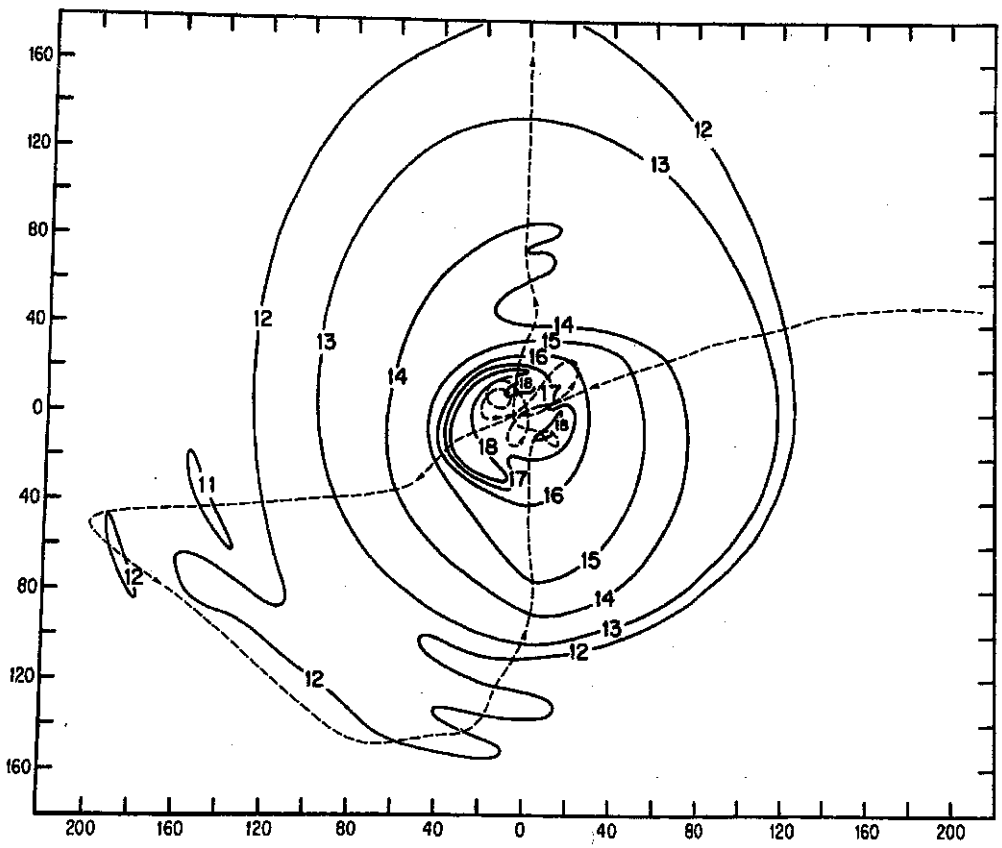

Figure 8.--Horizontal analysis of adjusted isotherms at 700 mb on November 25, in storm-relative coordinates.

maximum wind. Slight temperature decreases of 0.5° to 1.0°C were evident in the eye center. This lowering of temperature is an indication that subsidence at this level was most intense just inside the eyewall, a characteristic found in other Atlantic storms. For example, Shea and Gray (1973) also show that, on the average, in 21 hurricanes the highest adjusted temperatures were a few kilometers inside the radius of maximum wind. Temperature anomalies (deviations from the apparent near-environmental temperature of 12°C) inside the eye were about 6°C. Beyond a radius of 100 km, temperature gradients were weak and small-scale fluctuations were caused, primarily, by the presence of convection or rain, or both. The response of the temperature probe when in cloud or rain is not known precisely. If the instrument were wetted upon penetration of cloud or rain, cooling would result, since the device would act as a wet bulb. (Shown in figure 9d, at 50 km west of the center, is a somewhat characteristic dip in the temperature trace that has also been seen in Atlantic hurricane flight data. Without cloud water measurements it is difficult to evaluate this cooling effect. A reasonable estimate of up to 1° cooling caused by liquid water is indicated from experience with Atlantic flight data.)

4.2 Profiles

The profiles for the east-west leg are presented in fig. 9. The storm was moving slowly on this day (301° at 2.2 m s^{-1}), and, therefore, the relative winds (fig. 9c) would differ little from the actual winds (not shown). This slowness is reflected in the nearly identical profiles of actual and relative wind. The tangential wind profiles indicate a flat wind profile outside the eye region, with the eye having a diameter of approximately 100 km. The wind profiles also show a region of maximum wind between 90 and 140 km to the north of the storm center, which is the location of the relative outflow maximum. The relative radial component also indicates that the eye region was generally an area of slight inflow or pure tangential wind, while outside the eye region a small component of outflow existed. As on the previous day, the east-to-west profiles of tangential and radial wind show that little influence was exerted by the storm motion, which was very slowly westward. The eye radius had decreased from the 130 km of the previous day to 50 km on this day, to 50 km about 31 hours later.

The thermodynamic profiles show that the place of maximum temperature, minimum relative humidity, and relative maximum of adjusted Θ_E was just inside the radius of maximum winds. The relative dryness of this area within central parts of the eye region is illustrated by a minimum of mixing ratio and relative humidity. In contrast, in Hurricane Inez, Hawkins and Imbembo (1976), noted the maximum of mixing ratio to be in the central part of the eye. The difference can be explained by the sizes of the respective eyes. Inez was a small, intense storm (eye diameter <40 km), whereas Typhoon Irma was much larger (eye diameter about ~100 km). Turbulent mixing and detrainment of moist air near the eyewall clouds in Hurricane Inez could have moistened the eye region, whereas in Irma the inner eye was too remote to feel the effects of lateral mixing. This interpretation is supported by the observed maximum of moisture that was at and just inside Irma's maximum wind. The relative humidity was close to 100% outside the eye, and there was indication that the 700-mb air was drying with radial distance, as the mixing ratio profile illustrates.

The south-north leg (fig. 10) exhibited many of the same features as the east-west leg. The short, straight line segments apparent on these profile plots, and others to follow, are a manifestation of the compositing technique. They indicate that the aircraft did not go through the storm center (calm wind). A secondary maximum of wind occurred between 140 and 200 km radial distance to the north and radially outward from 100 km to the south. A plateau of 40-m-s^{-1} wind existed from the edge of the eye to about 100 km on both sides of the center. Here we choose the radius of maximum wind to be the point on the profile where the wind first stopped increasing with radial distance. The reason for calling this point the radius of maximum wind is not readily apparent, but Willoughby et al. (1981) have noted a similar wind structure with storms that have double concentric radar eye configurations; that is, the inner eye has a flat tangential wind character. The temperature and moisture profiles also indicate that there were sharp gradients (at least on the north side) within the presumed 40-km radius eyewall.

A maximum of relative radial outflow occurred coincident with the secondary tangential wind maxima. Temperature and moisture minima can be noted within the central portion of the eye. Relative humidity in the central portion of the eye region dipped to 60%, because of the temperature increase and moisture decrease. As other studies have indicated, the highest radial gradients of D-value and Θ_E were in the regions of maximum wind, which indicated the locations of the eyewalls.

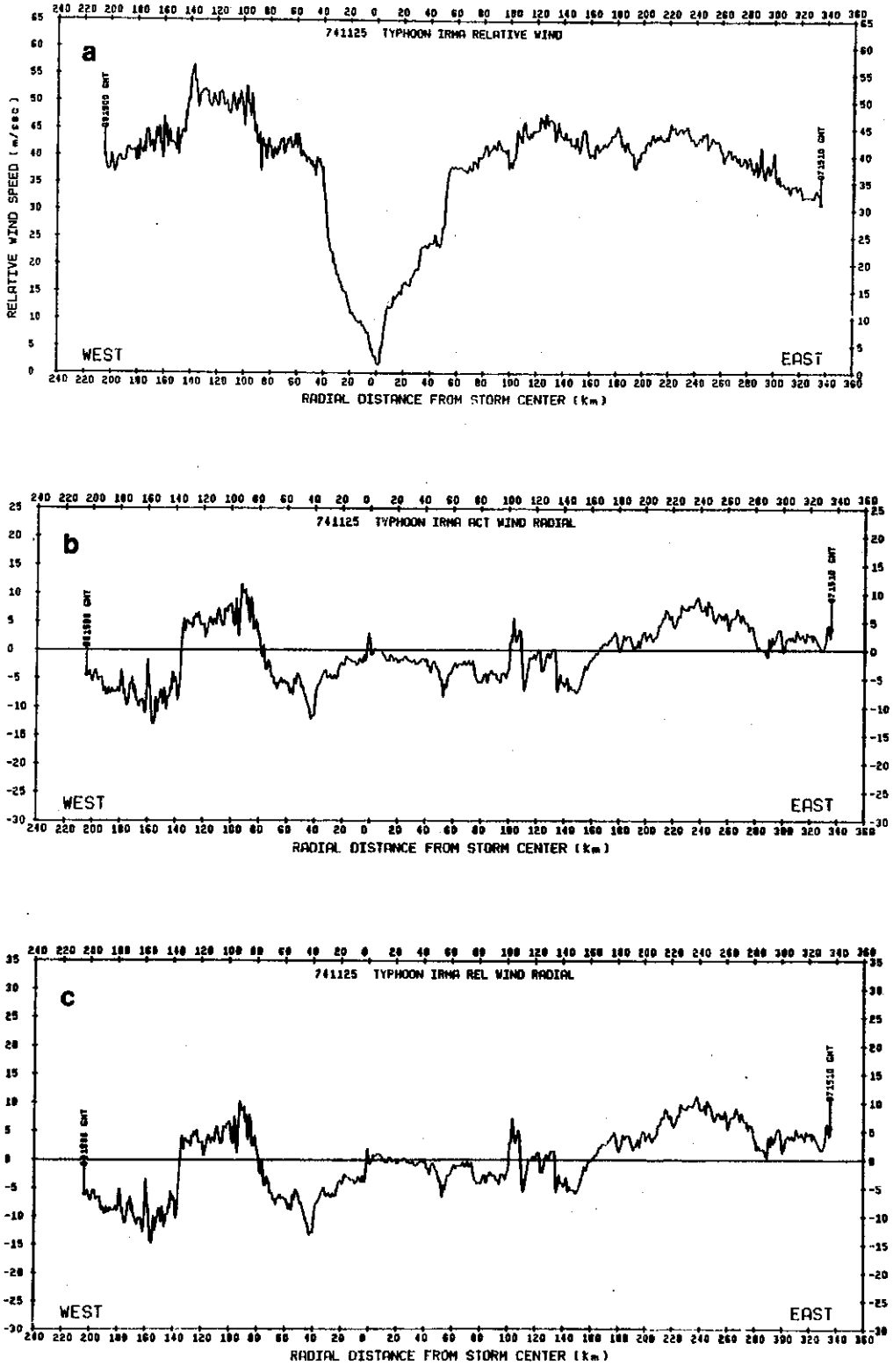

Figure 9.--November 25 east-west profiles: (a) relative tangential wind; (b) actual radial wind; (c) relative radial wind.

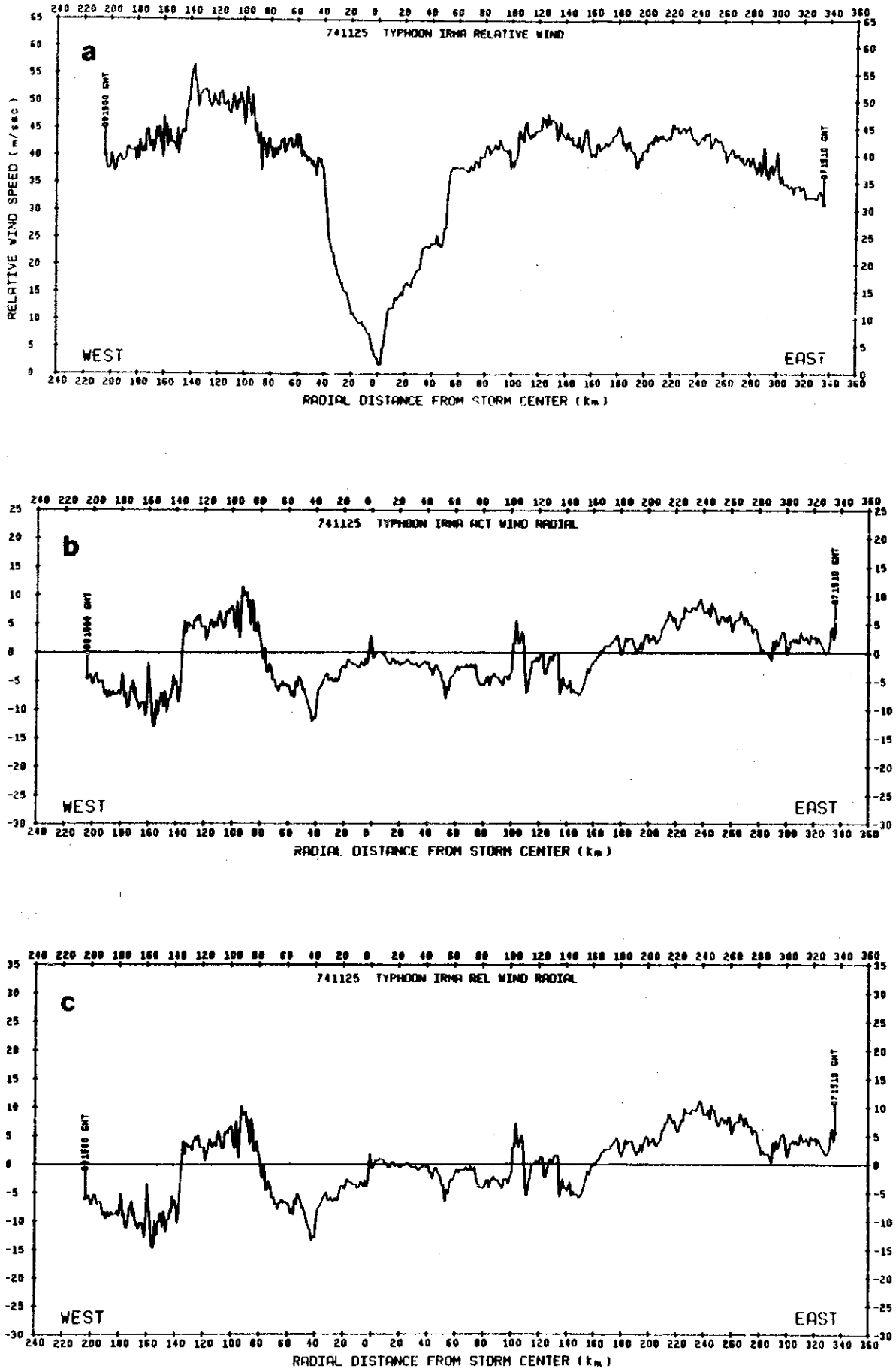

Figure 9.--November 25 east-west profiles: (a) relative tangential wind; (b) actual radial wind; (c) relative radial wind.

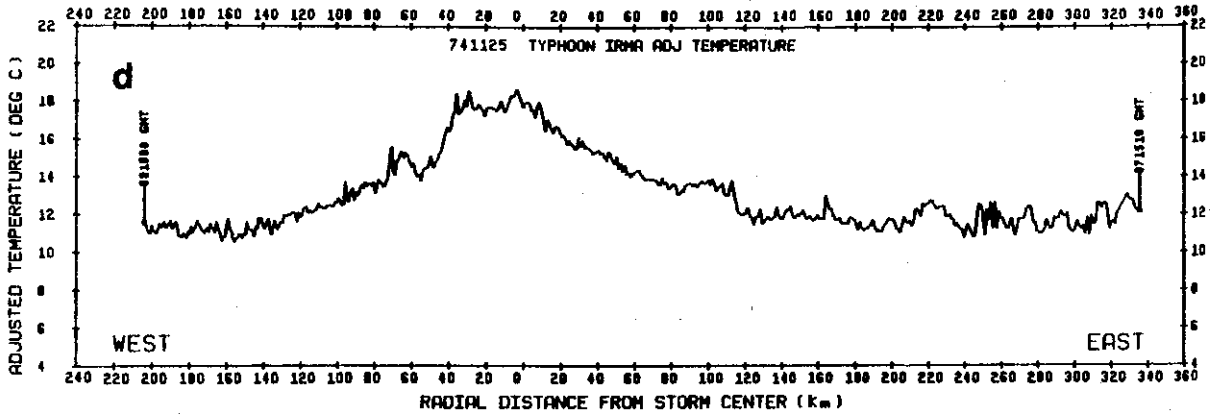

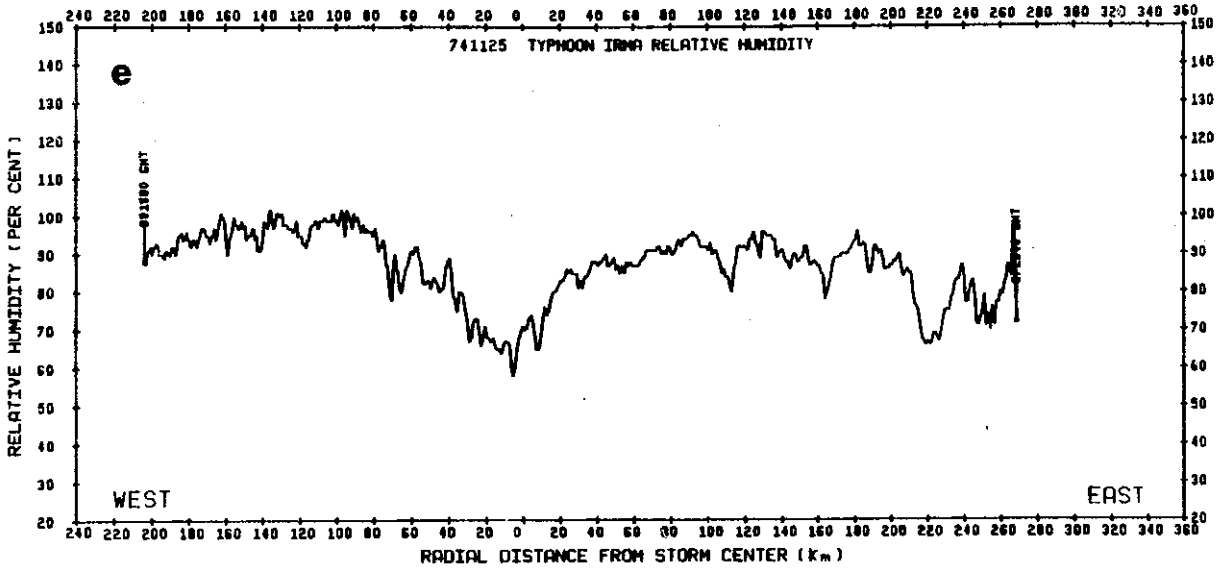

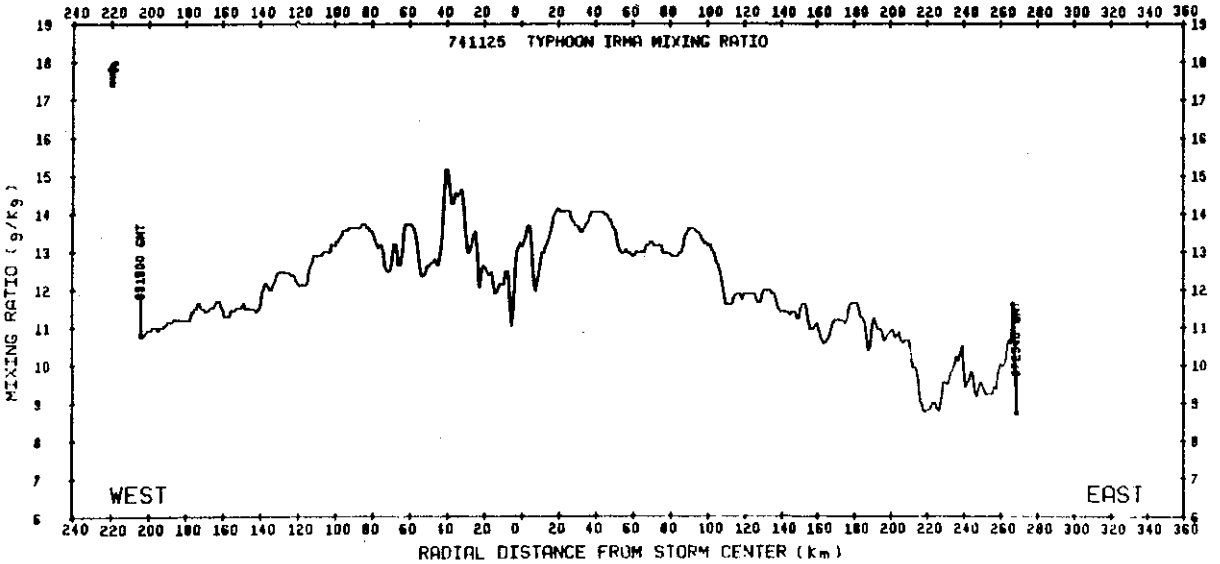

Figure 9.--Continued: (d) adjusted temperature; (e) relative humidity; (f) mixing ratio.

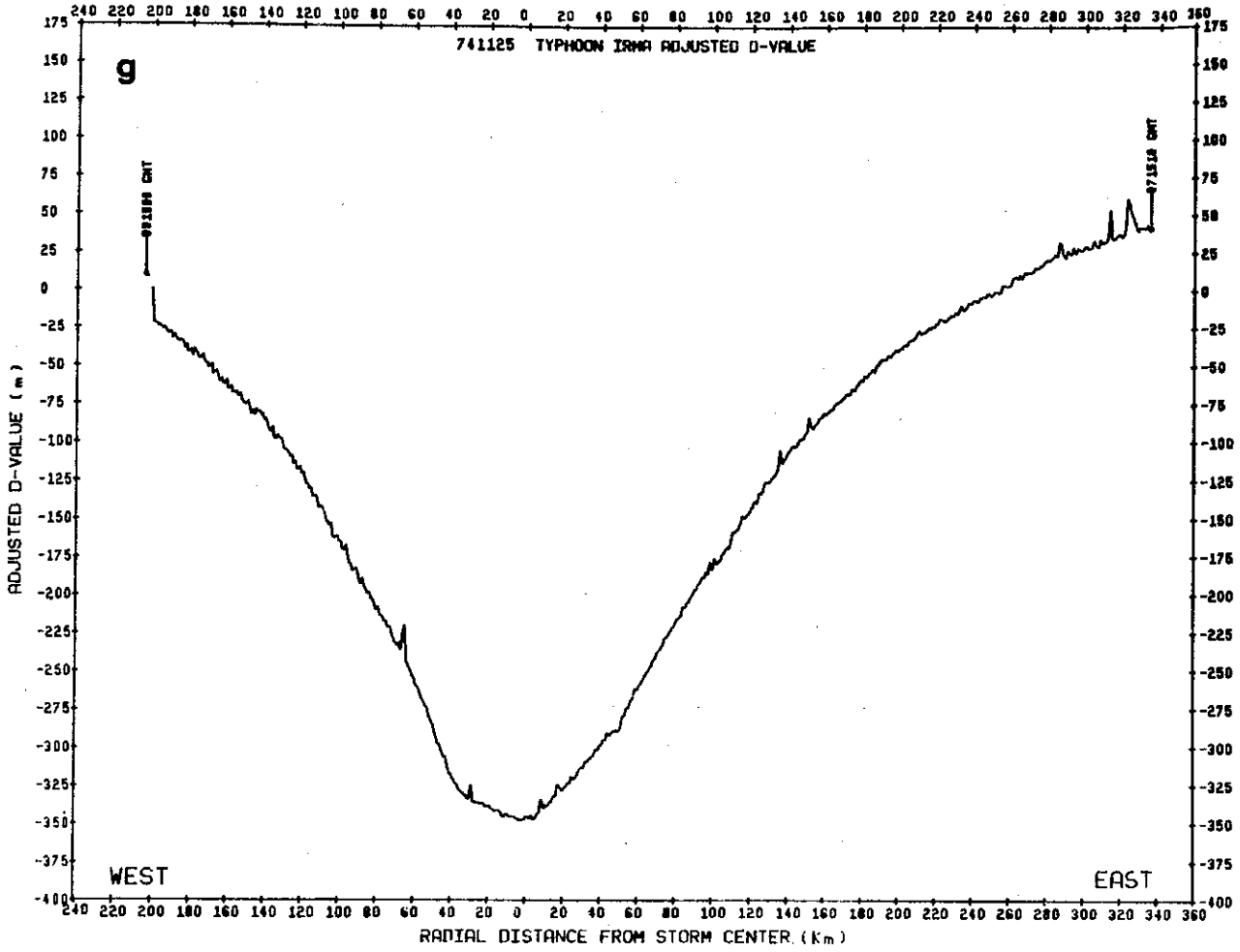

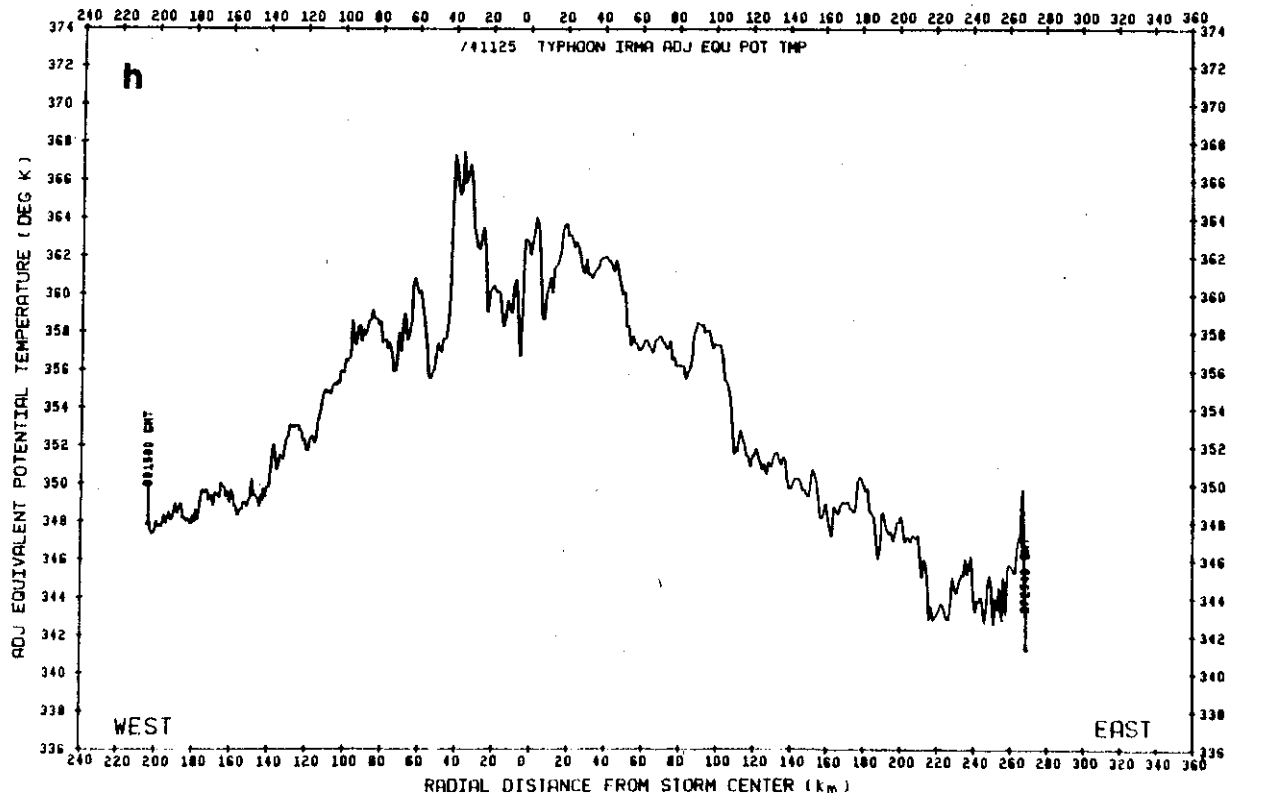

Figure 9.--Continued: (g) adjusted D-value; (h) adjusted equivalent potential temperature.

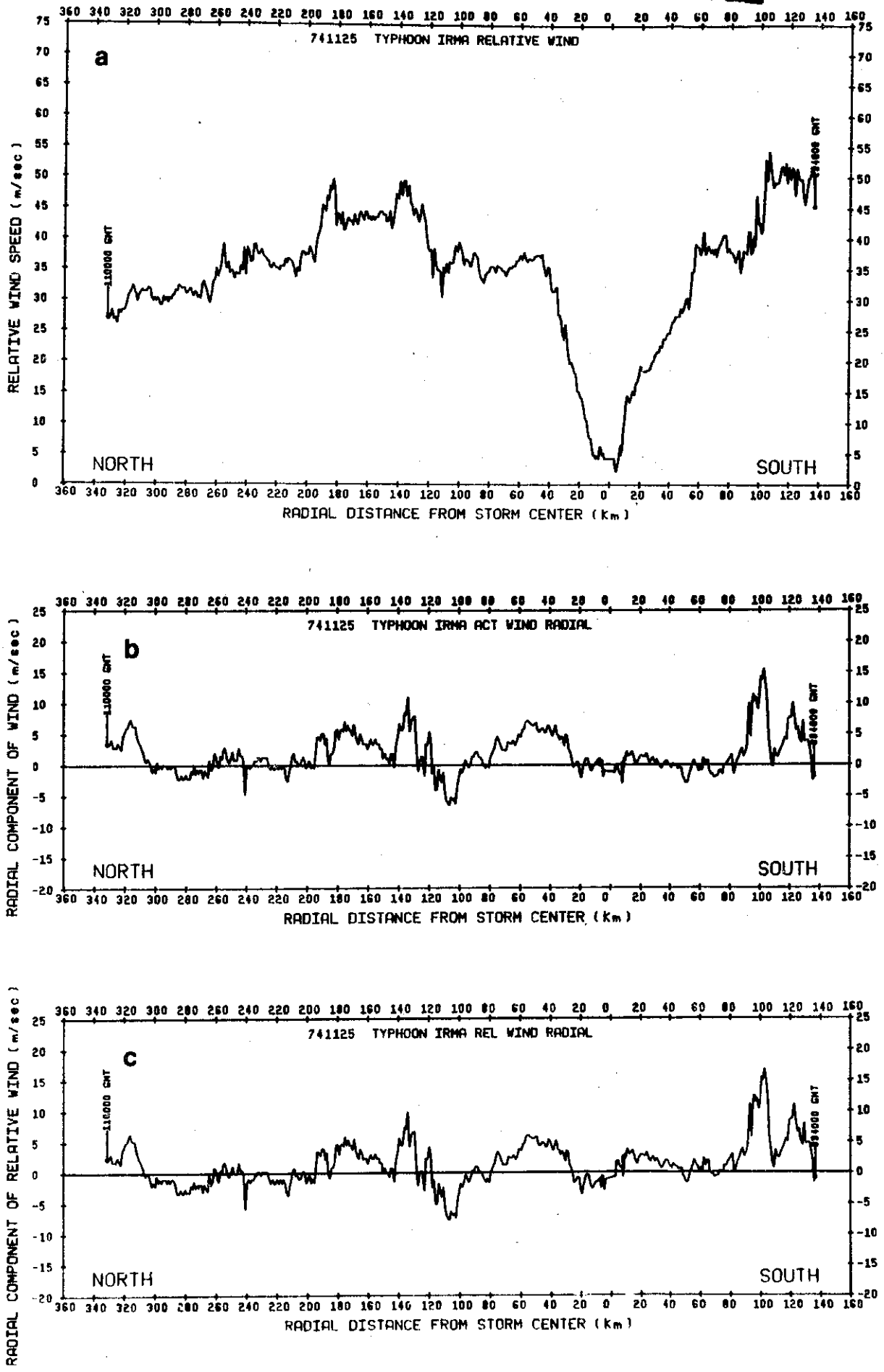

Figure 10.--November 25 south-north profiles: (a) relative tangential wind; (b) actual radial wind; (c) relative radial wind.

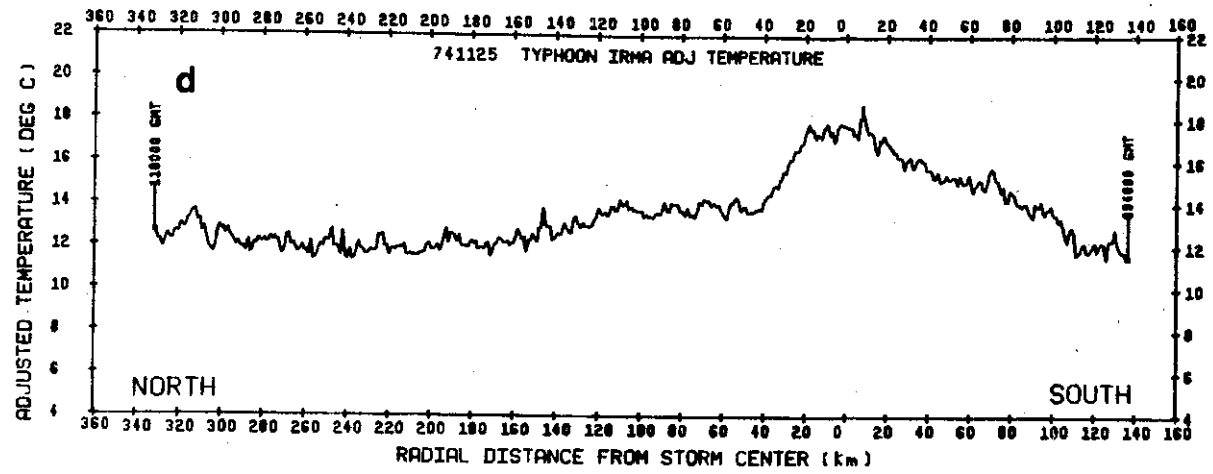

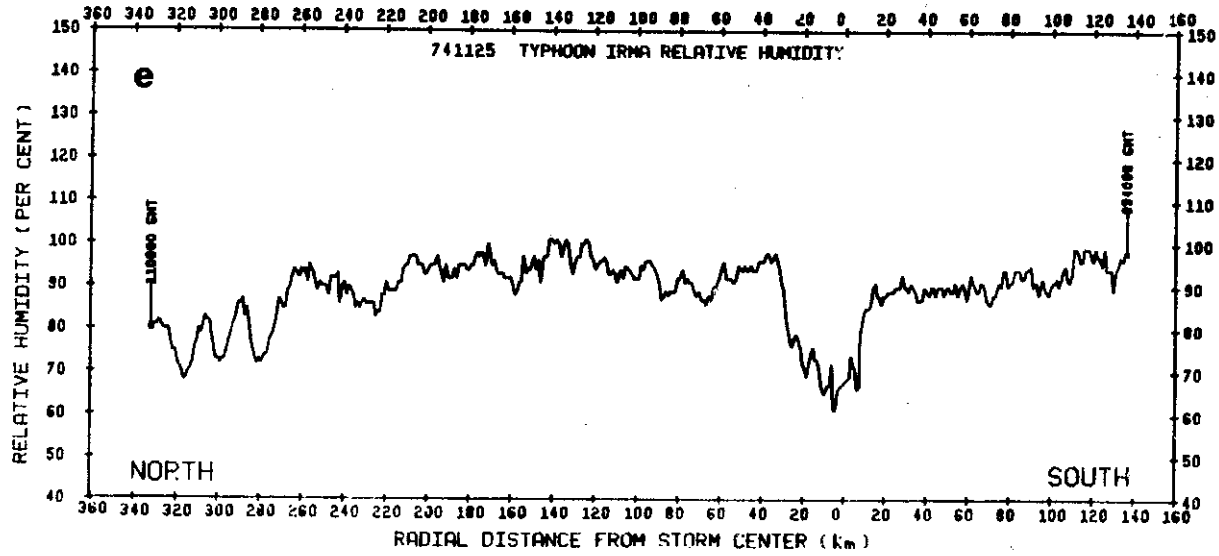

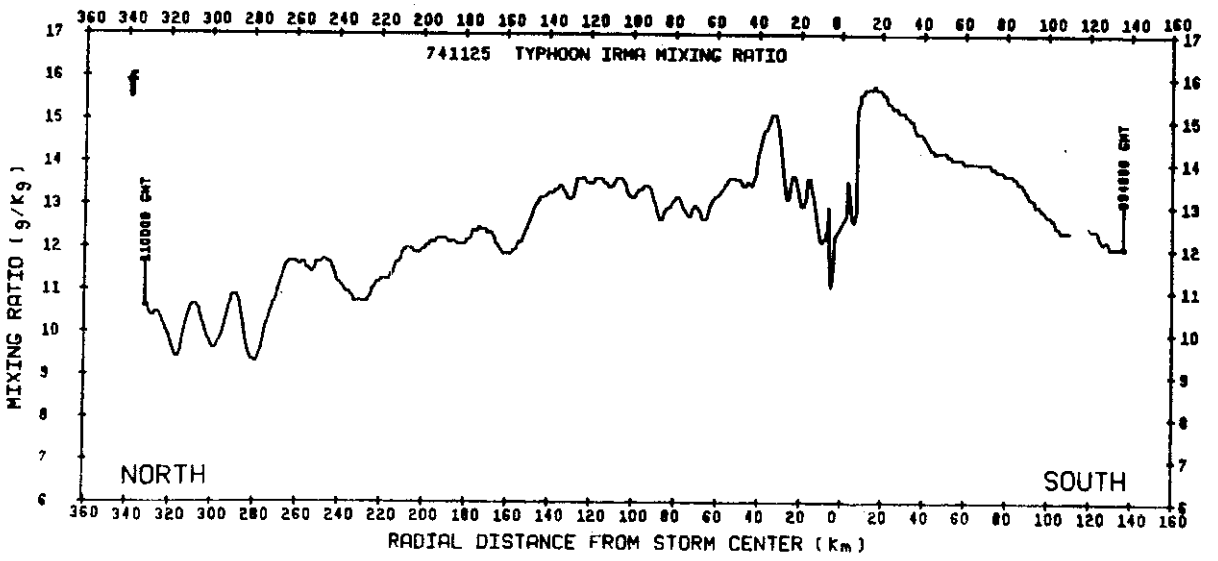

Figure 10.--Continued: (d) adjusted temperature; (e) relative humidity; (f) mixing ratio.

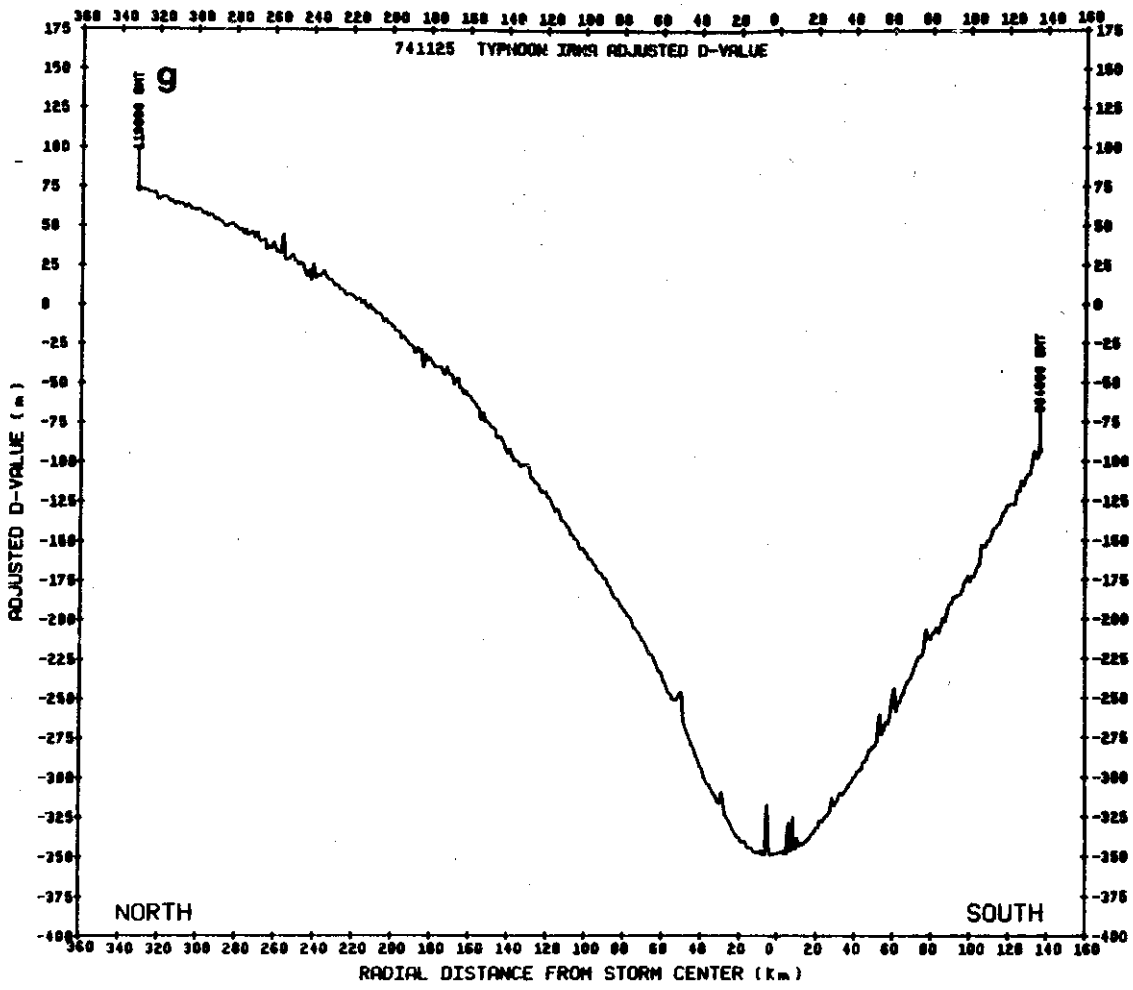

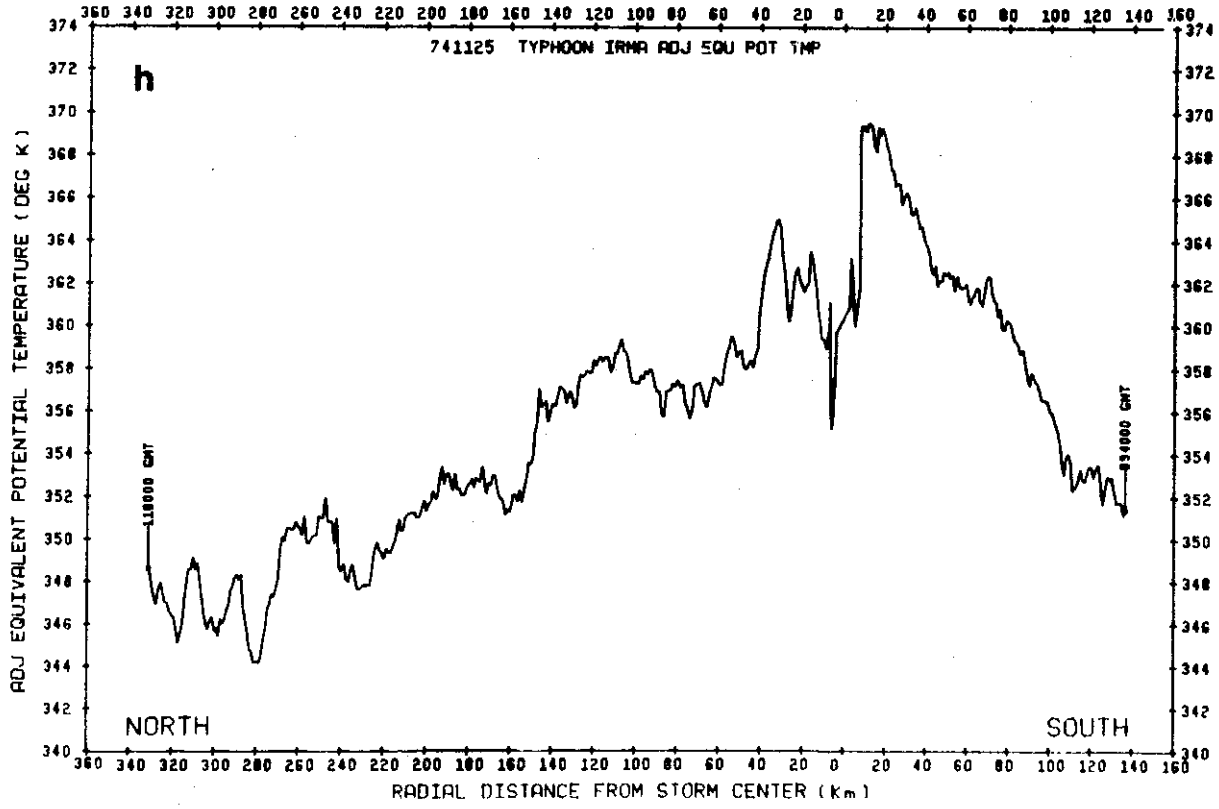

Figure 10.--Continued: (g) adjusted D-value; (h) adjusted equivalent potential temperature.

In summary, on this day Irma was very large, with two distinct wind maxima--one at the eye boundary (about 40 to 60 km radius) and one at a radial distance >100 km. The DMSP photographs (fig. 2) show that Irma had a cloud mass associated with the circulation extending as much as 250 km radial distance from the storm center. Maximum winds noted were nearly 55 m s^{-1} with temperature anomalies of 6°C inside the eye. Moisture values (mixing ratio) exceeded 15 g kg^{-1} in the eyewall region and just inside the eye. There was a somewhat unexpected dip in the moisture values at near eye center, which might be attributed to the large eye diameter.

These observations agree with the newer NOAA WP-3 aircraft data from mature storms as noted by Jorgensen (1982). In this context, the region of eyewall maximum wind was in the zone of maximum radar reflectivity, but the boundary of the radar echo and the clear eye was 3-5 km displaced inward. The maximum vertical velocity and gradients of Θ_E and D-value occurred at this boundary.

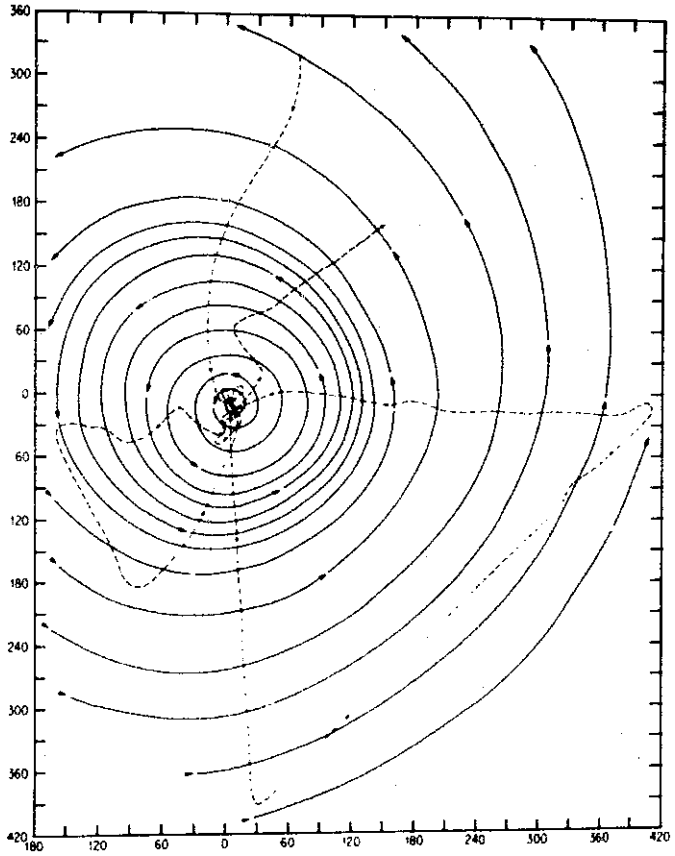

Figure 11.--Relative wind streamlines at 700 mb on November 26, in storm-relative coordinates.

5. STORM STRUCTURE ON NOVEMBER 26

5.1 Horizontal Analysis

The horizontal analysis of the relative wind streamlines is depicted in fig. 11. This analysis indicates a symmetric vortex with a very slight hint of outdraft. The isotach analysis (fig. 12) reveals that the maximum winds had increased 10-15 m s^{-1} in the previous 36 hours to 70-80 m s^{-1}. The

distance from the storm center. Maximum winds noted were nearly 55 m s^{-1} with temperature anomalies of 6°C inside the eye. Moisture values (mixing ratio) exceeded 15 g kg^{-1} in the eyewall region and just inside the eye. There was a somewhat unexpected dip in the moisture values at near eye center, which might be attributed to the large eye diameter.

These observations agree with the newer NOAA WP-3 aircraft data from mature storms as noted by Jorgensen (1982). In this context, the region of eyewall maximum wind was in the zone of maximum radar reflectivity, but the boundary of the radar echo and the clear eye was 3-5 km displaced inward. The maximum vertical velocity and gradients of θ_E and D-value occurred at this boundary.

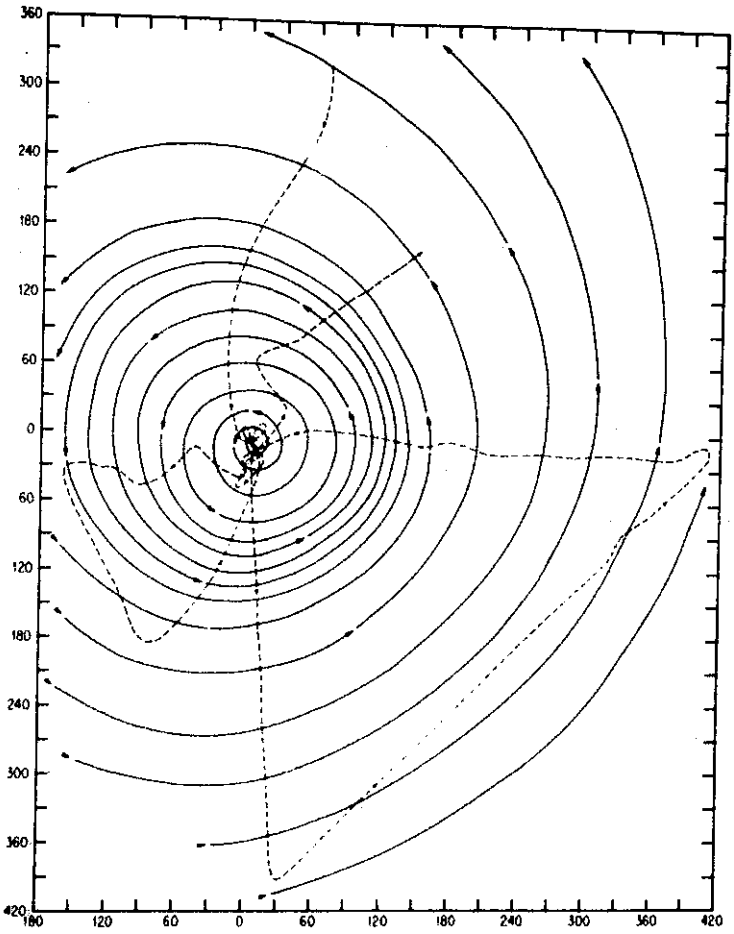

Figure 11.--Relative wind streamlines at 700 mb on November 26, in storm-relative coordinates.

5. STORM STRUCTURE ON NOVEMBER 26

5.1 Horizontal Analysis

The horizontal analysis of the relative wind streamlines is depicted in fig. 11. This analysis indicates a symmetric vortex with a very slight hint of outdraft. The isotach analysis (fig. 12) reveals that the maximum winds had increased 10-15 m s^{-1} in the previous 36 hours to 70-80 m s^{-1}. The

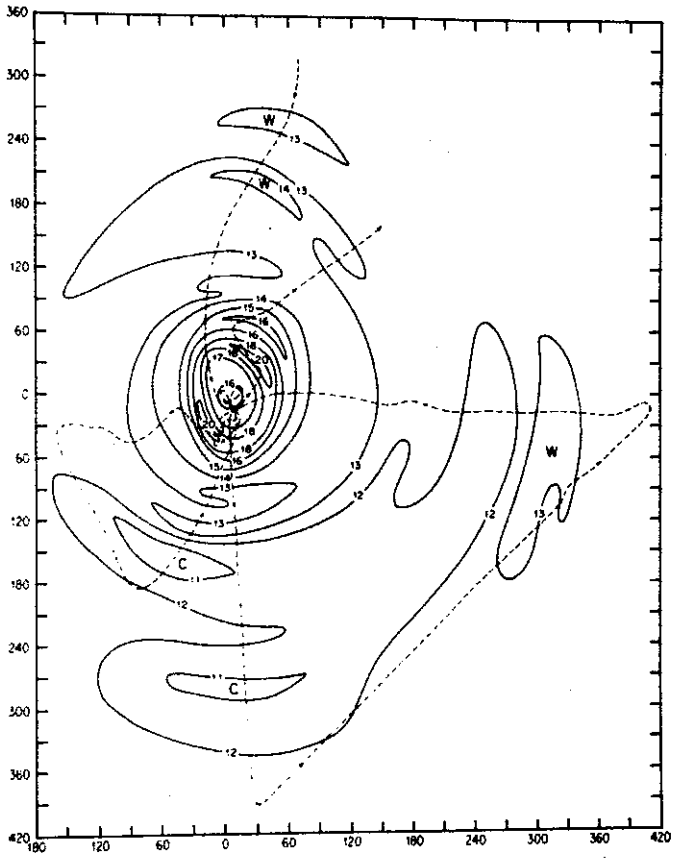

Figure 12.--Horizontal isotach analysis at 700 mb on November 26, in storm-relative coordinates.

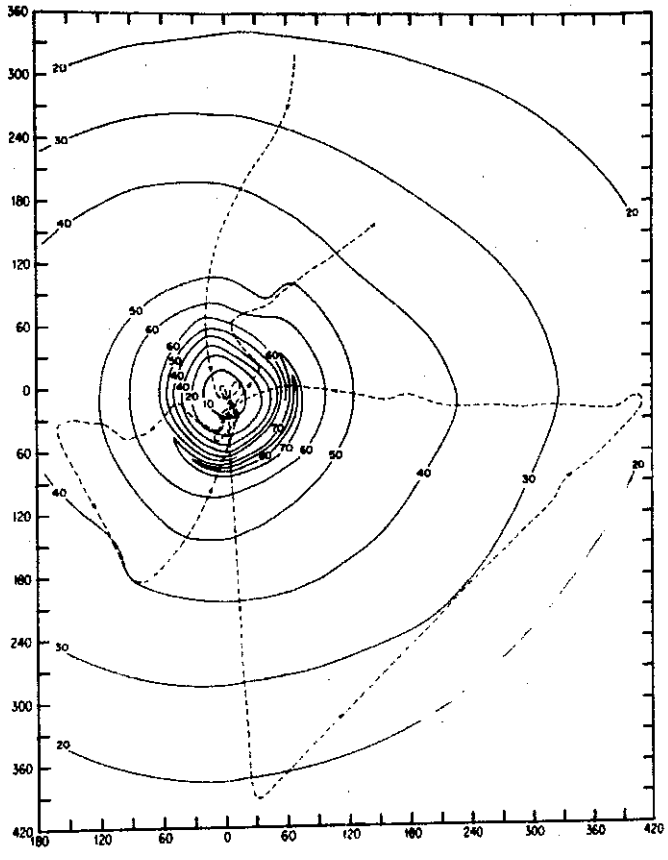

Figure 13.--Horizontal analysis of adjusted isotherms at 700 mb on November 26, in storm-relative coordinates.

relatively broad zone of maximum wind on November 25 was a sharp peak at about 60 km radial distance from the storm center. Maximum winds were located to the left rear part of the storm with respect to the direction of motion (275° at 5 m s^{-1}). This result is in contrast to other findings (Shea and Gray, 1973; LaSeur and Hawkins, 1963), which indicate that the strongest winds and strongest convection are usually found in the right front quadrant of the storm.

Horizontal analysis of adjusted temperature is presented in fig. 13. There is an 8°C anomaly in the eye from the apparent 12°C near environment, with the largest gradients in the eyewall region. Highest values of adjusted temperature were about 20°C and can be seen to have occurred in a ring just inside the radius of maximum wind. There was a 4°C temperature drop in the central part of the eye. Presumably, this thermal decline was caused by the large diameter of the eye, which allows the largest subsidence to occur near the eyewall. Note that there is a predominance of cooler temperatures to the south. This characteristic might be the result of advection of cooler temperatures from the north into the storm circulation, although no direct evidence is available to compute air trajectories over the large influence region of Irma. As shown in the sections that follow, this feature is common to other days of Irma as well.

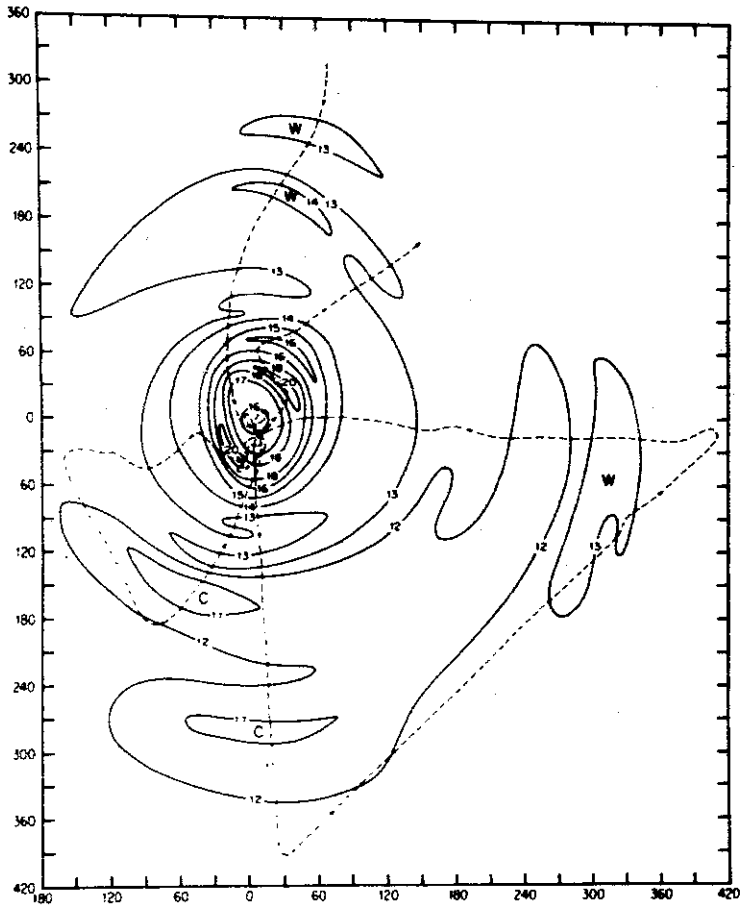

Figure 12.--Horizontal isotach analysis at 700 mb on November 26, in storm-relative coordinates.

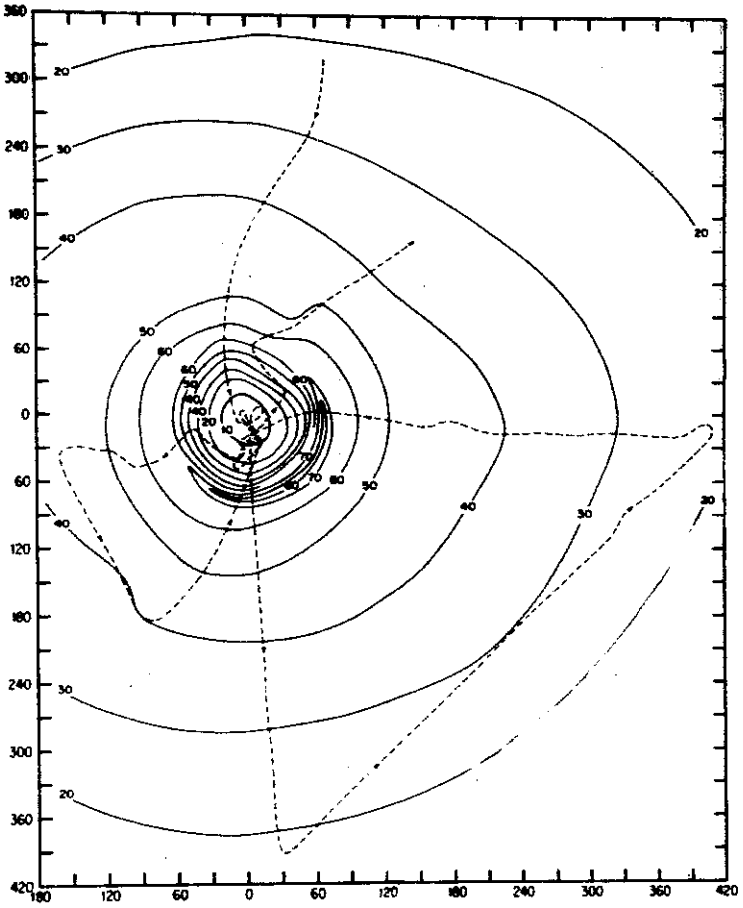

Figure 13.--Horizontal analysis of adjusted isotherms at 700 mb on November 26, in storm-relative coordinates.

relatively broad zone of maximum wind on November 25 was a sharp peak at about 60 km radial distance from the storm center. Maximum winds were located to the left rear part of the storm with respect to the direction of motion (275° at 5 m s^{-1}). This result is in contrast to other findings (Shea and Gray,

5.2 Profiles

The AWRS profiles for the November 26 north-south leg are illustrated in fig. 14. Storm motion on this day was 275° at 5 m s^{-1}. As a result of this motion, the relative wind was about 10 m s^{-1} lower on the north side than the south. The actual wind speed (not shown) on each side of the storm was about 70 m s^{-1}. Eye diameter had increased to about 160 km, with a well-defined single radius of maximum wind. It was on this day that the storm reached its maximum intensity. The storm had curved from a northwest track to a near-west heading in response to the steering currents and was imbedded within a region of little vertical shear with a strong 200-mb anticyclone aloft (not shown).

The radial wind profiles reveal that on the south side of the storm negative values or inflow predominated, while to the north, southwest, and west outflow was evident. These features are not thought to be caused by storm motion, as the actual and relative radial profiles are nearly identical. This finding is not at variance with other studies. Shea and Gray (1973) present plan views of mean radial winds that show outflow at midlevels ahead and to the right with respect to the storm's motion, with inflow predominating behind and to the left. The predominant feature of the radial wind is the sharp spike of outflow within the maximum wind regime on the south, west, and southwest profiles, indicating convergence of air from the eye into the eyewall. This is also seen in Atlantic hurricanes (Jorgensen, 1982).

The thermodynamic profiles reveal a slight change in the eye characteristics from the previous day. The relative humidity minimum of 60% is evident in the central part of the eye. Also shown is an adjusted temperature drop of about 4°, which is a much more pronounced dip than that of the previous day. Maximum temperatures occurred just inside both eyewalls, and the anomalies were 8°C. Maximum moisture values were about 15 g kg^{-1}, the same as the previous day. Θ_E profiles show the largest gradients in the eyewall region, as expected, and a relatively constant value within the eye of 364 K, except for a dip in the central part of the eye due to the moisture dip. The D-value profile shows the classically symmetric structure (spikes in the profile are caused by sharp aircraft rolls) and will be shown to be consistent, in the gradient wind sense, with the observed tangential winds.

The AWRS profiles for the east-west and northeast-southwest legs on November 26 are presented in figs. 15 and 16. They reveal much the same information as the north-south profile and are included for continuity. There were moisture and temperature minima in the central part of the eye and a corresponding dip in Θ_E, a well-defined single radius of maximum wind of about 75 m s^{-1} at a radial distance of 60 km, large values of radial outflow at the radius of maximum wind, particularly on the southwest side, and relatively subsaturated conditions toward the north and east, even within the eyewall and outer rainbands.

The data on November 26 indicate that Irma was a well-defined, large storm with maximum winds >75 m s^{-1}. The storm structure on this day agrees well with the composite of Atlantic storms of medium-to-high intensity presented by Shea and Gray (1972). They show that, for intense storms (that is, where central pressure is <945 mb), the wind profiles have sharper peaks and fall off more rapidly away from the radius of maximum wind than the broader profiles of wind for the moderate storms. Irma followed this pattern as well. On November 24 and 25 the wind profiles were rather broad and had two maximum regions. The intensification that took place on November 26 (down to 939 mb) was correlated with the narrowing of the wind profile. Maximum warming and drying were located within the eye in a ring adjacent to the maximum wind, and were more pronounced than on the previous day.

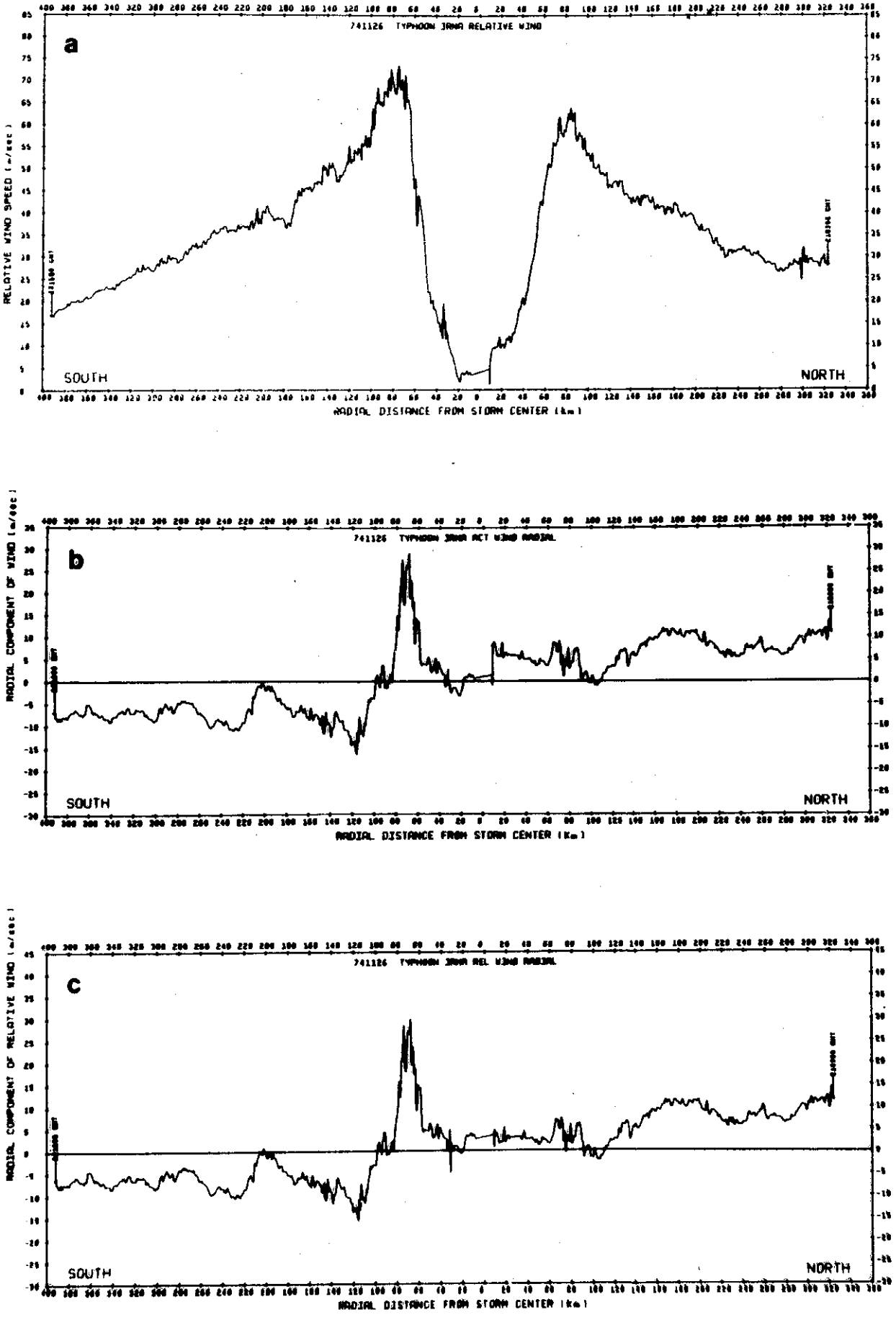

Figure 14.--November 26 north-south profiles: (a) relative tangential wind; (b) actual radial wind; (c) relative radial wind.

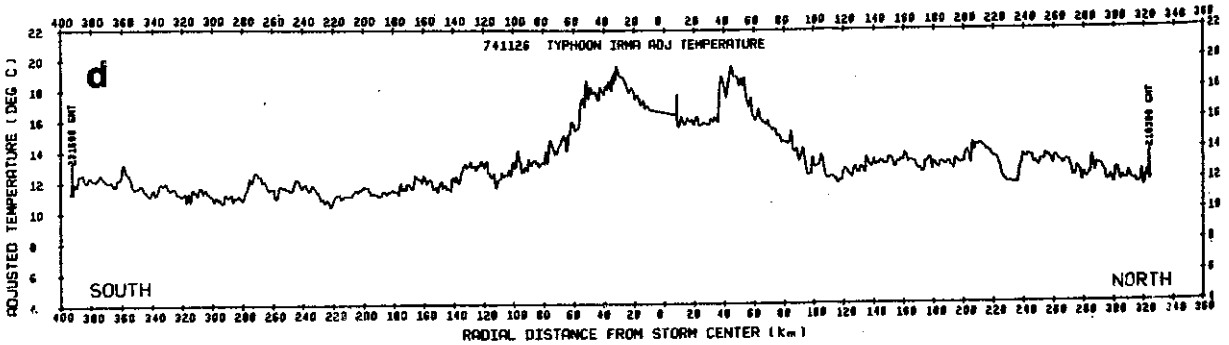

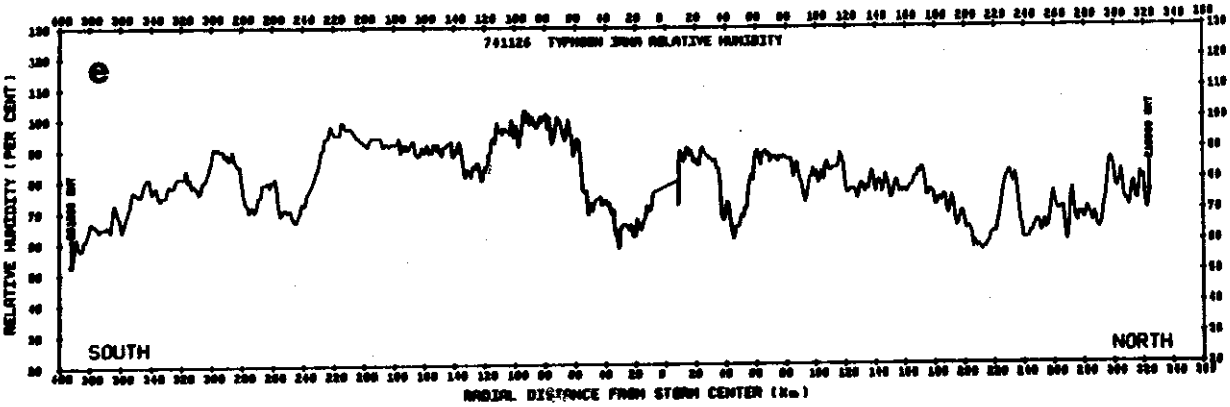

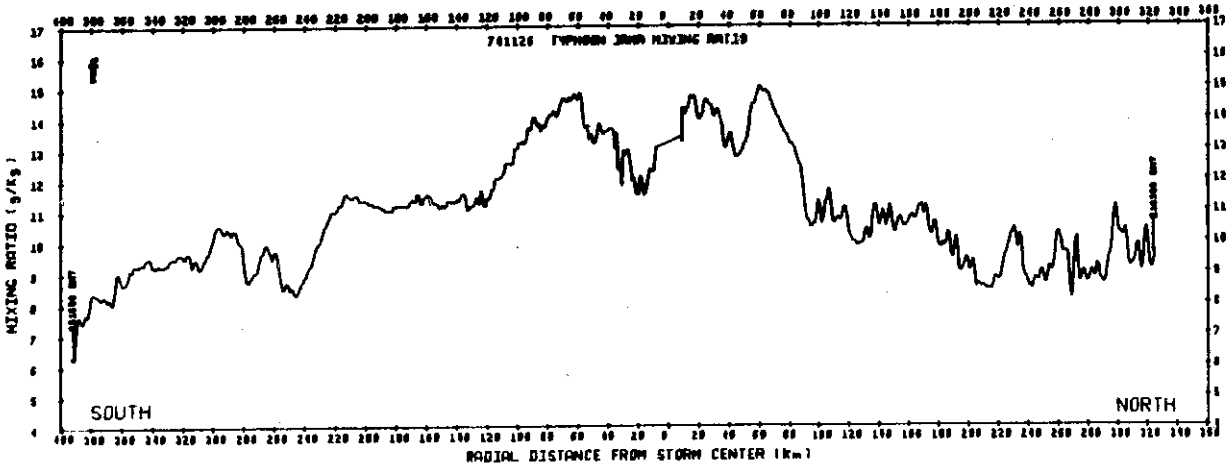

Figure 14.--Continued: (d) adjusted temperature; (e) relative humidity; (f) mixing ratio.

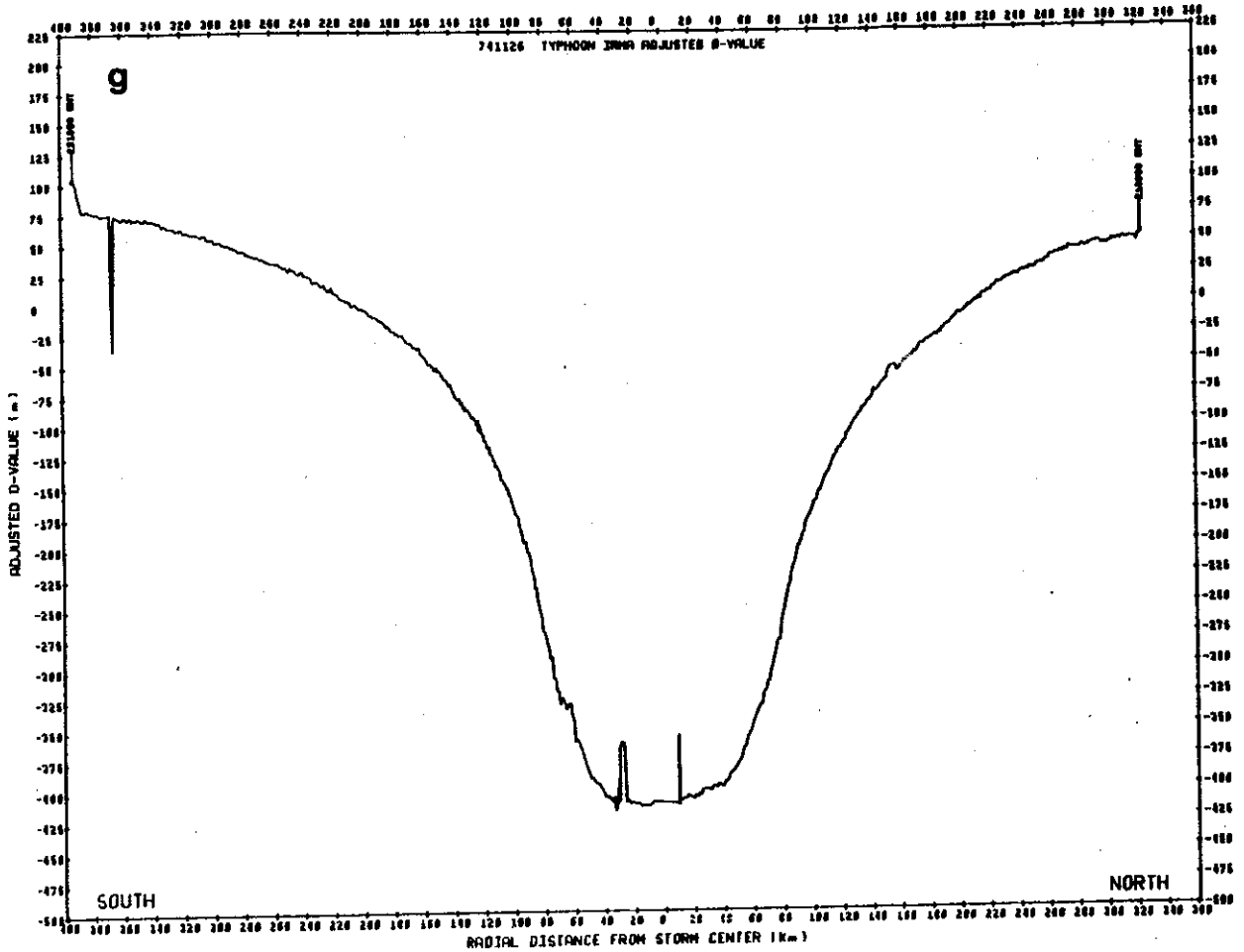

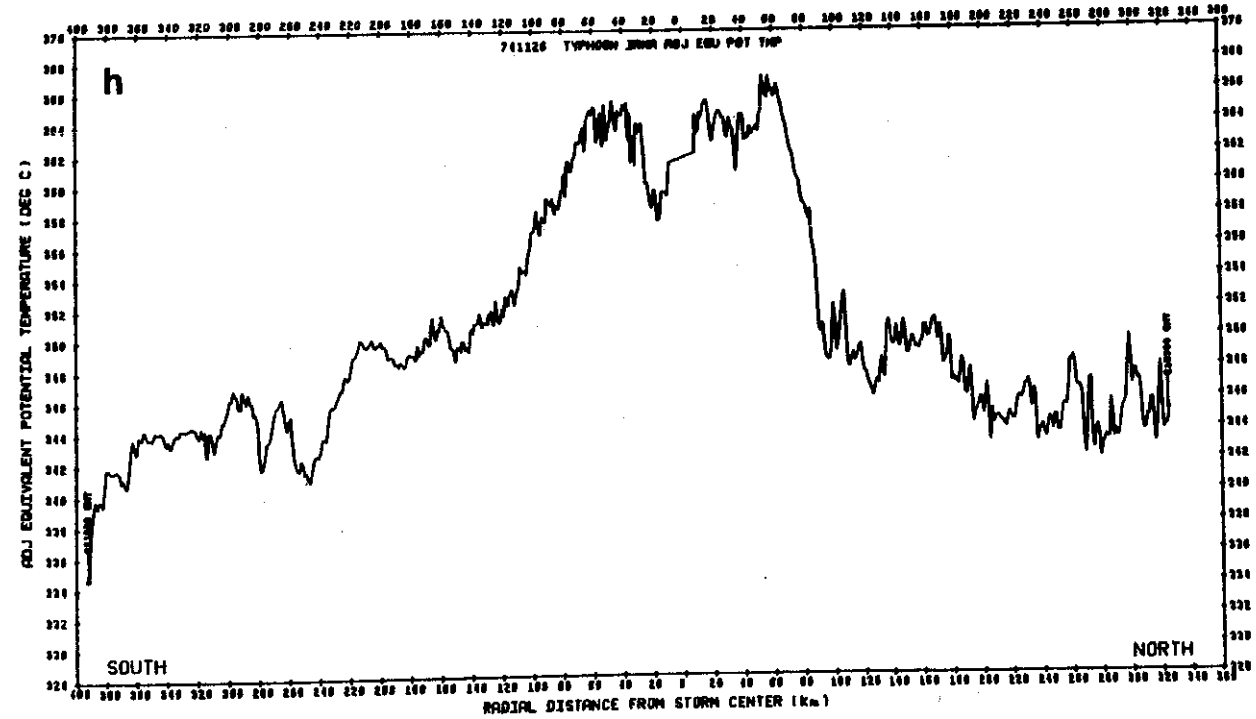

Figure 14.--Continued: (g) adjusted D-value; (h) adjusted equivalent potential temperature.

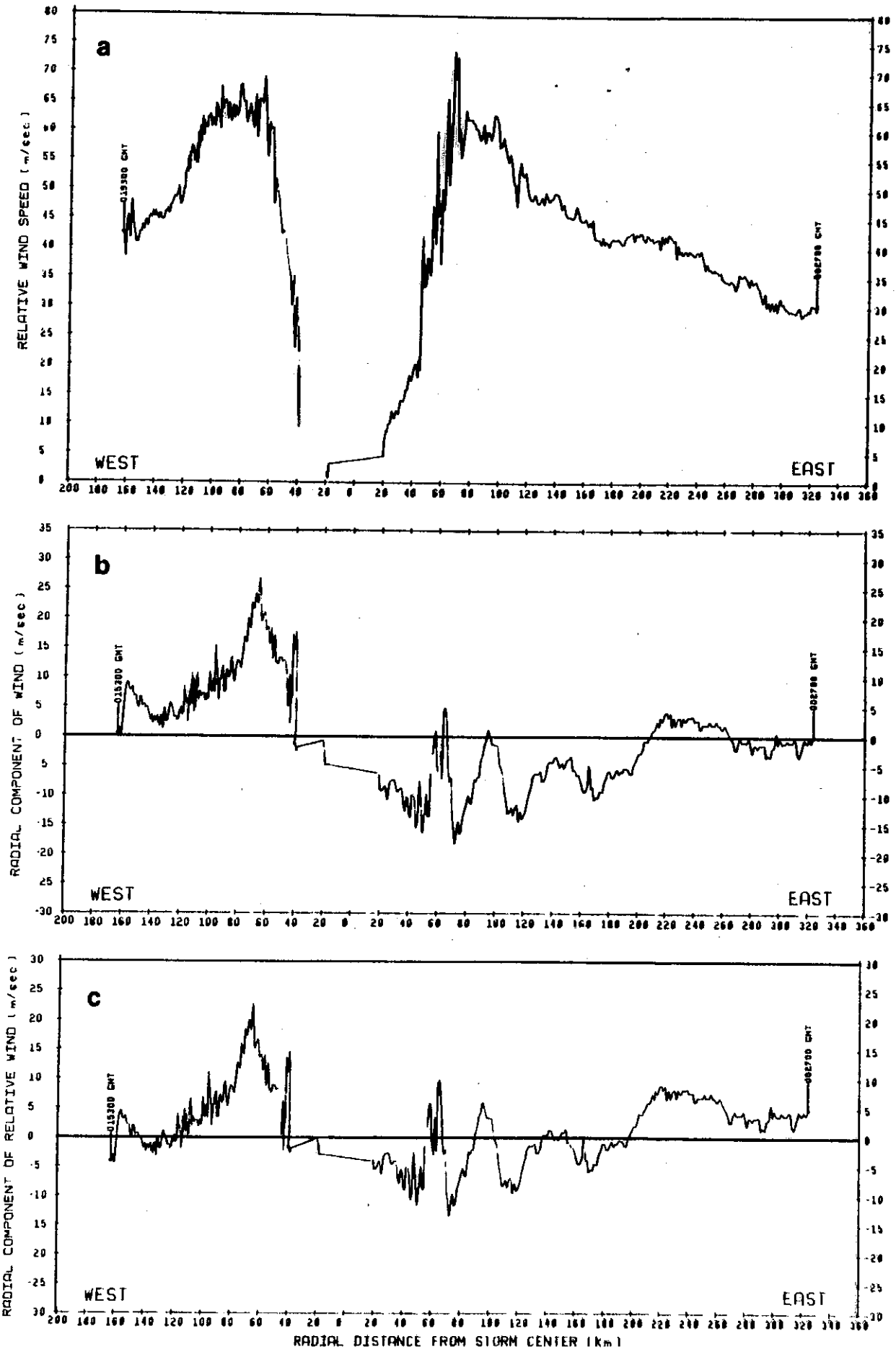

Figure 15.--November 26 east-west profiles: (a) relative tangential wind; (b) actual radial wind; (c) relative radial wind.

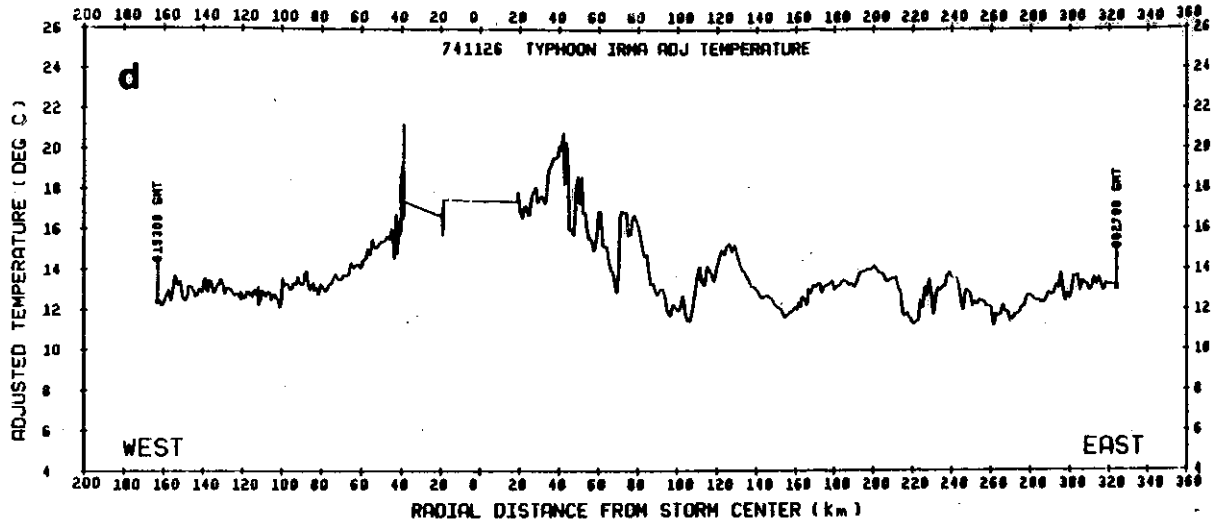

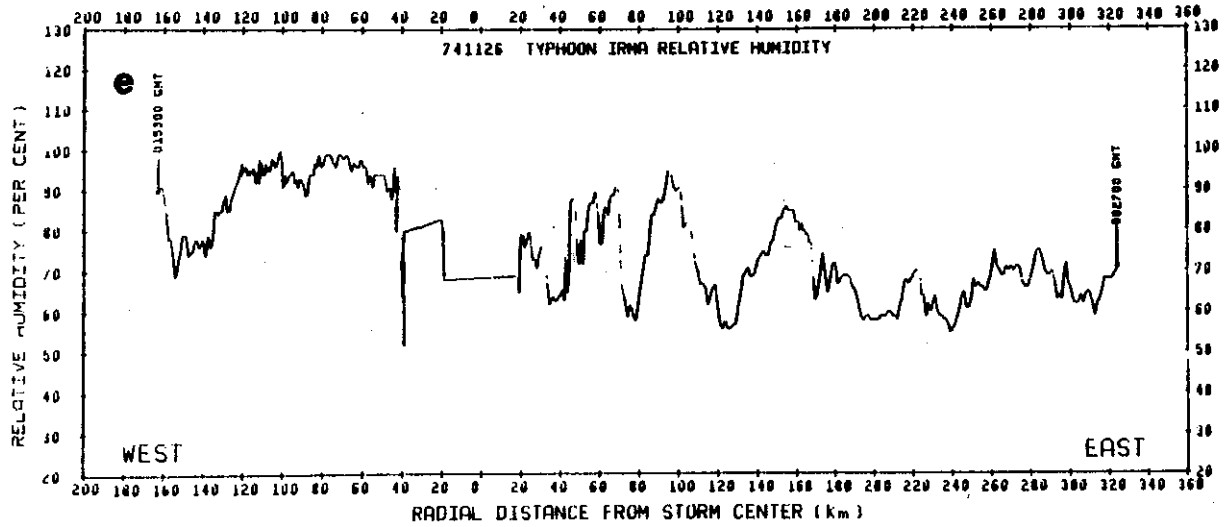

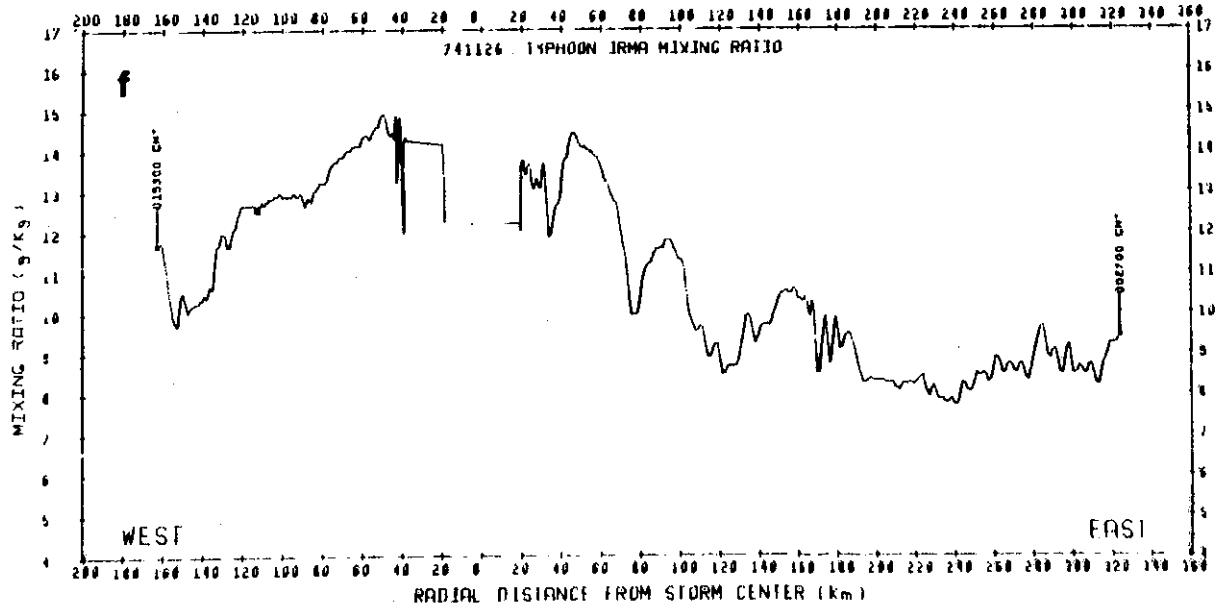

Figure 15.--Continued: (d) adjusted temperature; (e) relative humidity; (f) mixing ratio.

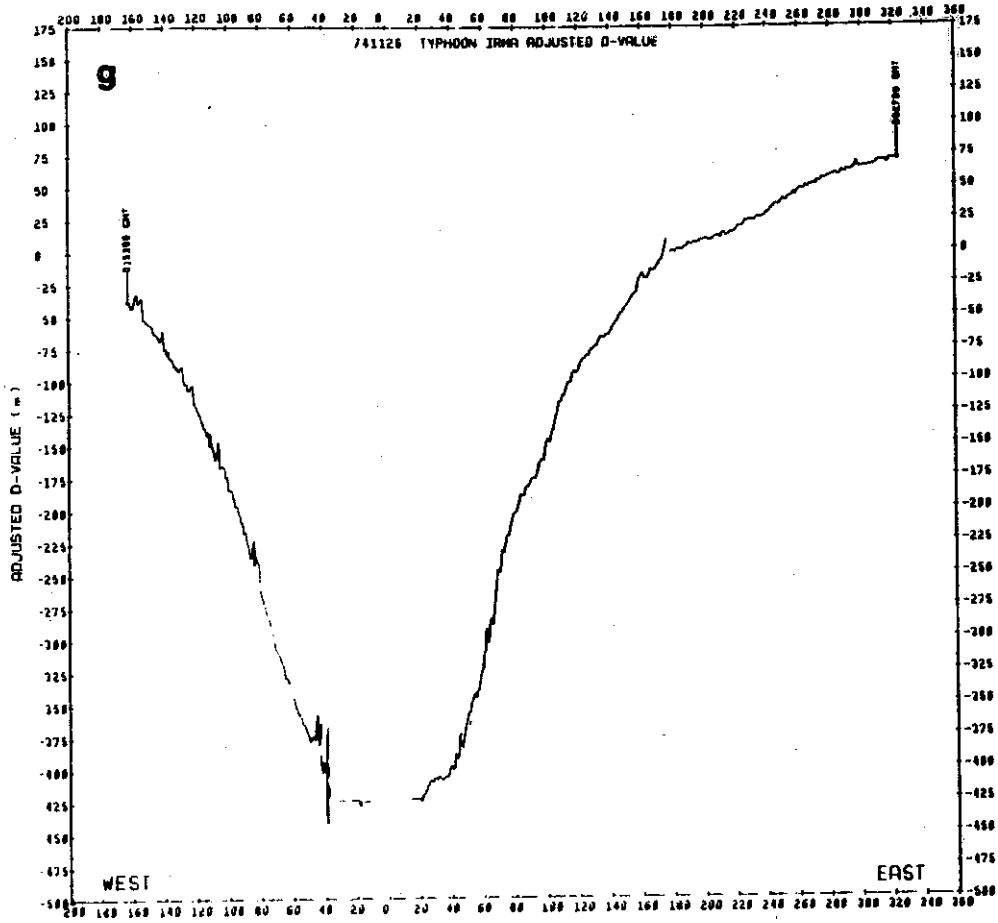

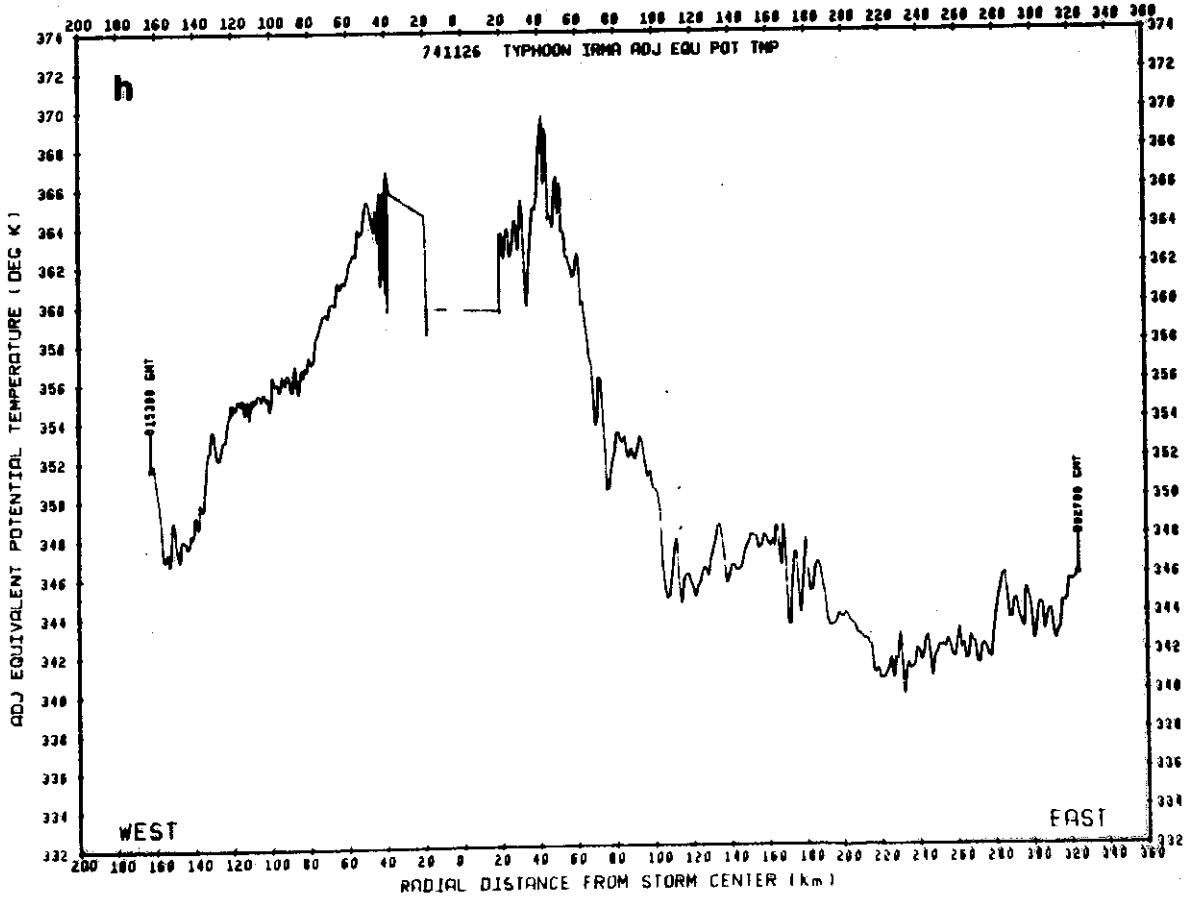

Figure 15.--Continued: (g) adjusted D-value; (h) adjusted equivalent potential temperature.

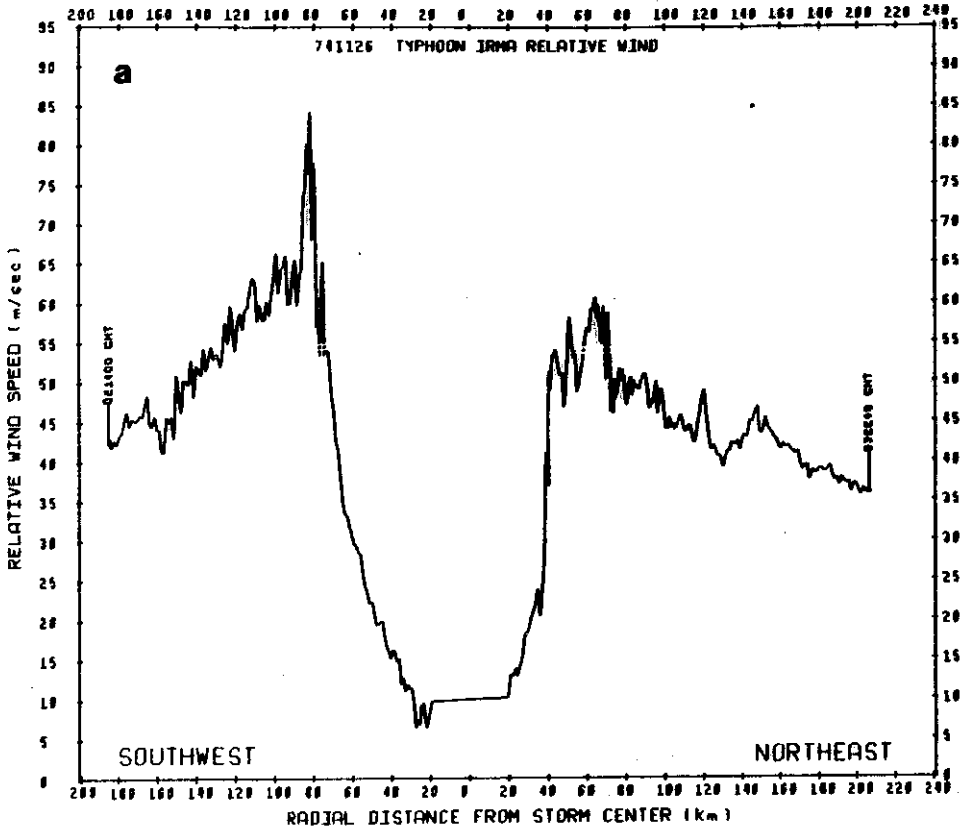

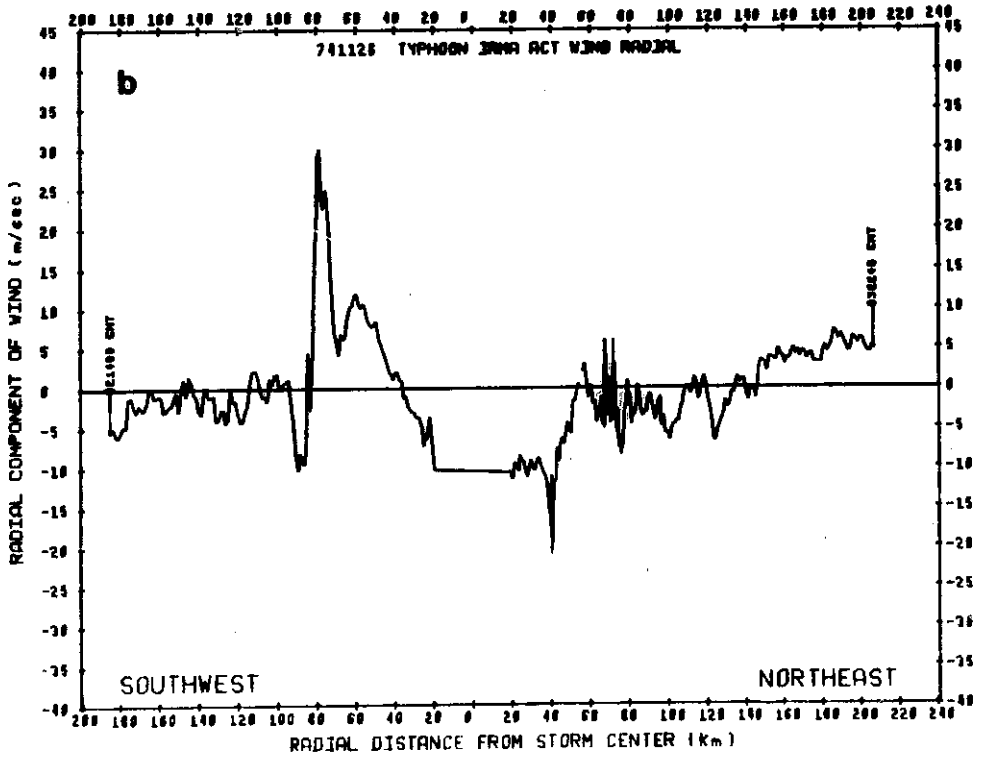

Figure 16.--November 26 northeast-southwest profiles: (a) relative tangential wind; (b) actual radial wind.

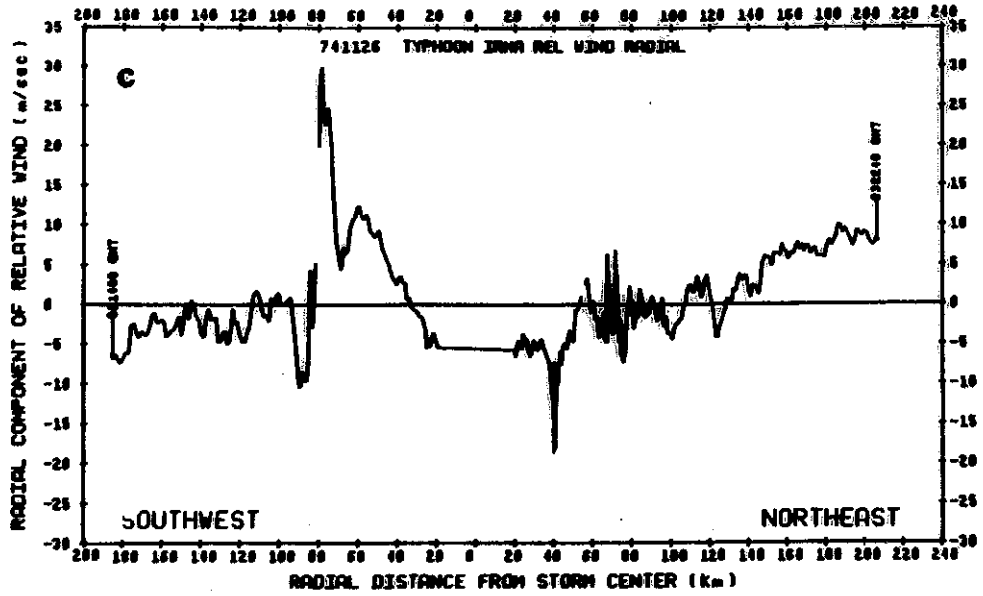

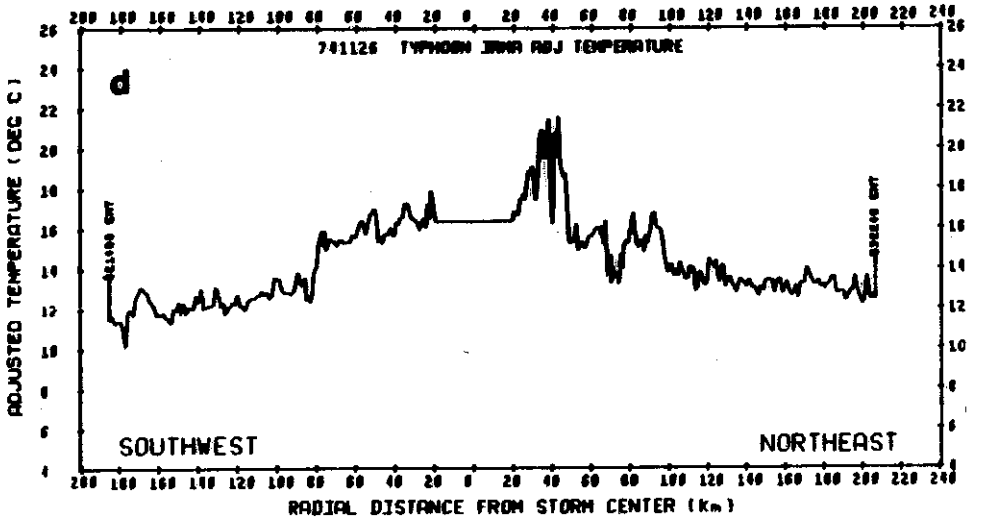

Figure 16.--Continued: (c) relative radial wind; (d) adjusted temperature.

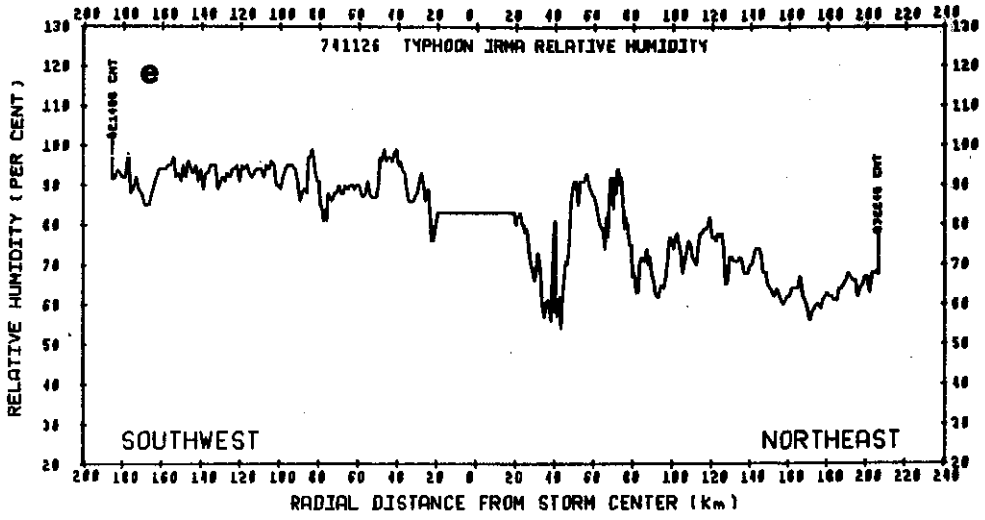

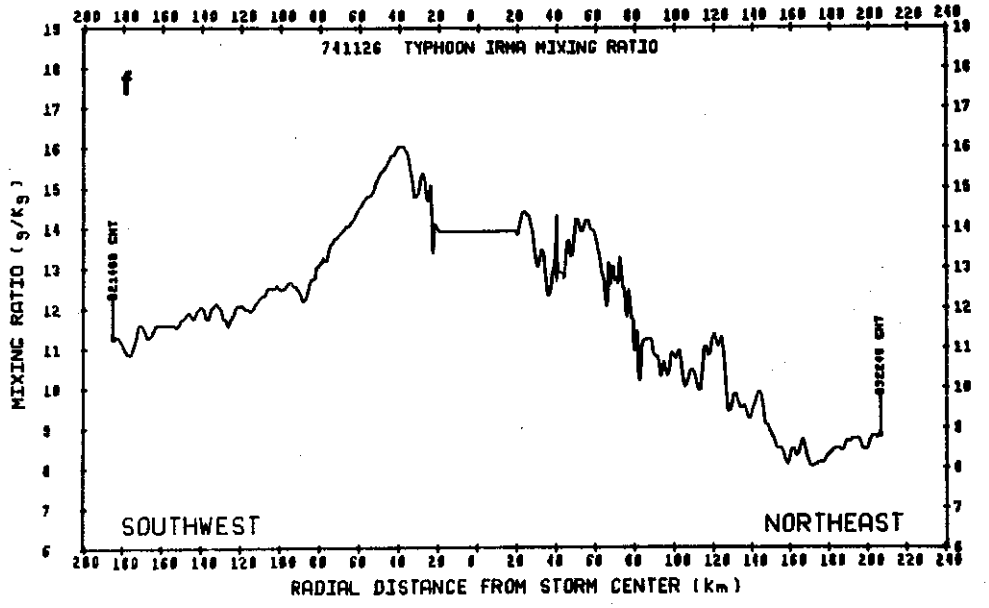

Figure 16.--Continued: (e) relative humidity; (f) mixing ratio.

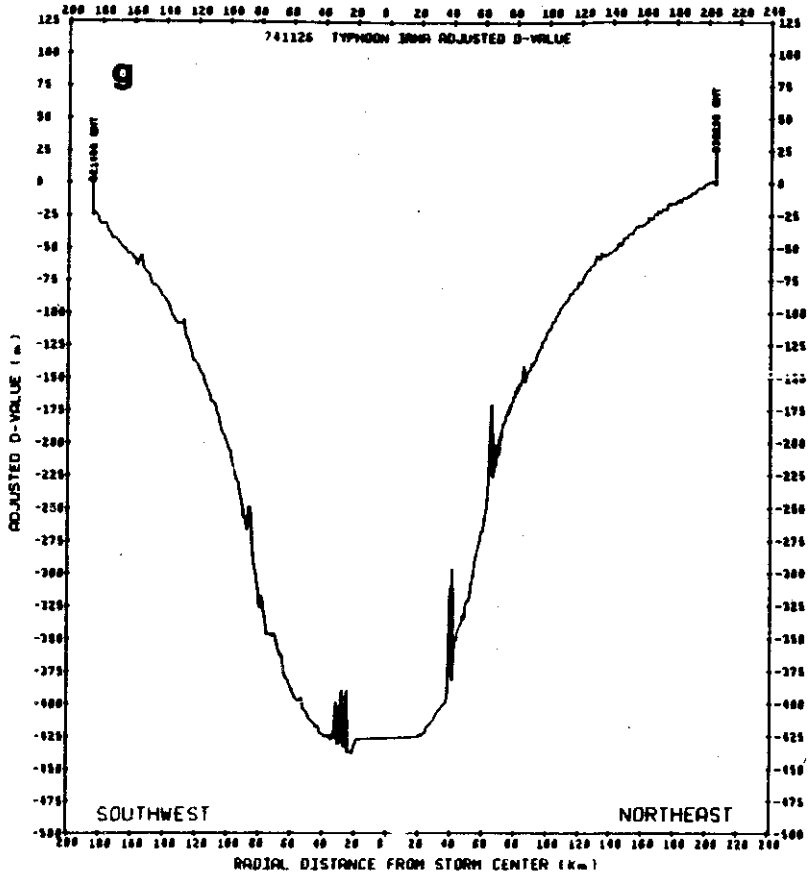

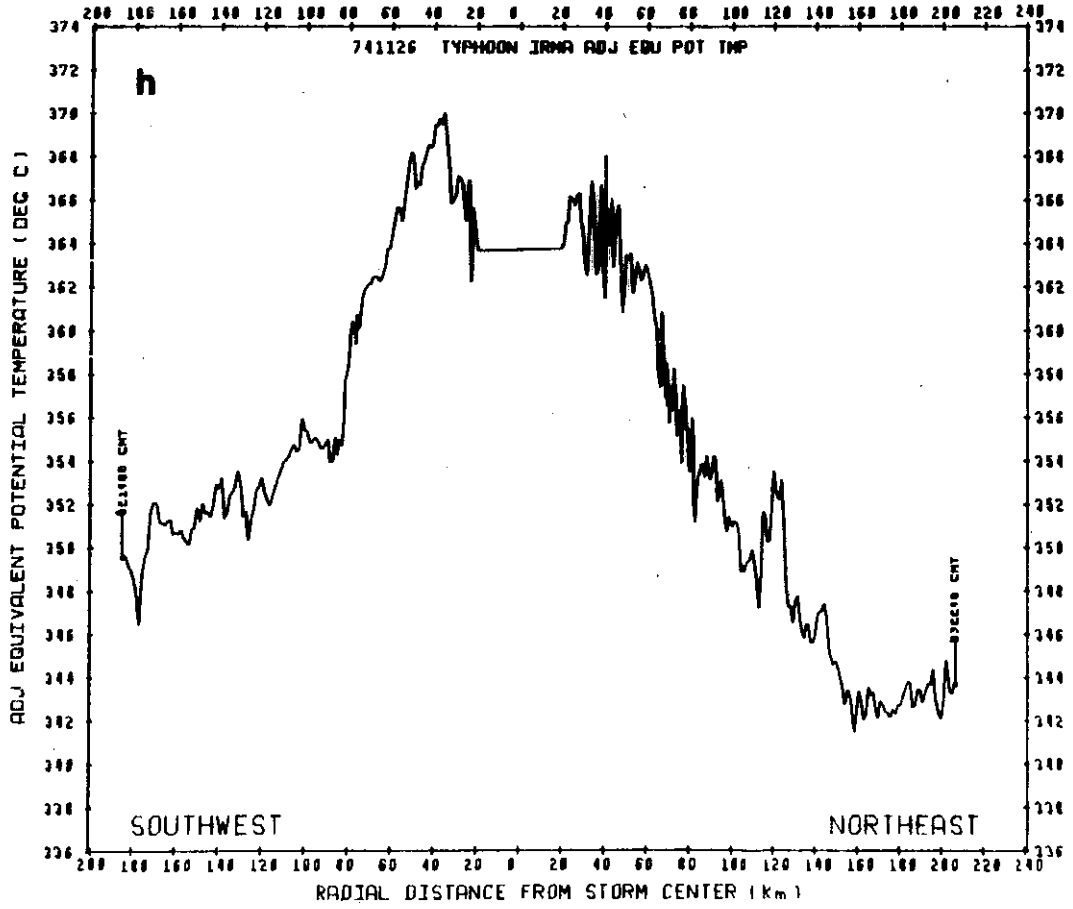

Figure 16.--Continued: (g) adjusted D-value; (h) adjusted equivalent potential temperature.

6. STORM STRUCTURE ON NOVEMBER 28

6.1 Horizontal Analysis

Typhoon Irma made landfall on the Philippine island of Luzon early on the November 28. The eye crossed the coastline about 60 km south of Baler and passed directly over Clark Air Force Base. The lowest central pressure experienced at Clark was 979 mb in the eye at 0700Z on November 28. Highest reported wind was a gust of 43 m s^{-1} at 0500Z. After leaving Luzon, Irma moved generally westward at slow speed (4 m s^{-1}) and began to reintensify. The AWRS aircraft began its investigation approximately 6 hours after the storm had entered the South China Sea on November 28.

The horizontal analysis of relative wind streamlines (fig. 17) indicates, as before, a nearly symmetric vortex with only the slightest hint of inflow. This is in contrast to the observations made before landfall that showed a slight outflow in the streamline pattern.

The storm had weakened considerably. The isotach analysis (fig. 18), indicates that the maximum wind speeds were only 25 m s^{-1} and were still to the south of the storm, but instead of a well-defined radius of maximum winds, there was a broad zone of winds from 20 to 25 m s^{-1}, similiar to that seen on November 24 and 25.

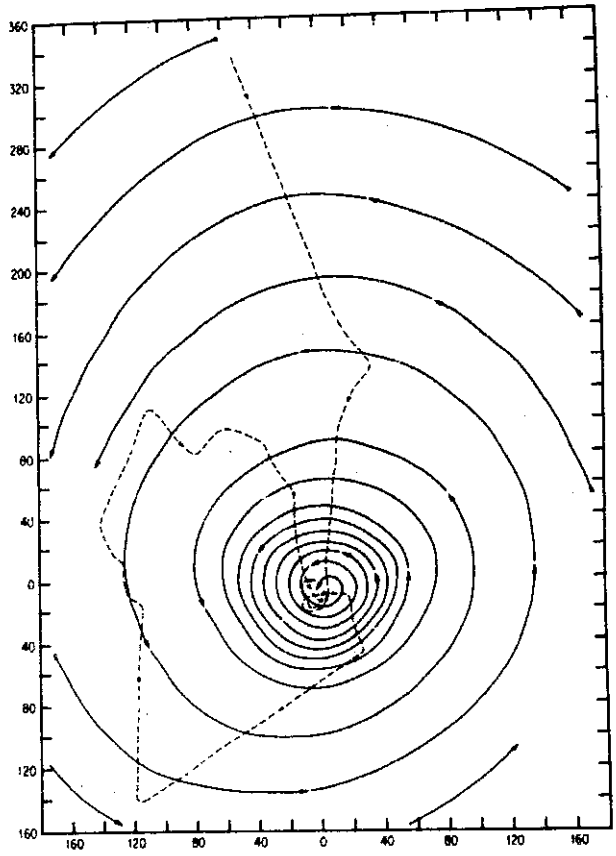

Figure 17.--Relative wind streamlines at 700 mb on November 28, in storm-relative coordinates.

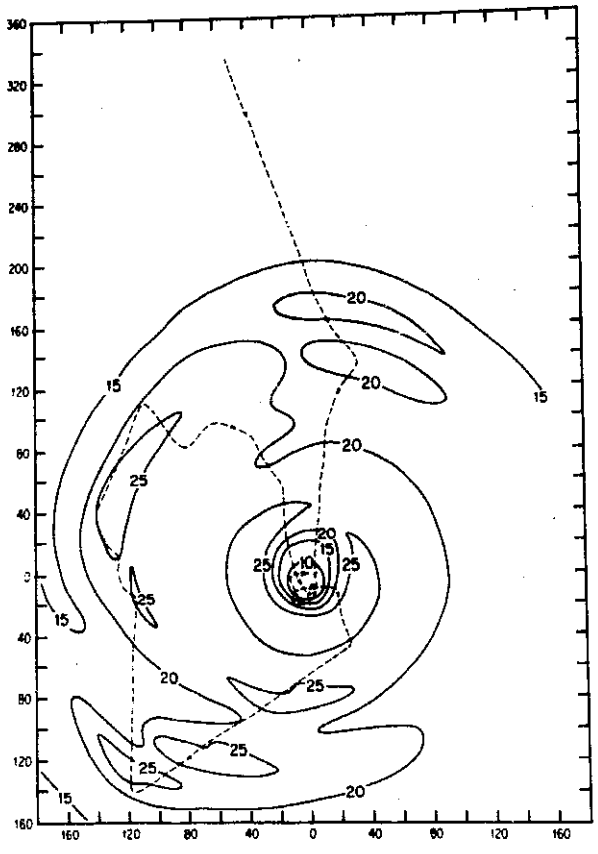

Figure 18.--Horizontal isotach analysis at 700 mb on November 28, in storm-relative coordinates.

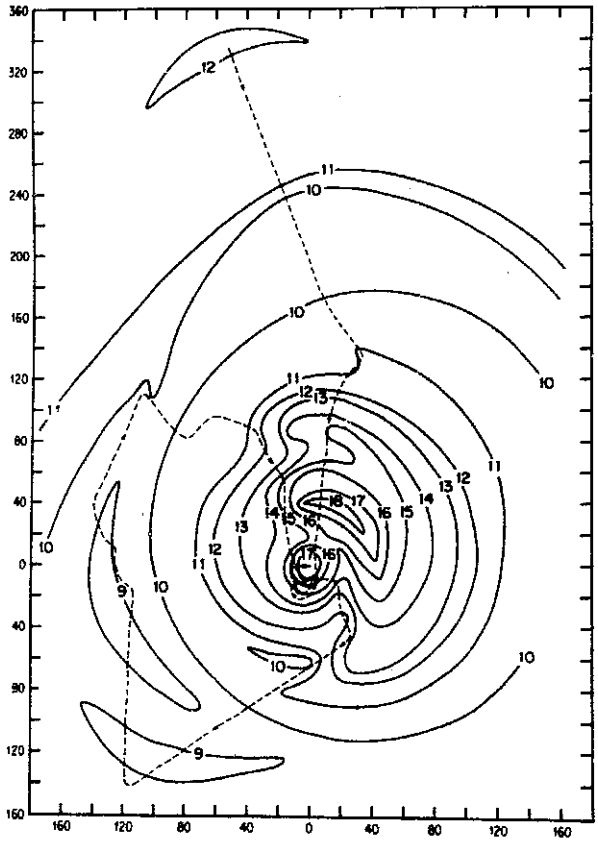

Figure 19.--Horizontal analysis of adjusted isotherms and 700 mb on November 28, in storm-relative coordinates.

The horizontal analysis of adjusted temperature is presented in fig. 19. Temperature anomalies are shown to have decreased to 5° to 6°C with generally cooler temperatures south of the storm center, as seen on previous days. Highest temperatures are found, not in the eye center, but, as before, generally to the northeast in an arc 20 km from the center.

6.2 Profiles

Profiles for the AWRS flight leg from the north to the southwest on November 28 are presented in fig. 20. The wind profiles indicate that one effect of landfall on the storm is to reduce the maximum wind to about 25 m s^{-1} and to decrease the eye diameter to about 50 km. The radial wind profiles show no distinct regions of inflow/outflow as evidenced on the previous day. There is now only a general region of slight inflow to the north and neutral (tangential) winds to the south.

The thermodynamic profiles do not exhibit the customary characteristics of hurricane conditions. The adjusted temperature profile shows that there was still a 5° to 6°C anomaly (from 12°C) which is quite high when one considers that the maximum wind was only 25 m s^{-1}. The highest temperature gradients to the southwest coincided with the eyewall determined from the wind profile. To the north, however, the temperature maximum was just inside the radius of maximum winds, but the temperature profile fell off gradually after that maximum. Relative humidity shows a relative minimum in the eye center (as low as 40%), but the radius of maximum wind was not the radius of highest humidity. This would indicate an absence of an eyewall region at the radius

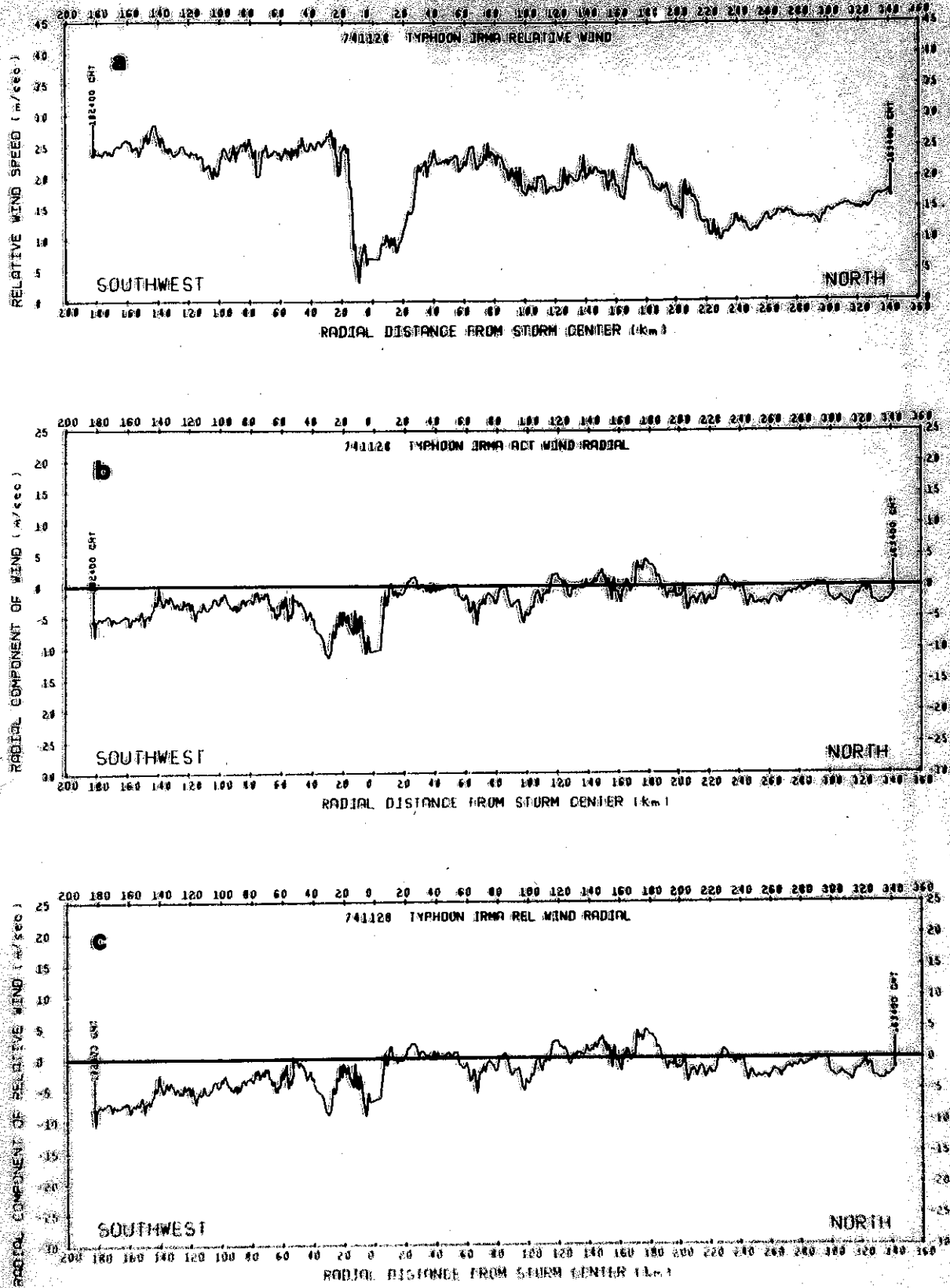

Figure 20.--November 28 north-southwest profiles: (a) relative tangential wind; (b) actual radial wind; (c) relative radial wind.

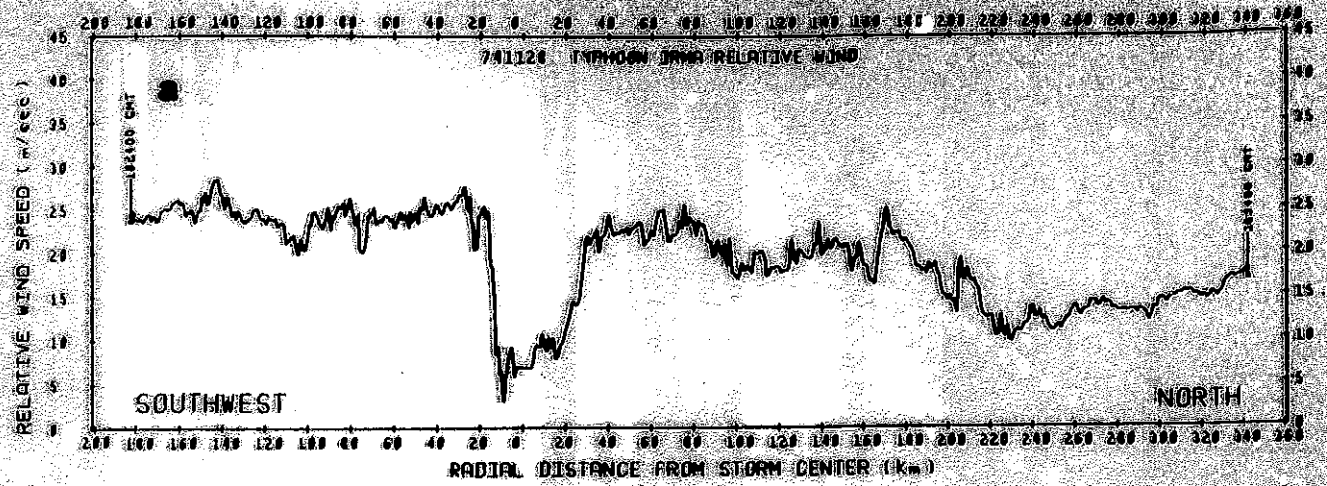
741128 TYPHOON IRMA RELATIVE WIND
a
SOUTHWEST
NORTH
RELATIVE WIND SPEED (m/sec)
RADIAL DISTANCE FROM STORM CENTER (km)

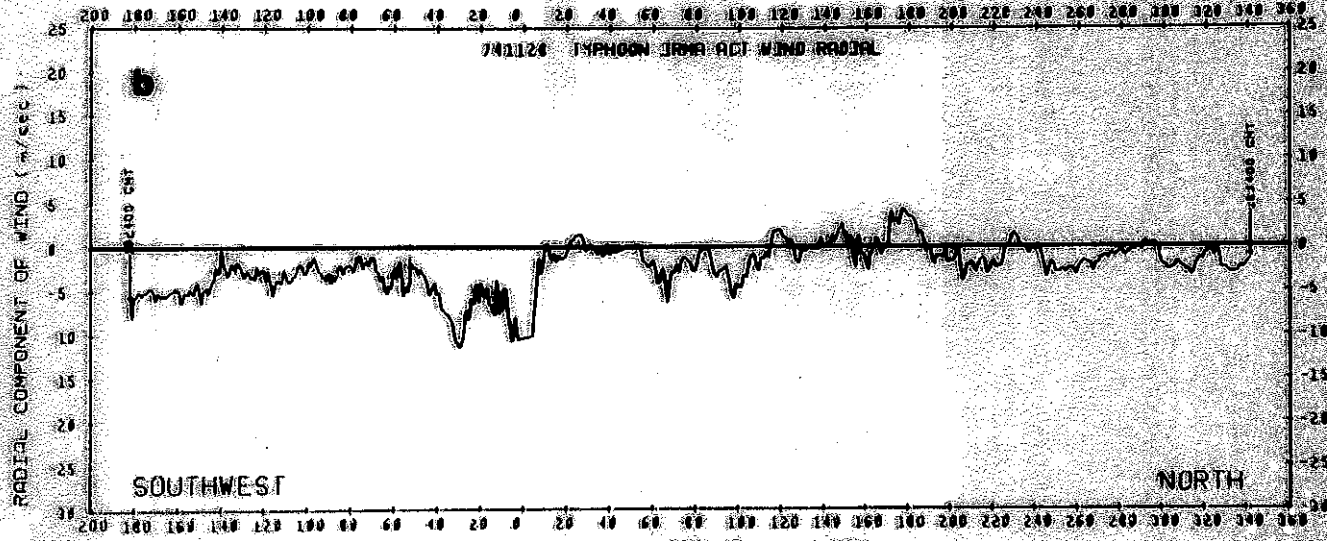
741128 TYPHOON IRMA ACI WIND RADIAL
b
SOUTHWEST
NORTH
RADIAL COMPONENT OF WIND (m/sec)
RADIAL DISTANCE FROM STORM CENTER (km)

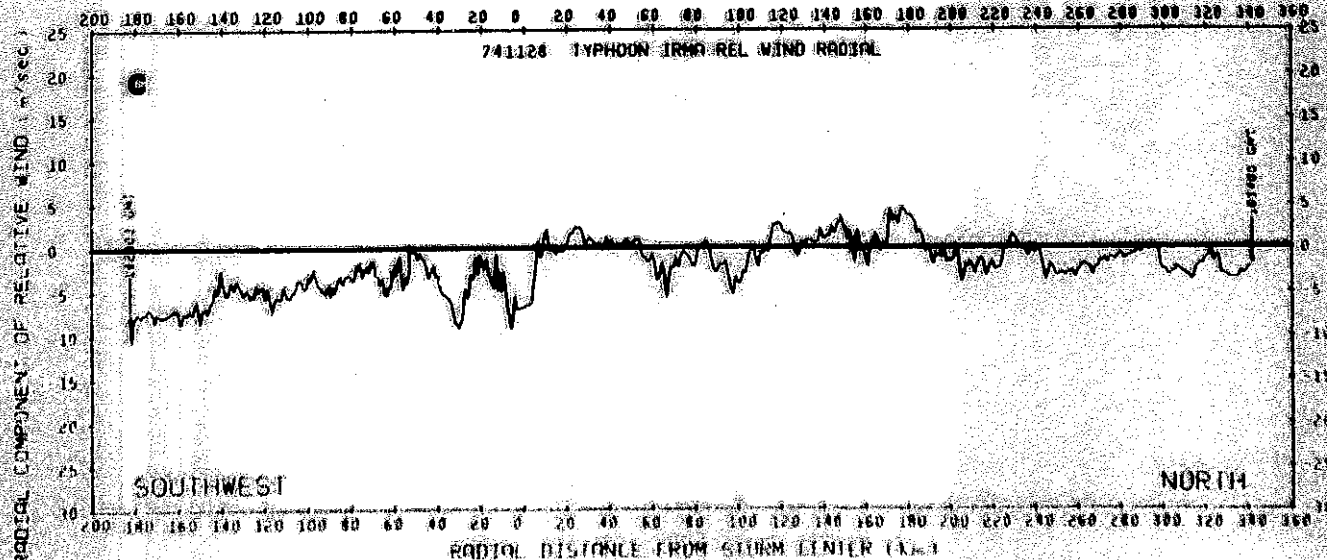
741128 TYPHOON IRMA REL WIND RADIAL
c
SOUTHWEST
NORTH
RADIAL COMPONENT OF RELATIVE WIND (m/sec)
RADIAL DISTANCE FROM STORM CENTER (km)

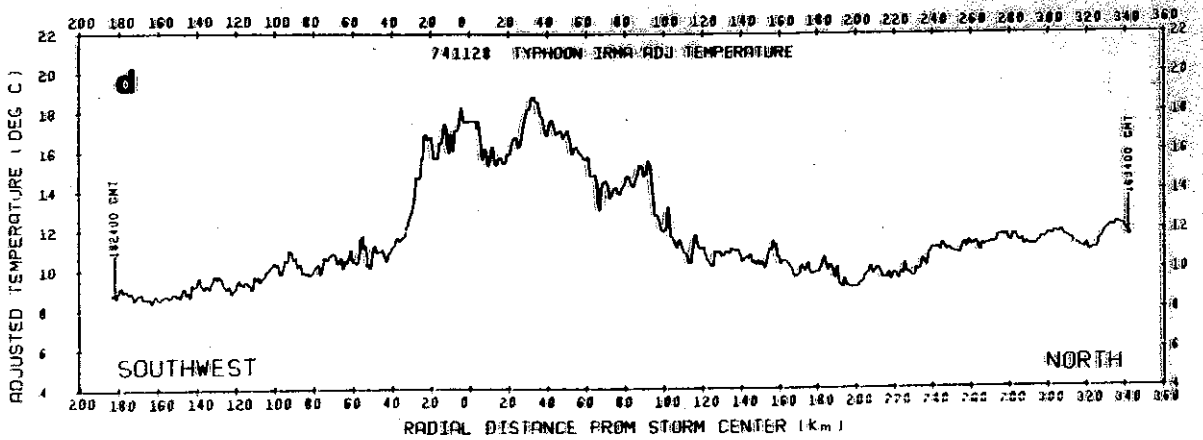

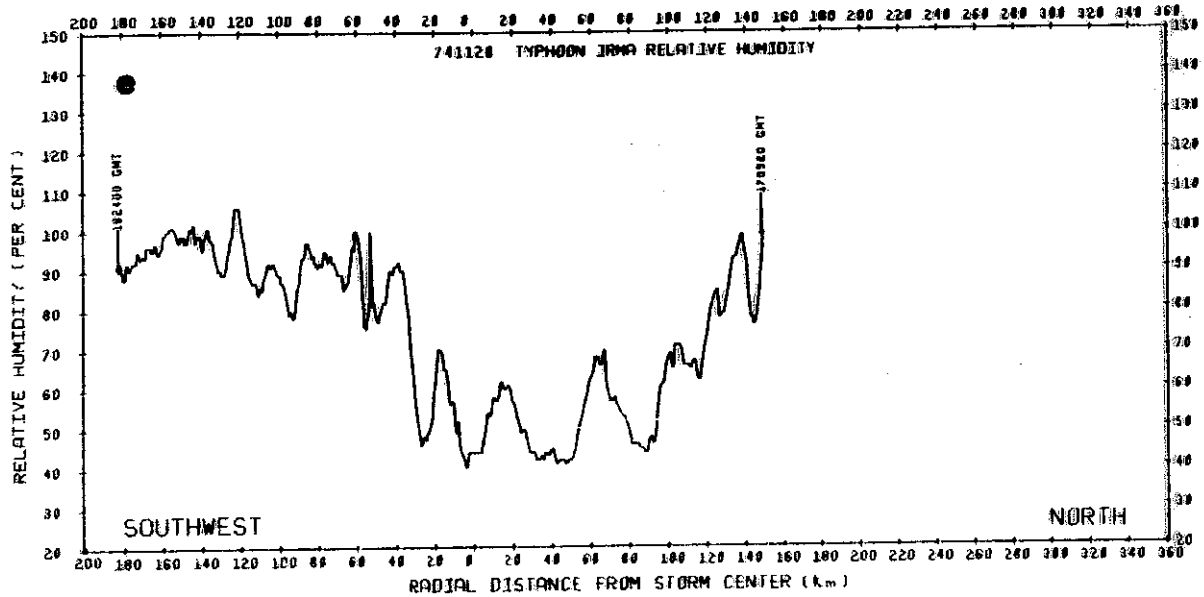

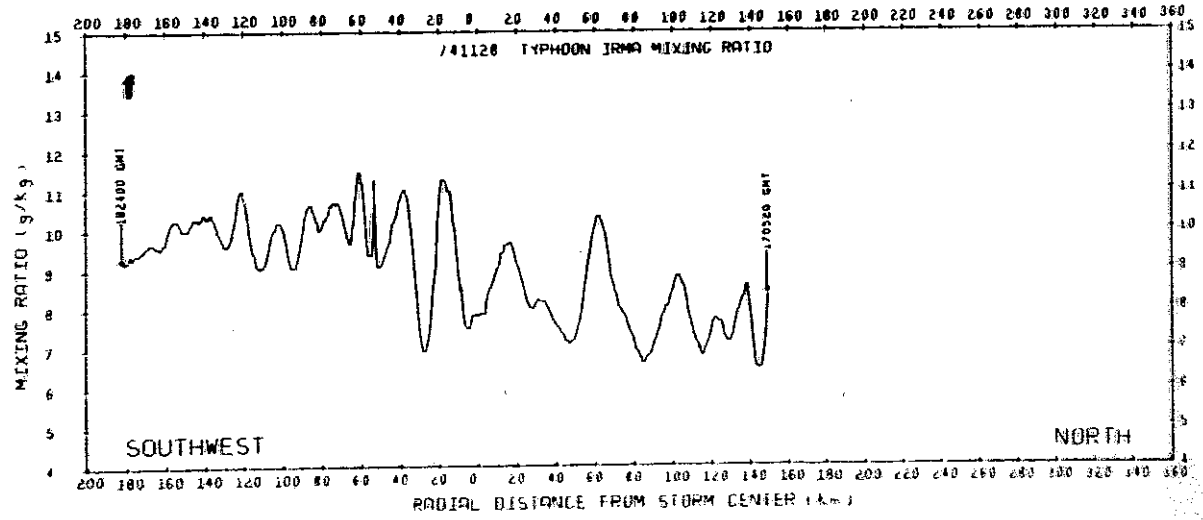

Figure 20.--Continued: (d) adjusted temperature; (e) relative humidity; (f) mixing ratio.

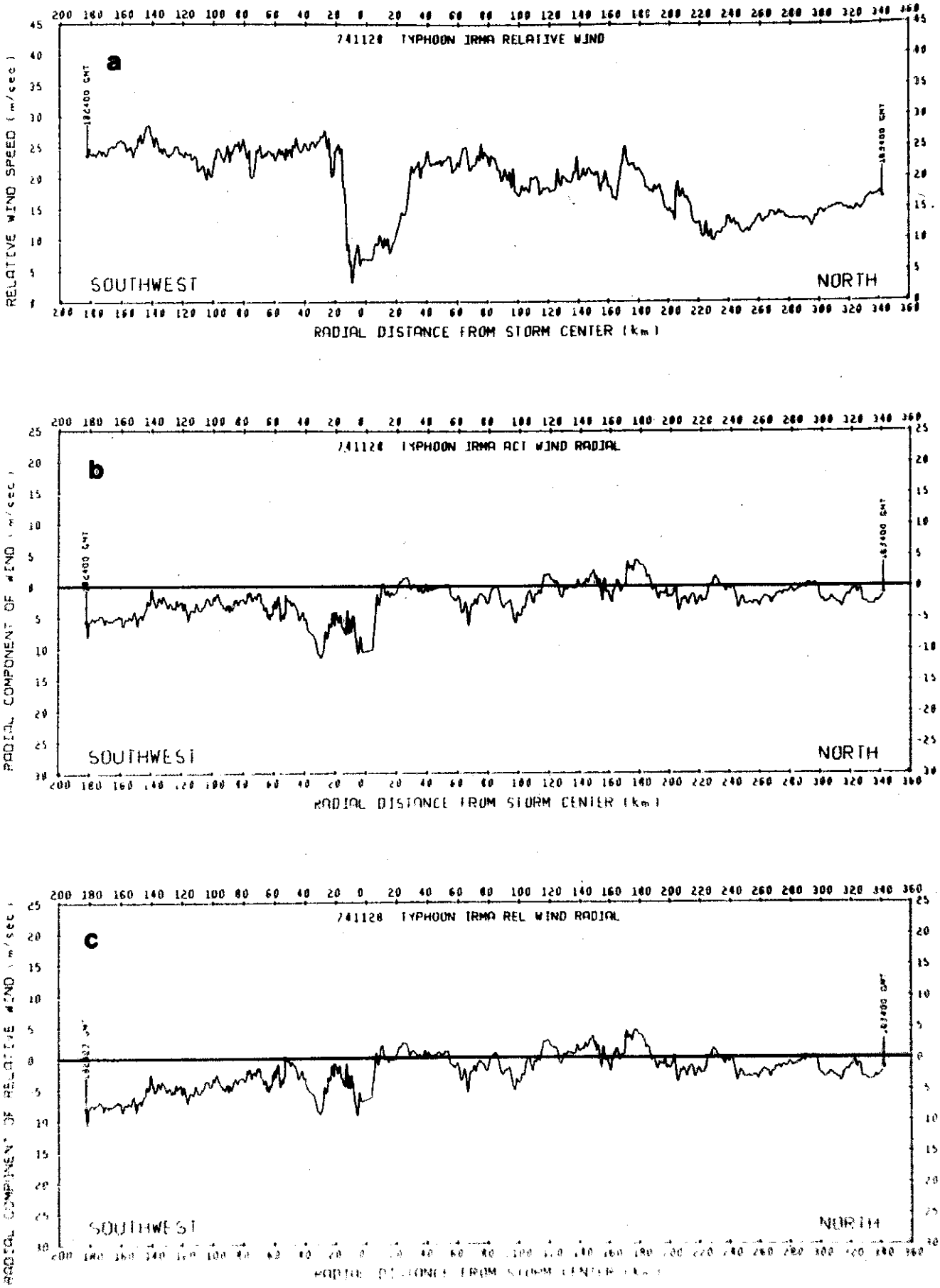

Figure 20.--November 28 north-southwest profiles: (a) relative tangential wind; (b) actual radial wind; (c) relative radial wind.

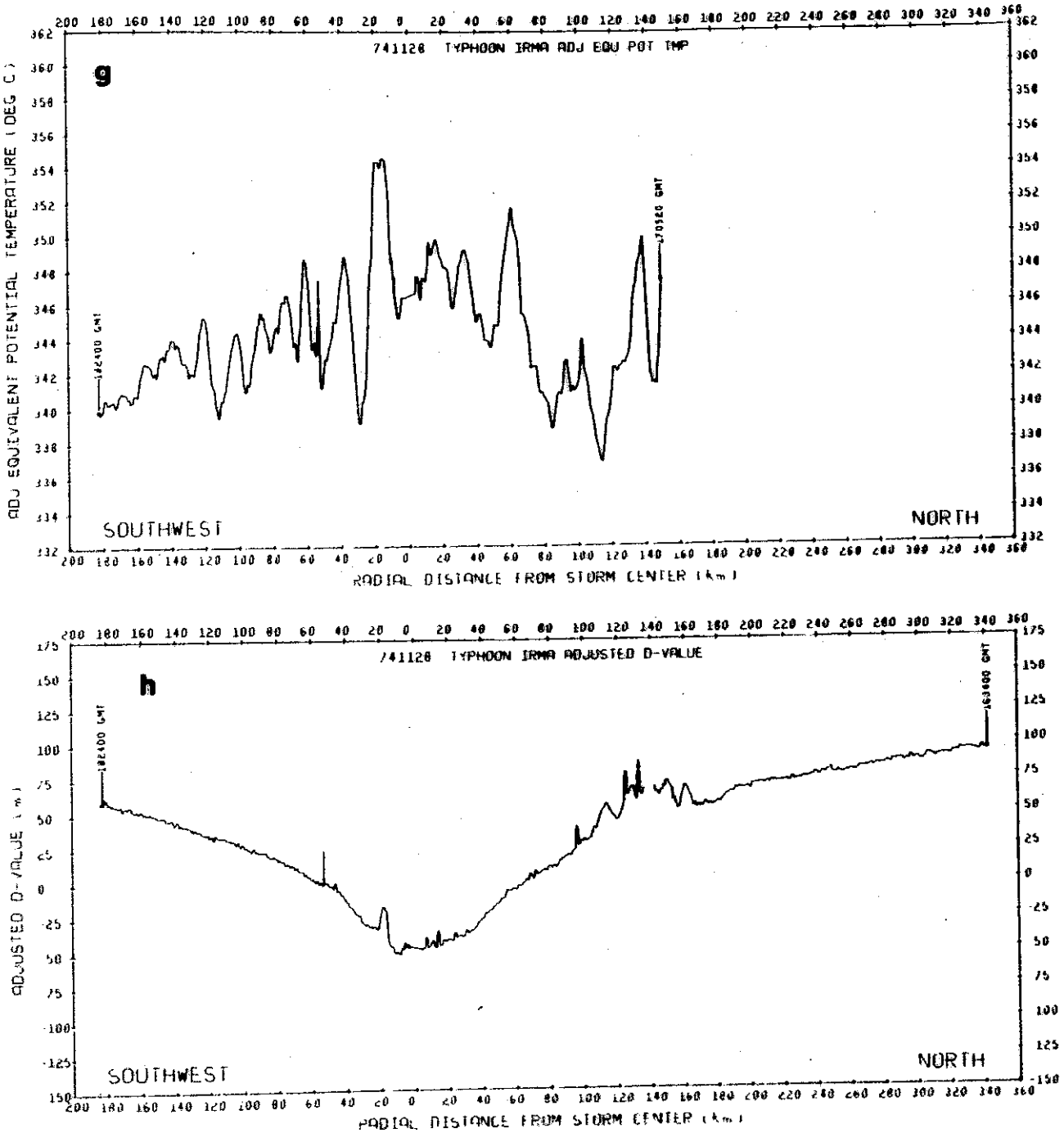

Figure 20.--Continued: (g) adjusted D-value; (h) adjusted equivalent potential temperature.

of maximum winds, with most of the convection having occurred beyond a radius of 50 km at this pass. Data beyond a radial distance of 150 km to the north were deleted from the graphs because of the malfunction of the dewpoint instrument. The Θ_E profile reveals nothing, except a gradual increase toward the storm center, an unusual characteristic that indicates a diffuse eyewall.

Figure 21 presents the AWRS profiles for the November 28 northwest-center leg. Radius of maximum wind is 45 km radial distance to the northwest, well correlated with the highest values of relative radial wind (outflow). Small values of inflow are evidenced beyond 60 km radial distance. The moisture

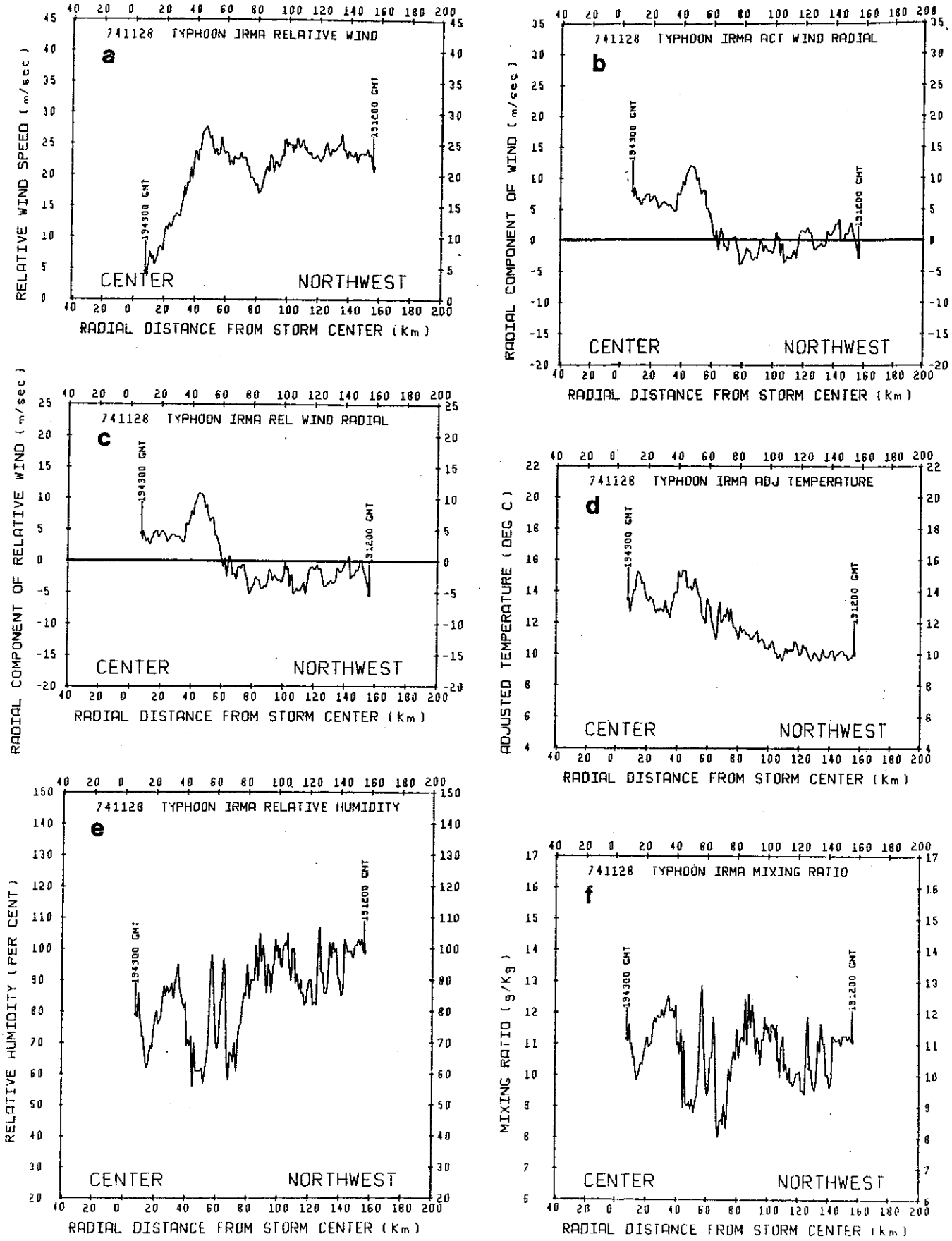

Figure 21.--November 28 northwest-center profiles: (a) relative tangential wind; (b) actual radial wind; (c) relative radial wind; (d) adjusted temperature; (e) relative humidity; (f) mixing ratio.

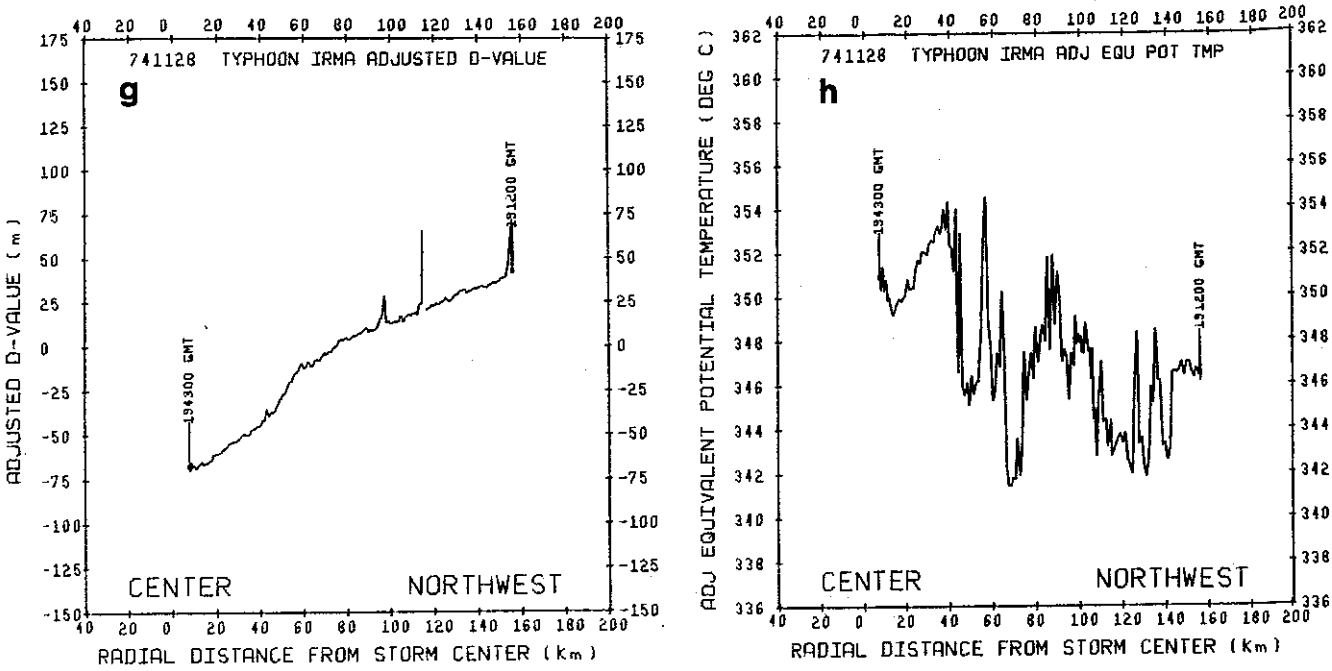

Figure 21.--Continued: (g) adjusted D-value; (h) adjusted equivalent potential temperature.

profiles indicate convection. This is supported by the Θ_E profile, which shows the highest gradient in this region.

An interesting aspect of the temperature profiles (figs. 20d and 21d) is the rapid increase from 9°-10°C 100 km to the north, to 16°-18°C in the eye, and the corresponding increase from 40 km to the southwest. On the most intense day, November 26, Irma's temperature at 200 km in all profiles was approximately 12°C. The 700-mb temperature on this day decreased to about 9°C, but the eye anomaly was only 1° to 2° cooler, at nearly the same latitude, indicating intrusion of Irma into a different air mass. The storm's recurvature to the north two days later also supports the indication of a cool trough to the west.

7. STORM STRUCTURE ON NOVEMBER 29

7.1 Horizontal Analysis

The horizontal analysis of the relative wind streamlines for November 29 is shown in fig. 22. As on other days, this analysis shows a nearly symmetric vortex with only a slight trace of outflow. The isotach analysis (fig. 23) shows that the maximum wind speed had increased about 10 m s^{-1} during the past 10 hours and had become concentrated into a definable radius of maximum winds. The storm had turned to a more west-northwest course and had picked up in forward speed to 5 m s^{-1}. Irma was still 24 hours from recurvature, however. The area of maximum winds was to the southwest and not in the right front quadrant as is typical of other storms.

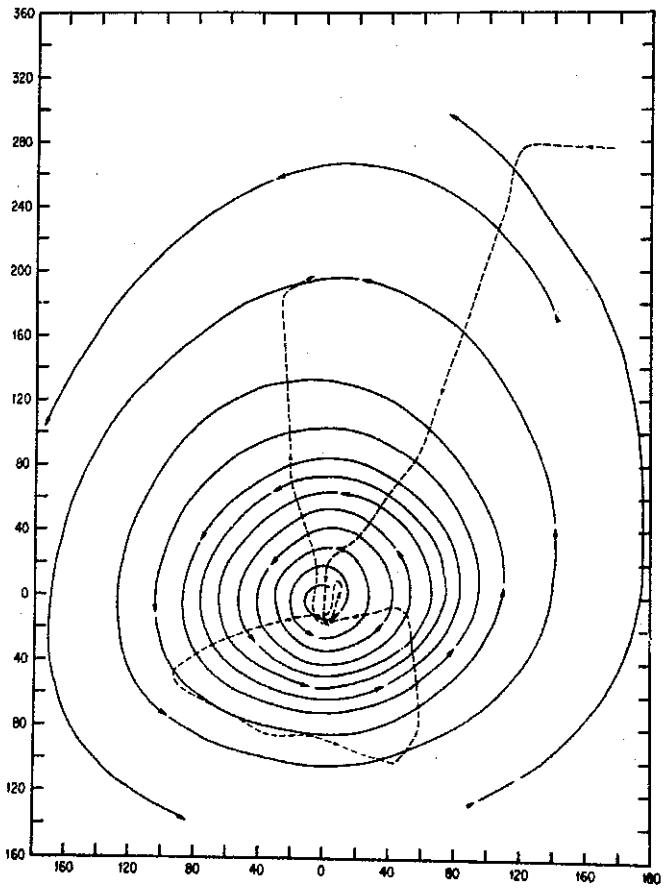

Figure 22.--Relative wind streamlines at 700 mb on November 29, in storm-relative coordinates.

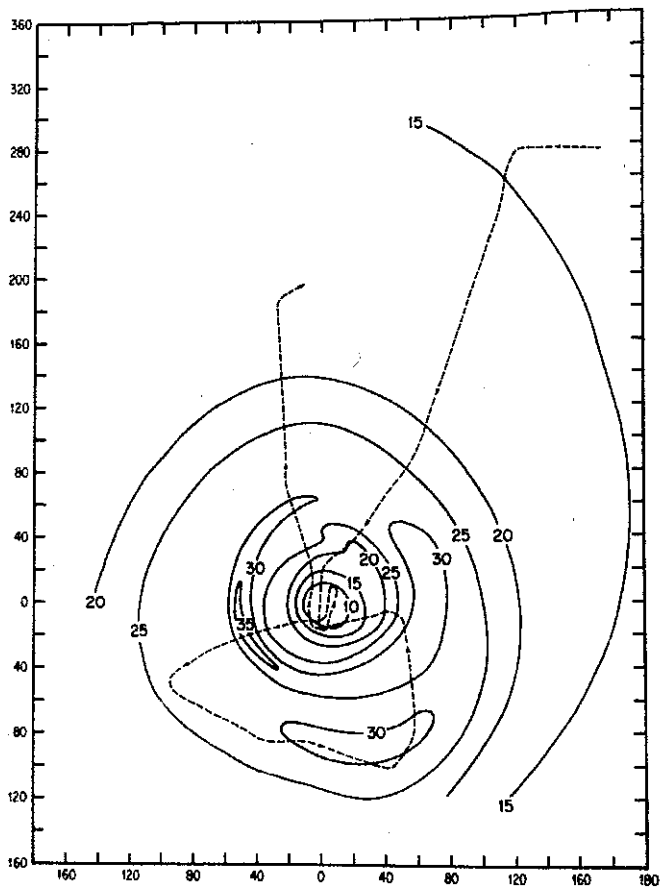

Figure 23.--Horizontal isotach analysis at 700 mb on November 29, in storm-relative coordinates.

The adjusted temperature analysis is presented in fig. 24. The region of maximum temperatures is, again, not in the eye center, but 20 to 30 km to the north, in an arc just inward of the maximum winds. A secondary maximum is located 80 to 100 km to the north-northwest. Irma was still intensifying on these last two days and had not yet been classified as a typhoon. Large asymmetries within developing storms have been noted previously (e.g., Sheets, 1967). The aircraft flight track did not go far enough south to confirm the relatively cold air evident on previous day.

7.2 Profiles

Profiles for the AWRS flight leg on November 29 from the northeast to the southwest are presented in fig. 25. As can be seen from the wind profiles, the eye diameter had increased to almost 100 km. The radial wind profiles show that there were distinct relative maxima (outflow) within each eyewall. As on previous days, slight inflow was present to the southwest outside the eyewall, with outflow everywhere to the north. Temperature maximum was not in the eye center, but was displaced 20 to 60 km northeast; in fact, the eye shows no distinct pattern on the adjusted temperature trace, just a general

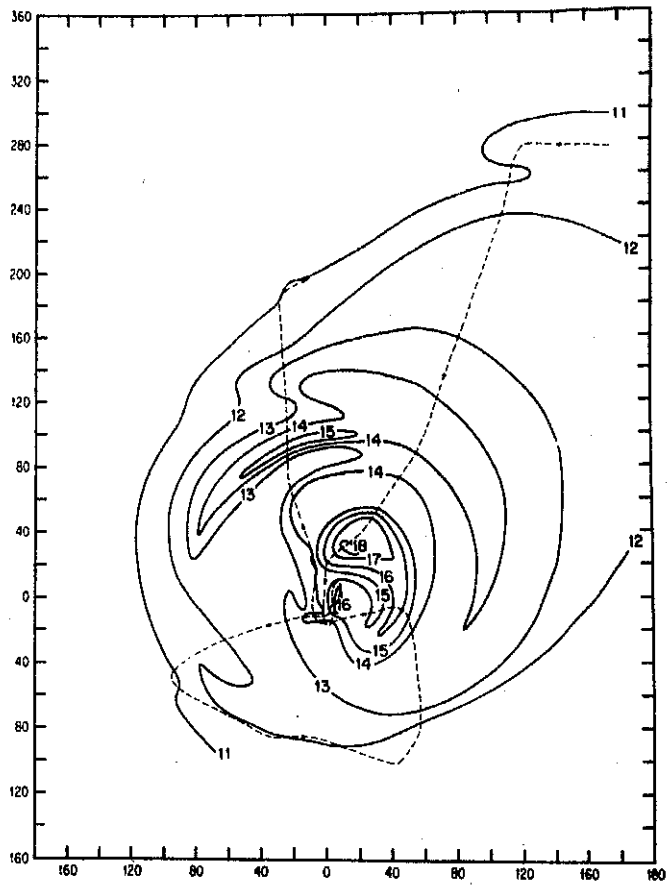

Figure 24.--Horizontal analysis of adjusted isotherms at 700 mb on November 29, in storm-relative coordinates.

decrease through the southwest. Moisture values show the opposite trend, however, with a relative maximum in the southwest eyewall and no distinct maximum in the northeast section. The net effect on the Θ_E profile is to create a relative maximum in the eye with largest gradients in the two eyewalls.

Profiles for the southeast-north leg on November 29 are depicted in fig. 26. These profiles also show an eye diameter of 100 km, with large asymmetries in the moisture profiles. Maximum moisture values were obtained in the eye center rather than in the convective eyewall. This indicates broken convection around the eye and a discontinuous eyewall, a fact confirmed by the observer flight logs. The lack of a well-defined zone of maximum outward radial flow (figs. 27b and 27c) in the north eyewall also supports the hypothesis of rather discontinuous eyewall convection. It has been noted (Jorgensen, 1981) that in Atlantic mature hurricanes, pronounced radial flow occurs only in the presence of a well-defined convection updraft and high radar reflectivity. In all other flight days, except the most intense day (November 26), generally saturated conditions prevailed outside the eye. Perhaps intrusion of drier air from the north, just before recurvature, is the explanation for the absence of moisture to the north on this day.

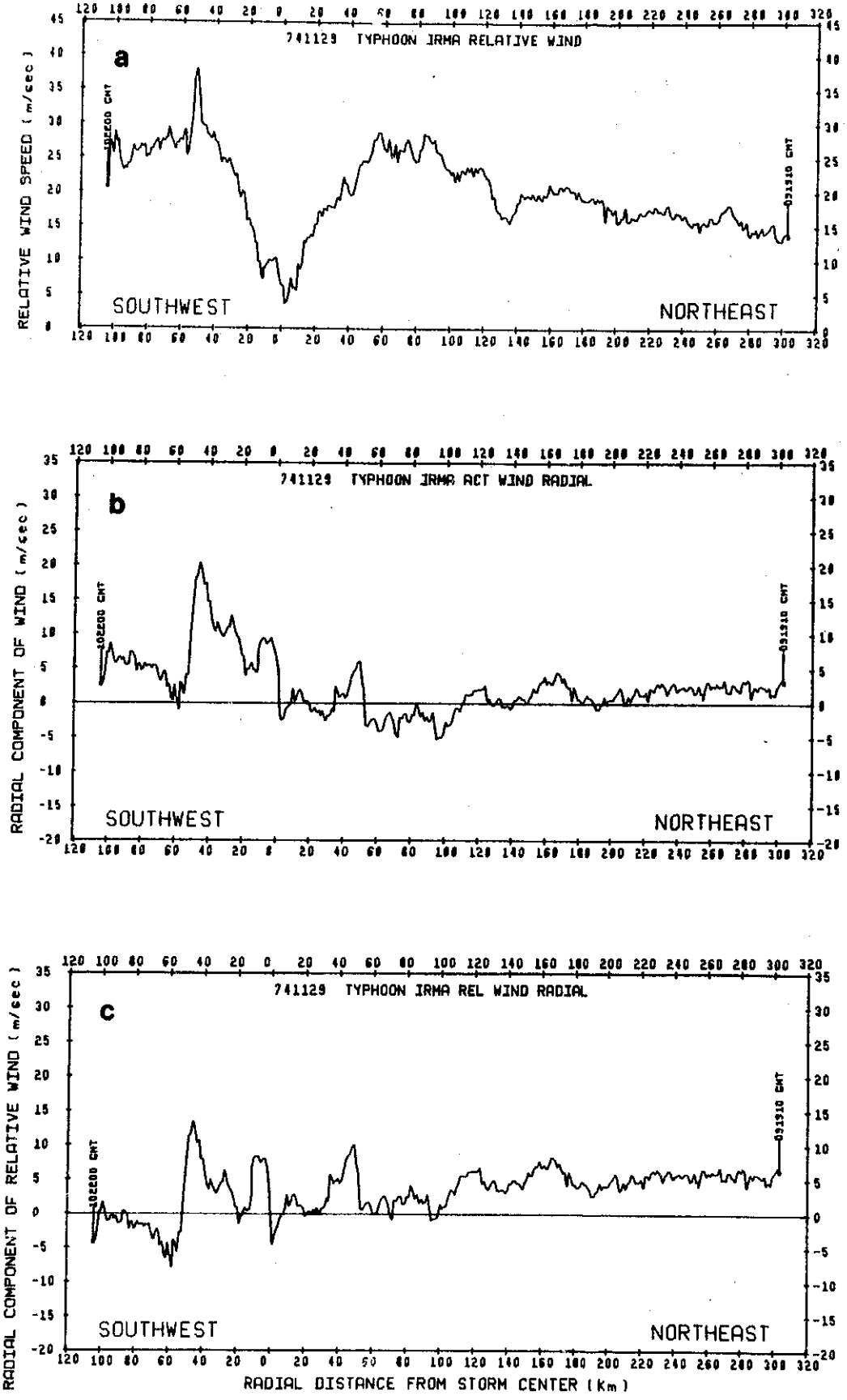

Figure 25.--November 29 northeast-southwest profiles: (a) relative tangential wind; (b) actual radial wind; (c) relative radial wind.

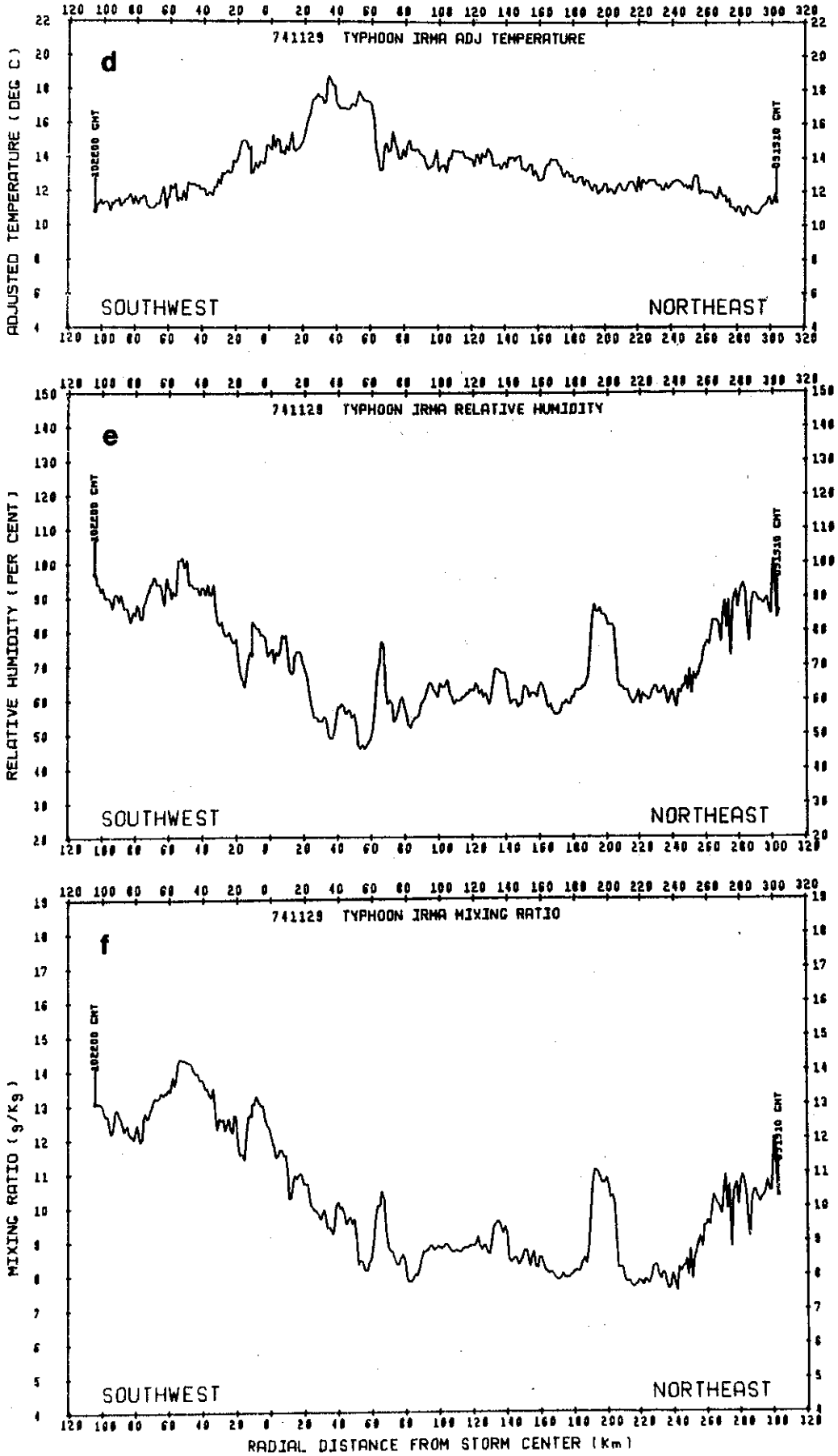

Figure 25.--Continued: (d) adjusted temperature; (e) relative humidity; (f) mixing ratio.

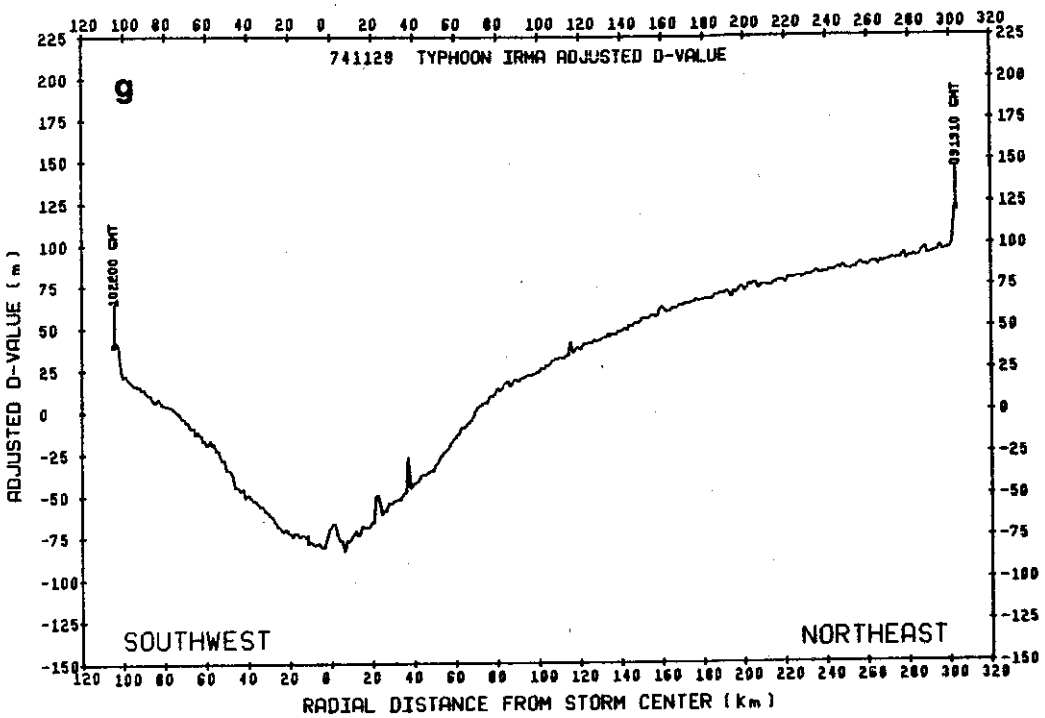

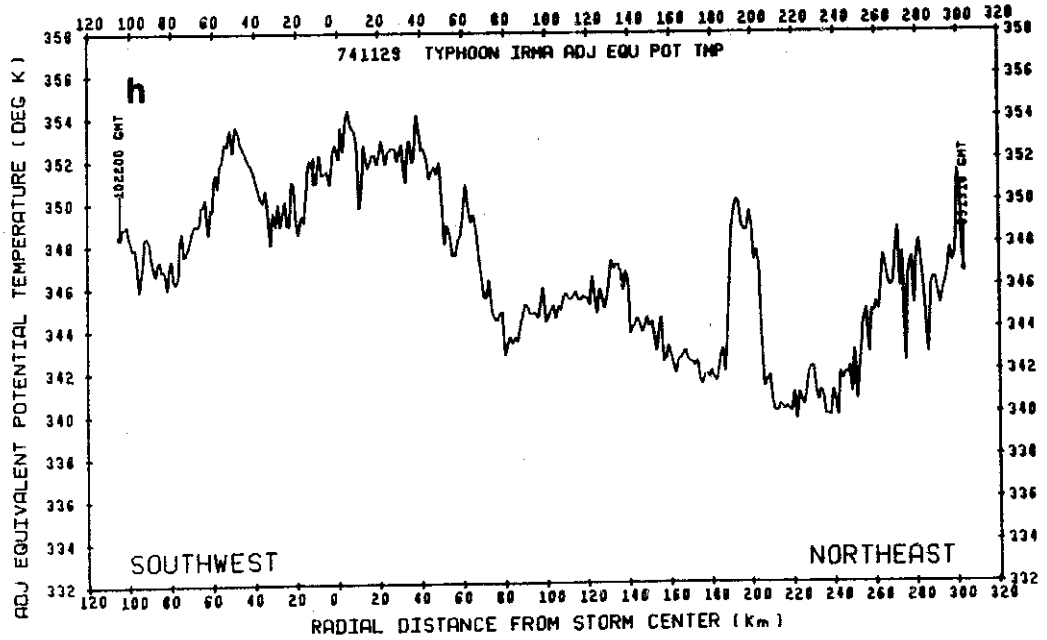

Figure 25.--Continued: (g) adjusted D-value; (h) adjusted equivalent potential temperature.

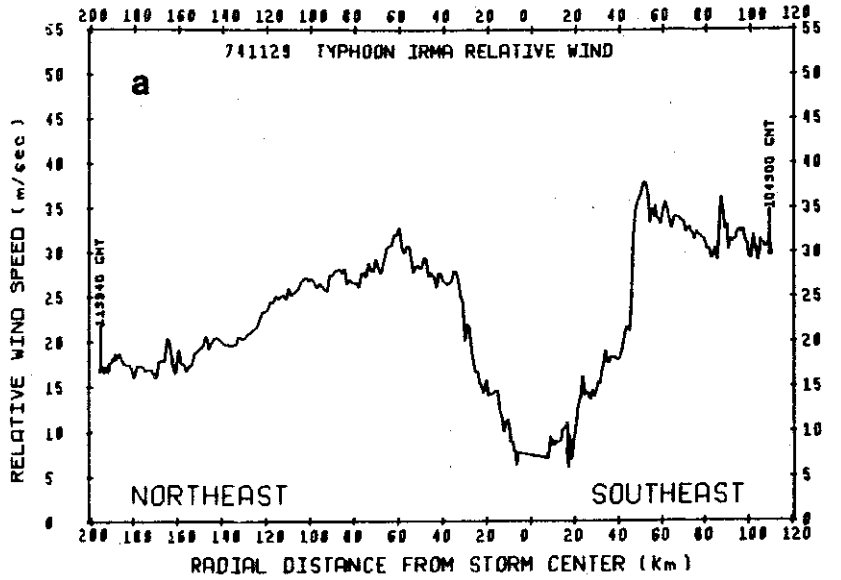

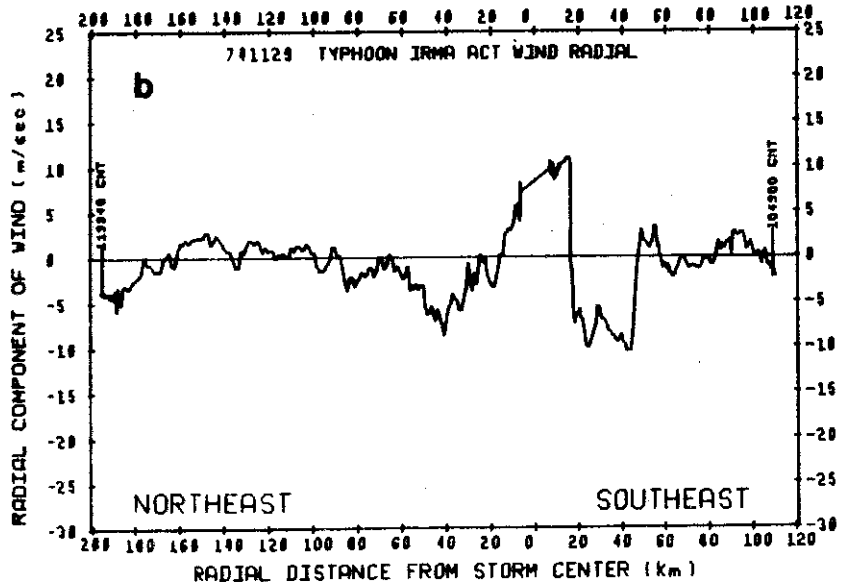

Figure 26.--November 29 southeast-northeast profiles: (a) relative tangential wind; (b) actual radial wind.

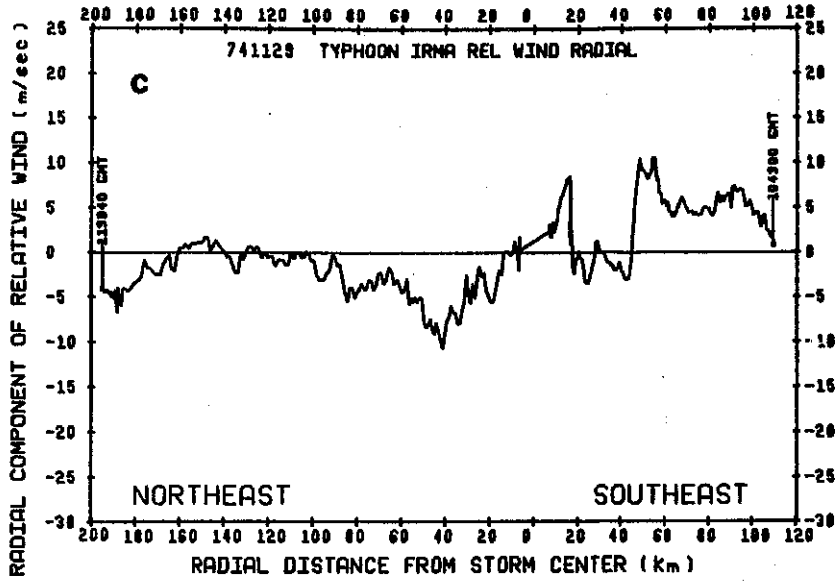

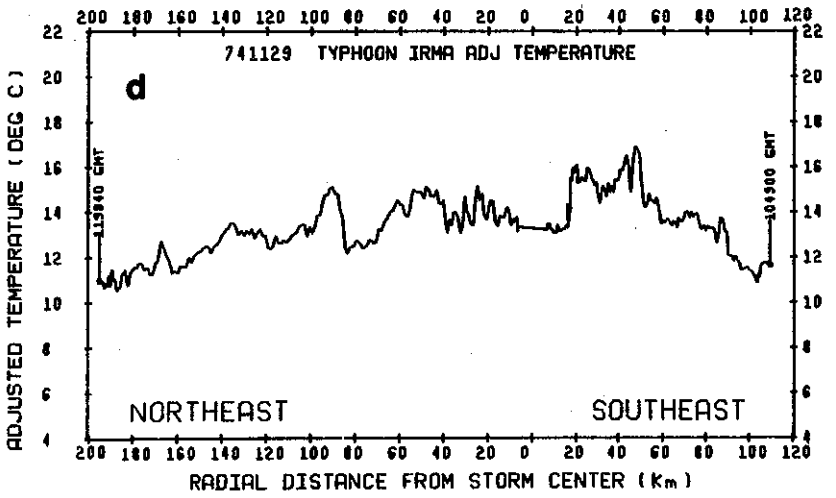

Figure 26.--Continued: (c) relative radial wind; (d) adjusted temperature.

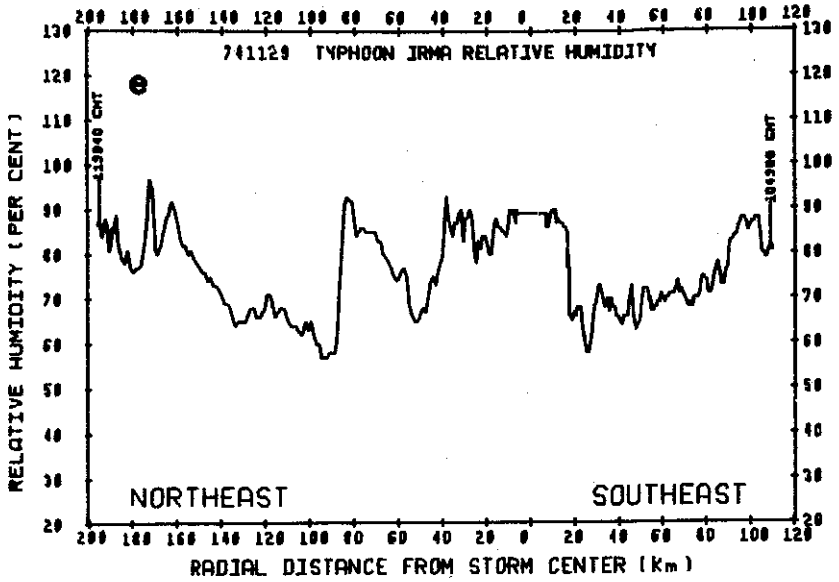

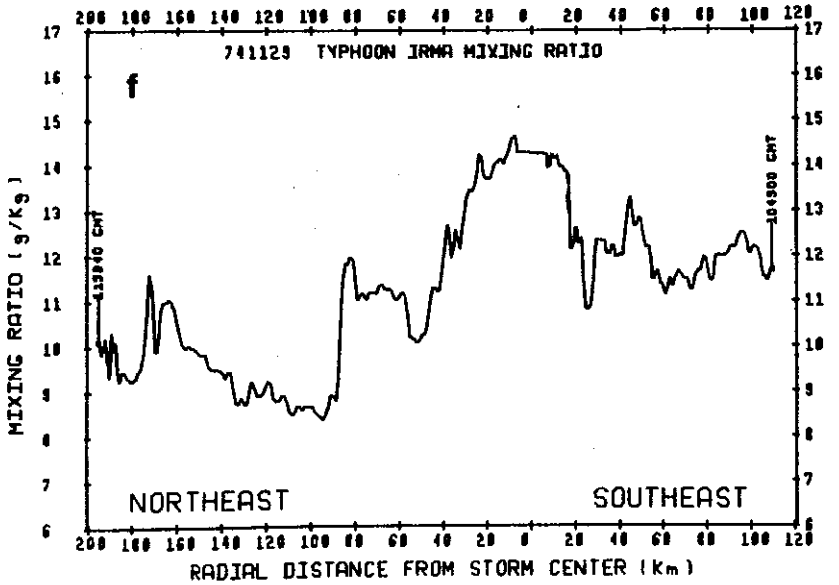

Figure 26.--Continued: (e) relative humidity; (f) mixing ratio.

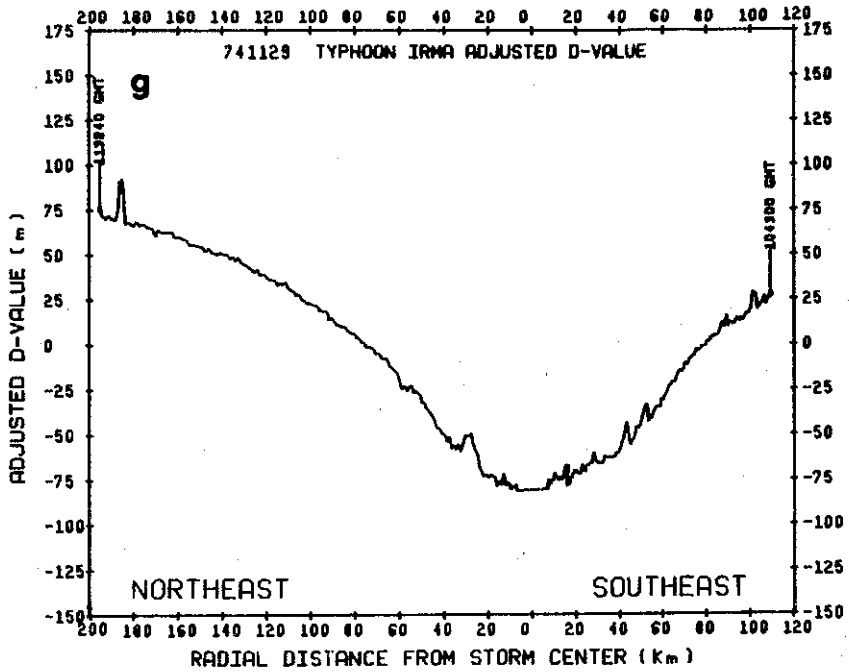

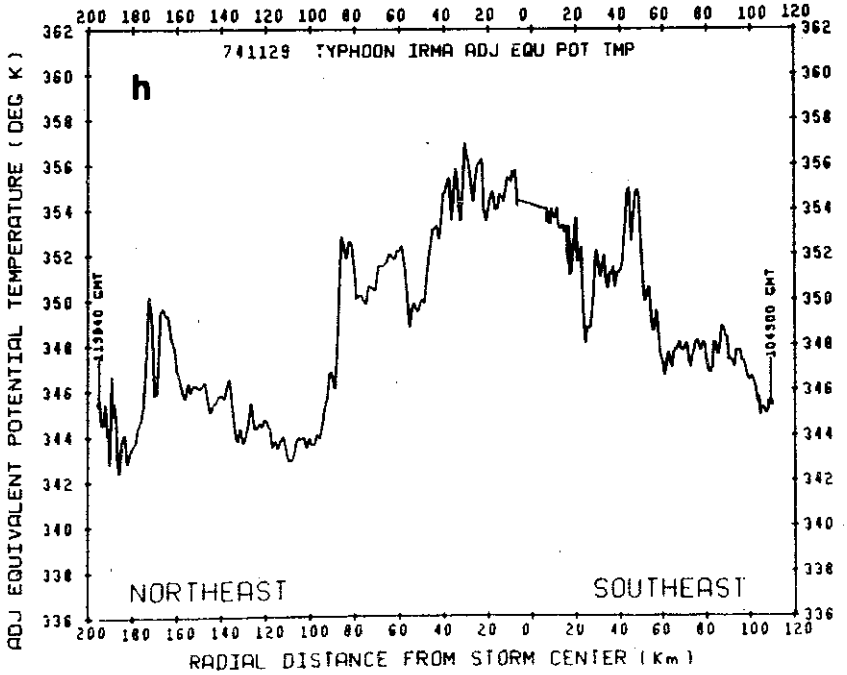

Figure 26.--Continued: (g) adjusted D-value; (h) adjusted equivalent potential temperature.

8. THE BALANCE BETWEEN WIND FIELD AND PRESSURE GRADIENT FIELD

The individual radial flight legs have been examined to determine the existence of supergradient winds. These winds have been hypothesized to be important in eyewall formation by Malkus (1958) and have been shown to exist by Shea and Gray (1973) in their composites. The wind data used by Shea and Gray were derived by the Doppler navigation instrument, which has been known to yield erroneous results when there is appreciable apparent surface motion below the aircraft from detection, by the Doppler beam, of sea spray caused by high wind velocities. Winds derived from the inertial navigation system used in this study do not suffer from this problem. Any comparisons of results derived from the two systems should be interpreted with the understanding that the Doppler winds may be underestimates of the real wind.

If no radial accelerations or radial friction were present, the pressure gradient force would balance the tangential wind field and the equation of motion would be

$$\frac{V_{g\Theta}^2}{r} + fV_{g\Theta} - \frac{\partial D}{g\partial r} = 0, \qquad (1)$$

where $V_{g\Theta}$ is the tangential wind in meters per second, f is the Coriolis parameter in meters per second, g is the gravitational acceleration in meters per second squared, D the adjusted D-value in meters, and r the radius of the trajectory curvature. The nearly circular streamlines and lack of appreciable change in storm central pressure during the period of aircraft investigation imply that the storm was in near-steady state. Radial distance from the storm center is, therefore, used as the radius of curvature.

When gradient wind is computed, the most difficult problem is the evaluation of the pressure gradient. The adjusted D-value, which is the height departure from the standard atmosphere, has, in general, a noise component of a few meters. In addition there are one or two data point spikes of 20 to 30 m (e.g., fig. 16g), which were probably caused by the nonstabilization of the radar altitude instrument, since these spikes were correlated to the roll of the aircraft during turns. These small-scale oscillations, as well as the large spikes, must be filtered before a gradient can be determined.

Several techniques of least-square polynomial approximation were tried in an attempt to find the best approximation to the D-value profile. A single, high-order polynomial was used over the entire half profile radially outward from the center for several profiles, but, although the profiles did approximate the largest gradients very well, oscillations developed in the derivative of the D-value polynomial near the end points. Lower-order polynomials were tried in an effort to filter the oscillations; however, these polynomials then underestimated the largest gradient of the D-value profile in the region of maximum winds. The oscillations are caused by the polynomial least-squares technique, that is, by the tendency of polynomials to go to infinity for large values of the independent variable. Thus, the error is likely to be large near the end points (Hamming, 1973). These oscillations contaminated the computed gradient wind, sometimes as much as 100 km from the end points. Another technique of least-squares polynomial approximation was then tried.

The new method consisted of the fitting of a low-order least-squares polynomial locally to an odd number of data points (typically 33) and then the use of the derivative of this curve to estimate the gradient of the D-value at the midpoint. In this way, the least-squares technique became smoother, removing high-frequency components associated with instrument error and cumulus-scale oscillations. A routine was also employed to remove data points that were in obvious gross error. This de-spiking routine checked for points that had residuals from a low-order polynomial that were at least 3 times the standard deviation for all the points. Those bad values were thrown out and a new polynomial was fit to the data. In this manner, a D-value function was generated for all data points in the profile (except for the 16 points at either end). The 16 points on either side of the data point were used as input to the curve-fitting routine. Since the data that were used were taken every 10 seconds, the aircraft traveled about 1.5 km between data points, so the smoothing interval is approximately 50 km.

Figure 27 illustrates the result of the computation of the gradient wind for six selected profiles on four flights during November 24 through 26 and November 28. The curves labeled V_g represent the computed gradient wind from the pressure field, and the lines marked V_θ are the observed relative tangential winds. It can be seen that the computed gradient wind agrees fairly well with the observed relative tangential wind in the region of the radius of maximum wind. Outside the radius of maximum winds, the agreement between the two winds is not so good, particularly beyond a radial distance of 200 km. The computed V_r exhibits an oscillating character at these large radial distances. The relative accuracy of the curve fit to the D-value field goes down at these large radial distances as determined by the correlation coefficient (a measure of the goodness of fit). In the high-energy region of the storm, (eyewall) values of the correlation coefficient generally were >.99. However, at large radial distances this value dropped to .93 or less, indicating that oscillations caused by instrument error and scales <50 km had an increasing effect on the estimation of the gradient, chiefly because the gradient and the noise level are the same order of magnitude. In addition, since, in the computation of the gradient wind, the gradient of the D-value is multiplied by the radial distance, the effect of small errors of $\partial D/\partial r$ on the computation of V_r is magnified at large radial distances. The good agreement between the computed gradient wind, V_r, and observed relative tangential wind, V_θ, at the radius of maximum wind is somewhat at variance with other studies. Shea and Gray (1973) have shown that, in the mean, the relative tangential wind exceeded the gradient wind from 105% to 150% at the radius of maximum wind, depending upon the value for the correction to the Doppler winds for water motion. Sheets (1973) has found in the case of Hurricane Debbie (1969) that, in general, the gradient wind overestimates the wind field for most areas of the high-energy region of the storm. The technique used in this study most closely resembles Sheets's filter "B," which smooths the D-value field with a low-pass filter and removes the significant contribution to the total signal for all scales of motion <50 km in wavelength.

Gray has remarked that the existence of supergradient winds at the radius of maximum winds is necessary to balance the inward acceleration in the inflow layer and to act as a ventilating effect for the air in the eye. As a whole, supergradient winds were not found at the radius of maximum winds for this data set, yet the radial winds frequently exhibited outflow from the eye into the eyewall region, thus ventilating the eye.

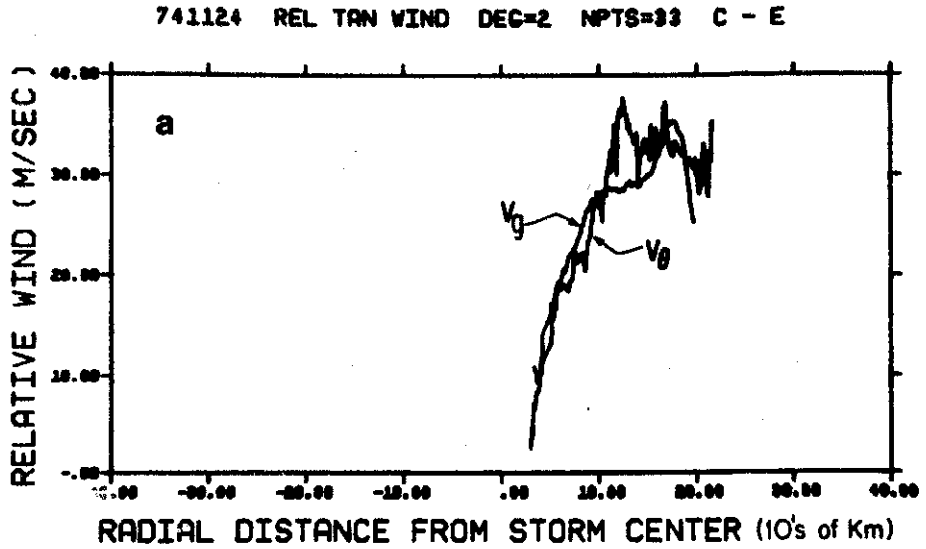

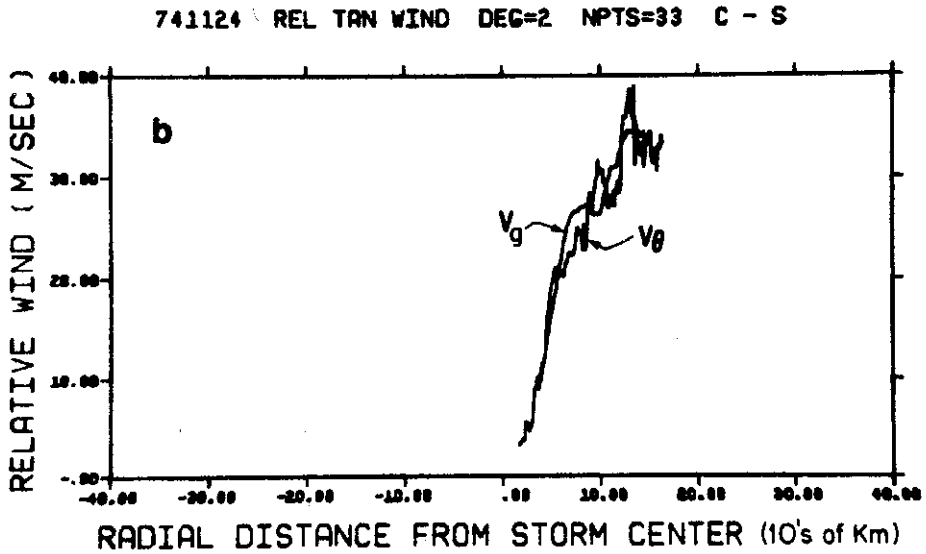

Figure 27.--Gradient wind computations for six selected profiles on four flights: November 24 (a) east-center and (b) south-center profiles.

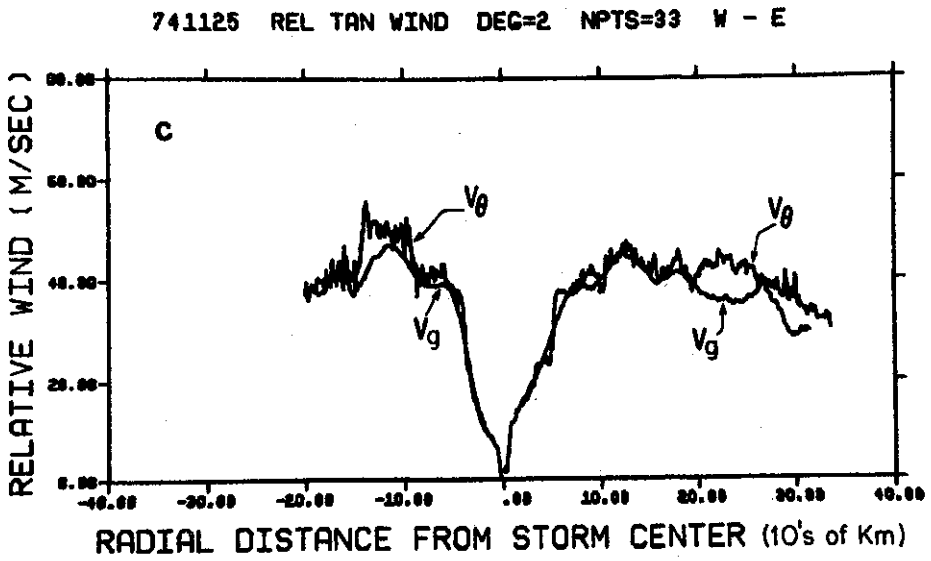

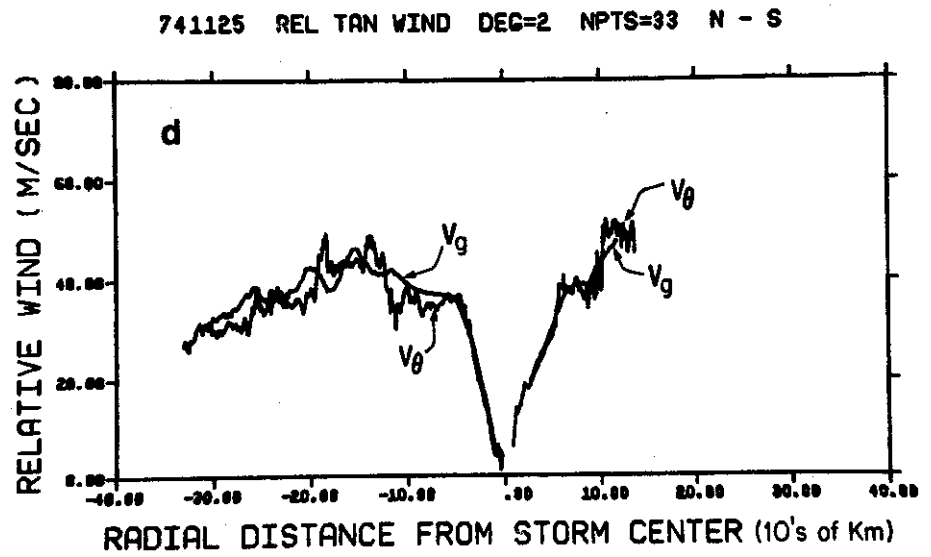

Figure 27.--Continued: November 25 (c) east-west and (d) south-north profiles.

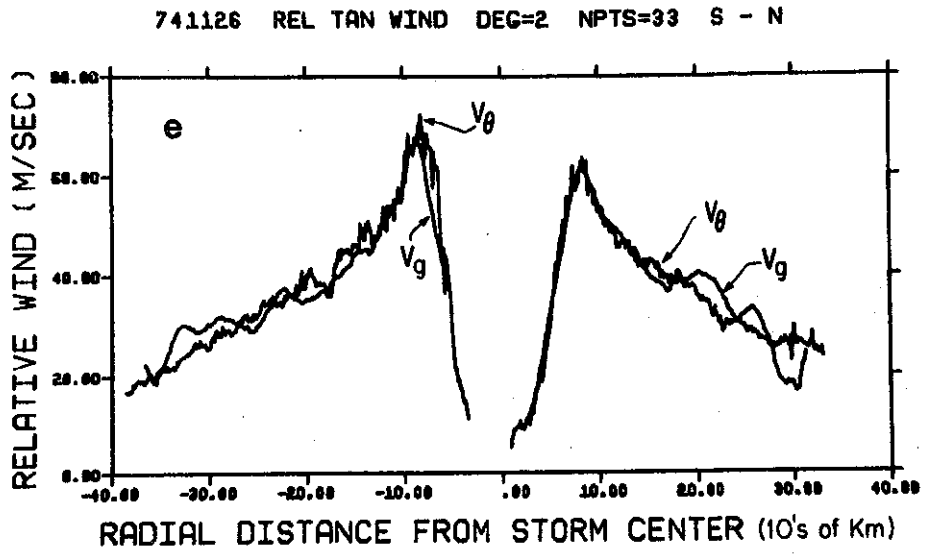

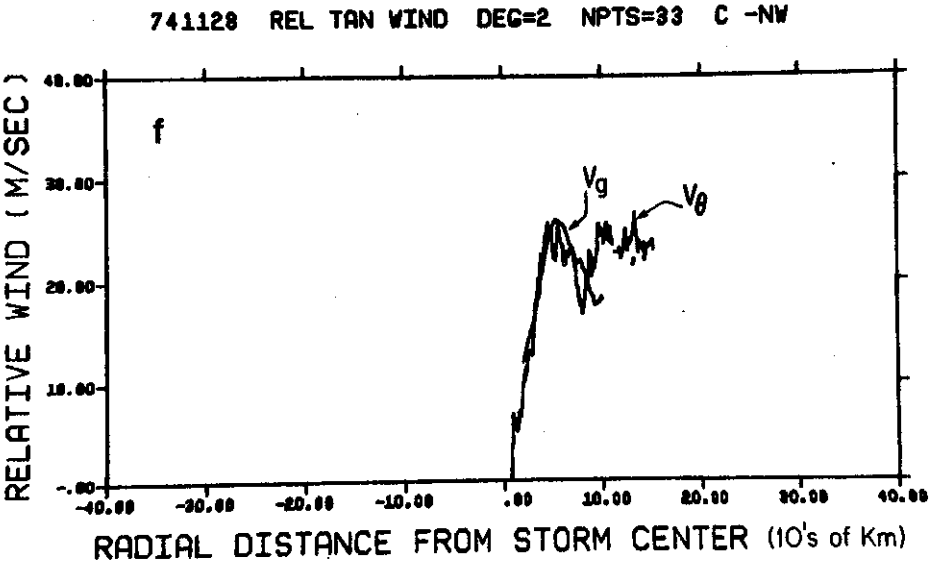

Figure 27.--Continued: (e) November 26 north-south profile; (f) November 28 northwest-center profile.

Gradient balance is indicated, regardless of storm state or speed, in the region of maximum wind. Beyond about 200 km radial distance, the relative accuracy of the computed gradient wind suffers to the extent that direct comparison with observed relative tangential wind is not possible.

9. SUMMARY AND CONCLUSIONS

Aircraft data from five reconnaissance flights into Typhoon Irma (November 24, 25, 26, 28, and 29, 1974) have been composited and analyzed relative to the moving storm center. Horizontal analyses of streamlines, isotachs, and adjusted temperature, and profile plots of the wind and thermodynamic quantities from the radial penetrations are presented for each flight. The five flights represent five stages of storm development, from a weak-to-moderate storm to a large, intense typhoon, and back to a weak storm after passage over Manila. Comparison of Irma's storm structure with mean hurricane structure as determined from Shea and Gray (1973) composites reveals striking similarities, in spite of the different instrumentation used in the respective studies. Comparisons with other case studies of individual hurricanes (Inez, 1966; Cleo, 1958) also reveal the similarity in structure of Pacific Typhoon Irma with Atlantic hurricanes, in spite of Irma's extensive horizontal dimensions and the large diameter of the storm's eye.

Data for four days were complete enough to construct horizontal analyses of streamlines, isotachs, and adjusted temperature. The analyses reveal similar structure in spite of large intensity changes. The 700-mb streamlines were nearly circular on the four days, indicating that the levels of inflow/outflow were always confined to the levels below/above 700 mb. The radial flow pattern on the most intense day was characterized by consistant inflow at 700 mb south and west of the center with outflow to the north and east. There are indications of this pattern on other days as well, although it is not as well worked. The most intense stage of development was characterized by a single predominant peak of maximum wind. The other, less intense stages of Irma were characterized by no steep decreases in tangential wind outside the eye; there are indications of multiple maxima of tangential wind on one of the days (November 25), a finding that Willoughby et al. (1981) noted in symmetric Atlantic hurricanes.

Temperature analyses indicate a consistent finding that the highest temperatures do not occur in the eye center, but in a ring adjacent to the radius of maximum wind. Cooler temperatures and slight inflow (leg-averaged) relative to the moving center are noted to the south and southwest of the storm center on all days with warm anomalies of temperature and slight outflow at 700 mb to the north.

Largest gradients of D-value and Θ_E are noted inward of the region of maximum wind with generally subsaturated conditions outside the eye on the most intense day, November 26. On November 24, 25, and 28, generally saturated conditions prevailed outside the eye, indicative of the effective actions of the convection in moistening the air outside the eye.

Gradient wind computations indicate that the D-value data (pressure and radar altitude) are accurate enough to make these computations directly possible. Irma's wind field above the 50-km scale appears to be in nearly gradient balance in the region of maximum wind. Beyond about 200 km radial

distance, however, the gradient in the D-value becomes small enough to be the same order as the oscillations produced by the instrument error and cumulus scale, and the relative accuracy of the computed gradient wind goes down.

10. ACKNOWLEDGMENTS

The author wishes to acknowledge the assistance of the late Billy M. Lewis, who provided insight into the data reduction and compositing procedure, and Dr. Harry F. Hawkins, who provided many worthwhile discussions on hurricane dynamics and the implications of gradient balance. Dr. Gordon Bell of the Royal Observatory in Hong Kong is greatly appreciated for his help in securing the synoptic maps and track of Typhoon Irma. Dr. Robert C. Sheets assisted in the derivation of the D-value adjustment algorithm.

Thanks go to Robert C. Bundgaard, Kama Aerospace Corporation, for his valuable assistance in determining the accuracy of the AWRS data, and to the U.S. Air Force for providing the data.

Dr. Steven Lord and Mr. Paul Willis provided many helpful comments during initial review of the manuscript.

11. REFERENCES

Annual Typhoon Report (1974): Fleet Weather Central/Joint Typhoon Warning Center, Guam, 116 pp.

Bell, G.A. (1975): Observations of the size of the typhoon eye. Typhoon Modification, WMO-No. 408, Geneva, 19-29.

Colon, J.A. (1964): On the structure of Hurricane Helene (1958). National Hurricane Research Project Rep. 72, NOAA/ERL, WMPO, Boulder, Colorado, 56 pp.

Hawkins, H.F., and S.M. Imbembo (1976): The structure of a small, intense hurricane--Inez 1966. Mon. Weather Rev. 104: 418-442.

Hawkins, H.F., and D.T. Rubsam (1968): Hurricane Hilda (1964). II: Structure and budgets of the hurricane on October 1, 1964. Mon. Weather Rev. 96: 617-636.

Hamming, R.W. (1973): Numerical Methods for Scientists. McGraw-Hill, 714 pp.

Jorgensen, D.P., 1982: Meso- and convective-scale characteristics common to several mature hurricanes: Part I, General observations by research aircraft. (Unpublished manuscript.)

LaSeur, N.E., and H.F. Hawkins (1963): An analysis of Hurricane Cleo (1958) based on data from research reconnaissance aircraft. Mon. Weather Rev. 91:694-709.

Lewis B.M., and D.P. Jorgensen (1978): Study of the dissipation of Hurricane Gertrude (1974). Mon. Weather Rev. 106:1288-1305.

Ley, G.W., and R.L. Elsberry (1976): Forecasts of Typhoon Irma using a nested-grid model. Mon. Weather Rev. 104:1154-1161.

Malkus, J.S. (1958): On the structure and maintenance of the mature hurricane eye. J. Meteorol. 15:337-349.

Melhart, L.J., and B.L. Fister (1975): Operational test and evaluation. Airborne Weather Reconnaissance System, OTE Final Report, HQ MAC/DOQT, Scott AFB, Illinois.

Shea, D.J., and W.M. Gray (1973): The hurricane's inner core region, I: Symmetric and asymmetric structure. J. Atmos. Sci. 30:1544-1564.

Sheets, R.C. (1967): On the structure of Hurricane Ella (1962), ESSA Tech. Memo. IERTM-NHRL 77, NOAA/Environmental Research Laboratories, Boulder, Colo., 33 pp.

Sheets, R.C. (1973): Analysis of hurricane data using the variational optimization approach with a dynamic constraint. J. Appl. Meteorol. 12: 963-976.

Willoughby, H.E., J.A. Clos, and M.G. Shorebah (1981) Concentric eyewalls, secondary wind maxima, and the evolution of the hurricane vortex. (Unpublished manuscript.)

Appendix: Adjusting a D-Value to a Reference Pressure Surface

From the equation of state,

$$P = \frac{R^*}{\overline{m}} \rho T \ ,$$

where P is pressure in millibars, R* the universal gas constant, 8.31×10^7 erg mol^{-1} K^{-1}, $\overline{m}$ the mean molecular weight of dry air, 28.966 g mol^{-1}, ρ the air density in grams per cubic centimeter, and T the temperature in kelvins, and from the hydrostatic equation

$$dP = \rho g dZ \ ,$$

where g is the acceleration of gravity in square centimeters, we obtain

$$\frac{-R^* \overline{T}_v}{\overline{m}g} \int_{P_1}^{P_2} \frac{dp}{P} = \int_{Z_1}^{Z_2} dZ \ , \qquad \text{(A.1)}$$

where $\overline{T}_v$ is the mean virtual temperature between the heights Z_1 and Z_2 of the two pressure surfaces P_1 and P_2. By integration

$$\Delta Z = Z_2 - Z_1 = 29.2898 \, \overline{T}_v \ln \frac{P_1}{P_2} \quad \text{[meters]}. \qquad \text{(A.2)}$$

If Z_1 = adjusted height (RH), Z_2 = height of aircraft (RA), P_1 = pressure height of reference level (P_{ref}), and P_2=P, then

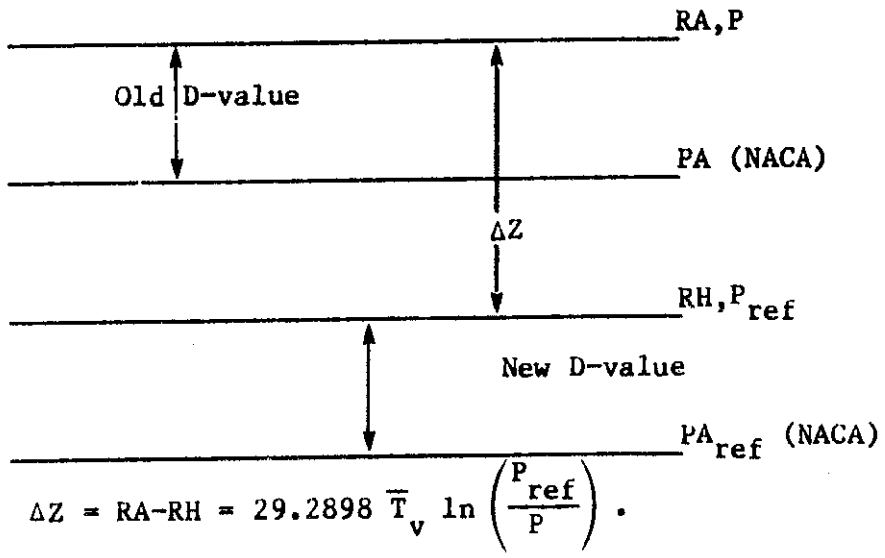

$$\Delta Z = RA-RH = 29.2898 \, \overline{T}_v \ln \left(\frac{P_{ref}}{P} \right) .$$

The new reference height is then

$$RH = RA - \Delta Z \ ,$$

and the new (adjusted) D-value is

$$D_{adj} = RH - PA_{ref} \ .$$

$\overline{T}_v$ can be approximated by

$$\overline{T}_v = [2T_v + (PA - PA_{ref})\ \delta]/2 \ ,$$

where δ is the mean tropical lapse rate, which is 5.577°C km^{-1}, and T_v is the virtual temperature given by

$$T_v = (T-273.16)\ \frac{1 + 1.609w}{1 + w} \ ,$$

where w is the mixing ratio.

This method of approximation for D-value adjustment was compared with an exact iterative method. It was found that, as long as the distance over which the adjustment is being made is <100 mb, the approximation differs from the exact by <1 m.

Environmental Research LABORATORIES

The mission of the Environmental Research Laboratories (ERL) is to conduct an integrated program of fundamental research, related technology development, and services to improve understanding and prediction of the geophysical environment comprising the oceans and inland waters, the lower and upper atmosphere, the space environment, and the Earth. The following participate in the ERL missions:

AL *Aeronomy Laboratory.* Studies the physics, dynamics, and chemistry of the stratosphere and the surrounding upper and lower atmosphere.

AOML *Atlantic Oceanographic and Meteorological Laboratories.* Study the physical, chemical, biological, and geological characteristics and processes of the ocean waters, the sea floor, and the atmosphere above the ocean, including tropical meteorology such as hurricanes and tropical weather systems.

ARL *Air Resources Laboratories.* Study the diffusion, transport, dissipation, and chemistry of atmospheric pollutants; develop methods of predicting and controlling atmospheric pollution; monitor the global physical environment to detect climatic change.

GFDL *Geophysical Fluid Dynamics Laboratory.* Studies the dynamics of geophysical fluid systems (the atmosphere, the hydrosphere, and the cryosphere) through theoretical analysis and numerical simulation using powerful, high-speed digital computers.

GLERL *Great Lakes Environmental Research Laboratory.* Studies hydrology, waves, currents, lake levels, biological and chemical processes, and lake-air interaction in the Great Lakes and their watersheds; forecasts lake ice conditions.

NSSL *National Severe Storms Laboratory.* Studies severe-storm circulation and dynamics, and develops techniques to detect and predict tornadoes, thunderstorms, and squall lines.

OWRM *Office of Weather Research and Modification.* Conducts a program of basic and applied research to advance the understanding and define the structure of mesoscale phenomena, to improve short-range weather predictions and warnings, and to identify and test hypotheses for beneficially modifying weather processes.

PMEL *Pacific Marine Environmental Laboratory.* Monitors and predicts the physical and biochemical effects of natural events and human activities on the deep-ocean and coastal marine environments of the Pacific region.

PROFS *Prototype Regional Observing and Forecasting Service.* Evaluates and integrates advanced meteorological measurement, forecasting, and communication/dissemination technologies into functional mesoscale weather forecast system designs for transfer to operational agencies such as NWS, NESS, and FAA.

RFC *Research Facilities Center.* Operates instrumented aircraft for environmental research programs; provides scientific measurement tools, logged data, and associated information for meteorological and oceanographic research programs.

SEL *Space Environment Laboratory.* Studies solar-terrestrial physics (interplanetary, magnetospheric, and ionospheric); develops techniques for forecasting solar disturbances; provides real-time monitoring and forecasting of the space environment.

WIM *Weather Modification Program Office.* Plans and coordinates ERL weather modification projects for precipitation enhancement and severe storms mitigation.

WPL *Wave Propagation Laboratory.* Develops, and applies to research and services, new methods for remote sensing of the geophysical environment.

U.S. DEPARTMENT OF COMMERCE
National Oceanic and Atmospheric Administration
BOULDER, COLORADO 80302